August 2018

A Controls-Oriented Approach For Modeling Professional Drivers During Ultra-High Performance Maneuvers

Jeffery Ryan Anderson
Clemson University, jra3@g.clemson.edu

A Controls-Oriented Approach For Modeling Professional Drivers During Ultra-High Performance Maneuvers

---

A Dissertation
Presented to
the Graduate School of
Clemson University

In Partial Fulfillment
of the Requirements for the Degree
Doctor of Philosophy
Automotive Engineering

---

by
Jeffery R. Anderson
August 2018

Accepted by:
Dr. Beshah Ayalew, Committee Chair
Dr. Timothy Rhyne
Dr. Ardalan Vahidi
Dr. Robert Prucka

Abstract

In the study of vehicle dynamics and controls, modeling ultra-high performance maneuvers (i.e., minimum-time vehicle maneuvering) is a fascinating problem that explores the boundaries of capabilities for a human controlling a machine. Professional human drivers are still considered the benchmark for controlling a vehicle during these limit handling maneuvers. Different drivers possess unique driving styles, i.e. preferences and tendencies in their local decisions and corresponding inputs to the vehicle. These differences in the driving style among professional drivers or sets of drivers are duly considered in the vehicle development process for component selection and system tuning to push the limits of achievable lap times. This work aims to provide a mathematical framework for modeling driving styles of professional drivers that can then be embedded in the vehicle design and development process.

This research is conducted in three separate phases. The first part of this work introduces a cascaded optimization structure that is capable of modeling driving style. Model Predictive Control (MPC) provides a natural framework for modeling the human decision process. In this work, the inner loop of the cascaded structure uses an MPC receding horizon control strategy which is tasked with finding the optimal control inputs (steering, brake, throttle, etc.) over each horizon while minimizing a local cost function. Therein, we extend the typical fixed-cost function to be a blended cost capable of optimizing different objectives. Then, an outer loop finds the objective weights used in each MPC control horizon. It is shown that by varying the driver's objective between key horizons, some of the sub-optimality inherent to the MPC process can be alleviated.

In the second phase of this work, we explore existing onboard measurements of professional drivers to compare different driving styles. We outline a novel racing line reconstruction technique rooted in optimal control theory to reconstruct the driving lines for different drivers from a limited set of measurements. It is demonstrated that different drivers can achieve nearly identical lap times while adopting different racing lines.

In the final phase of this work, we use our racing line technique and our cascaded optimization framework to fit computable models for different drivers. For this, the outer loop of the cascaded optimization finds the set of objective weights used in each local MPC horizon that best matches simulation to onboard measurements. These driver models will then be used to optimize vehicle design parameters to suit each driving style. It will be shown that different driving styles will yield different parameters that optimize the driver/vehicle system.

Dedication

To my amazing wife, Liesel. I love you with all of my heart. I could not be more blessed than to walk through life with you. We finally crossed the finish line!

Acknowledgments

There are so many people to whom I am grateful for their support and encouragement that it would be impossible to include everyone here. This, like all other accomplishments in life, proves the adage that nobody accomplishes anything alone.

First, I would like to express my sincerest gratitude to my advisor, Dr. Beshah Ayalew. Over these past five years, I have learned an incredible amount from him. Not only academically but in all aspects of life. He has been a mentor, role model, and a friend. I sincerely appreciate the freedom that he has given me to explore this area of research, as well as the encouragement he gave me to be persistent when things were tough. I am truly grateful to have had the opportunity to work with him these past five years.

To all of my committee members: Dr. Timothy Rhyne, Dr. Robert Prucka, and Dr. Ardalan Vahidi thank you for challenging me to become a better student. I greatly appreciate all the insight and pointed questions which helped to hone and polish this research into what it has become. I especially appreciate the coursework which formed my fundamentals. Dr. Rhyne, your tires course was incredible and Dr. Vahidi, your optimal control class helped give me the foundation for much of this work.

My employer Michelin has graciously sponsored me during this pursuit. I am extremely thankful for this experience. Allowing me the flexibility to be successful working through the Ph.D. process while still allowing me to contribute at work has been a rewarding process in which I have learned a great deal about both the subject matter and myself. Specifically, Alex Papadatos, Olivier Gerardin, Dan Osborne, and Guillaume Jaillard, thank you all so much for this incredible opportunity and the ability to study this fascinating field.

Finally, I want to thank Lee Willard and Ryan Pawlowski who went above and beyond to help out and support this endeavor. You all have been a fountain of wisdom, support, and encouragement and for that I am grateful.

My family and friends have been an immense source of optimism and comfort throughout this journey. I can never thank everyone enough for their continued help and encouragement. They have been an incredible source of both strength and stability constantly keeping me grounded while helping me to see the light at the end of the tunnel (which I thought would never come).

Throughout my Ph.D. work, I cannot quantify the knowledge I have gained. I can, however, sum up the more practical aspects of high-performance vehicle development with two quotes. The first encouraged me to rely on fundamentals as they never fail while the latter reminded me that sometimes even sound logic is not enough. I truly believe both understandings are crucial in developing useful material for the ultra-high-performance sector.

"*Who gave you permission to do that?*" - Management

"*Sir Isaac Newton.*" - Lee Willard (Michelin Ultra-High-Performance Tire Designer)

"*Predicting lap time is bad karma.*" - Jim Mero (GM Test Driver for Corvette)

Table of Contents

List of Tables

List of Figures

Chapter 1

Introduction

In this dissertation, we aim to better understand and provide a mathematical framework for modeling the human element of high-performance driving. Professional drivers are considered the pinnacle of performance when it comes to limit handling and minimum-time maneuvering. In the automotive industry, these drivers are used as tools to evaluate vehicle performance and provide the final validation check on many automotive development programs. Their subjective impressions tune the vehicle's subsystems and overall all feel. In motorsports, race teams meticulously tune vehicles around their team's drivers to provide a competitive platform. Different human drivers possess unique driving styles which lead to different tunings to suit a particular style. In this work, we will present a method of modeling different drivers driving styles. Using this framework, the vehicle can then be numerically optimized for a particular driving style.

Vehicle minimum-time maneuvering is a direct result of the human spirit to push the human/machine system to the limits of performance. Shortly after the invention of the automobile, man took to racing. The first recorded race of two vehicles over a prescribed path occurred in 1867 with home-built steam engine vehicles [6]. The first organized motoring competition took place some years later, in 1894, in France [7]. As the years progressed motorsports formalized into a myriad of different groups and series which has led to the vibrant sport that is auto racing today. While the motorsports industry has a direct con-

nection with this problem, it trickles into much of the automotive industry as a whole. High-performance vehicles (i.e., sports cars and luxury vehicles) include performance targets in their development programs that benefit from the study of minimum-time vehicle maneuvering. Professional drivers are still considered the benchmark of limit-handling performance. By gaining a better understanding of how these drivers operate, we can better design automotive safety systems that can operate at an equivalent level of performance. Technologies such as obstacle avoidance, where time-optimal operation is critical, can benefit from researching this problem [8]. Additionally, solutions to these problems reach outside of the automotive industry and can influence the gaming industry [9] and even education [10].

Minimum-time vehicle maneuvering problems are among some of the most complicated and challenging problems to model and solve. The general mission of a driver during this type of driving is to negotiate a set road or maneuver in minimum-time while obeying constraints that take the form of vehicle dynamics and the track to be traversed. The complicated nature of this arises from a few key areas. Frictional forces between the tire and road are incredibly complicated and highly nonlinear with respect to control parameters (i.e., slip quantities). Moreover, the behavior of this friction is highly dependent on the road surface, thermal conditions, and tire solicitation. Modeling the vehicle dynamics also introduces complications with suspension effects and aerodynamics. Both of these items are well researched, and techniques for dealing with these effects exist albeit there is always a trade-off between model fidelity and computational cost. While much research exists and shall be reviewed in the subsequent chapters, full comprehension of the 'human' aspect of driving is still not fully achieved. Much of the existing literature has concentrated on creating an 'ideal' driver model while it is well accepted that different drivers have different styles in accomplishing the minimum-time objective. They can achieve similar performances utilizing their different styles [11]. The goal of this work is to further the study of the 'human' aspect of controlling a vehicle during limit handling maneuvers and present a method for modeling these aspects. The key contribution of this dissertation will be to provide a frame-

work to mathematically model the human element of driving during ultra-high performance maneuvers and then a means of optimizing a vehicle for a particular driving style.

1.1 Motivation

Racing and motorsports possess a very distinct connection to this work [1] with millions of research dollars being spent for milliseconds of lap time improvement [12]. This research also reaches to other areas of the automotive industry, such as high-performance vehicles. These vehicles are a key segment to original equipment manufacturers (OEMs). In the United States, just under 90% of OEMs sell a vehicle that participates in this segment. Nearly all OEMs at some time or another have demonstrated prototype cars in this segment. Sports and sport luxury cars account for nearly three-quarters of a million vehicle sold per year [13]. This trend is not limited to the OEMs; suppliers also play a vibrant role in this segment. For example, ultra-high performance tires account for 17% of the replacement tire market in the US. This contribution is worth over five billion dollars per year [14]. These companies are heavily investing in research and development and acquiring substantial revenue through this channel.

As technologies advance and driver assistance systems become more prevalent, gaining a better understanding of how professional drivers accomplish minimum-time driving becomes increasingly important. Driver assistance algorithms should feel 'natural' to their human counterpart and be able to perform as good as a human can. A critical area where this is the case is obstacle avoidance where a vehicle is controlled typically on the vehicle performance envelope to avoid an imminent collision. Another domain that this work contributes to is to the concept of automated proving grounds. By automating the testing component of vehicles, human errors can be mitigated, and a consistent test can be realized. This work is still in its infancy but has had important research activity [15]. From here, the obvious extension is autonomous driving where a vehicle needs to be able to perform with the same capability as a human. Research has also been established in the area of au-

tonomous racing [16]; moreover, commercial race series have established themselves around this concept, i.e., Roborace [17].

1.2 Research Overview

The research goal is divided into three phases. First, we will find a suitable framework for modeling the human element of driving. Next, onboard measurements will be studied to demonstrate the differences we aim to model. The mathematical framework will then be applied to the onboard data to create a model of a particular driving style. Lastly, we will use the identified driver model to optimize vehicle parameters.

1.2.1 Mathematical Framework

In the first phase of the work, we will identify a mathematical framework that is capable of modeling differences in driving styles. We explore Model Predictive Control (MPC) as it has been shown to model the human decision process [18]. MPC traditionally uses a fixed-cost function which practically approximates a global goal. In other words, a minimum-time vehicle maneuvering problem is typically solved with a fixed time-optimal cost in each MPC horizon. This approximation is sub-optimal as MPC neglects any information outside of the scope of the current horizon. Just because time is minimized in each horizon, does not mean that time will be minimized globally.

Professional drivers are able to learn racing circuits and find strategies to globally minimize maneuvering time. For instance, in certain sections of the track, it can be advantageous to sacrifice maneuvering time to maximize velocity and 'setup' for the next section on the course. This strategy is especially true on a curve followed by a long straight section of track [19]. Motivated by how drivers learn different sections of a race track, we explore a blended MPC cost that is capable of capturing different objectives. In this work we consider minimizing time and maximizing velocity at the exit of the horizon; however, this could be further extended to include any suitable objective. Next, an outer loop optimizer learns the

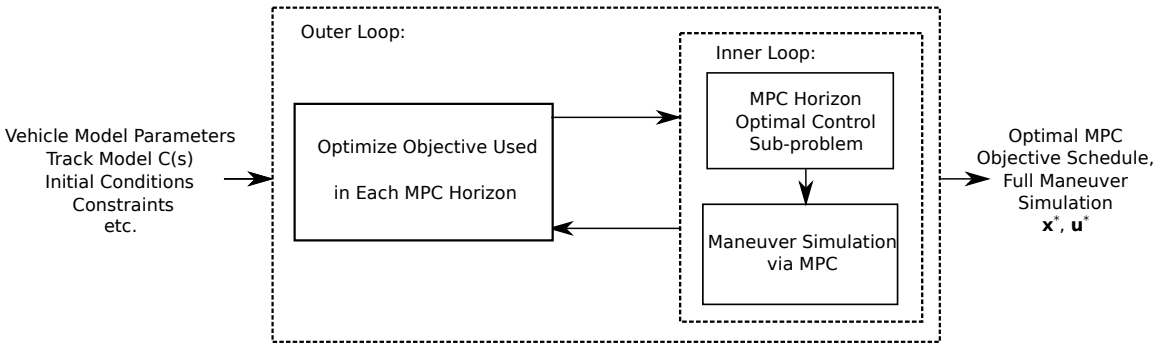

Figure 1.1: Overview of the proposed cascaded optimization. The optimal state and control variables are denoted as $\mathbf{x}^*$ and $\mathbf{u}^*$, respectively.

ideal schedule of the objectives used in each local MPC horizon. This cascaded optimization structure can be seen in Figure 1.1. This structure allows path information outside of the current MPC horizon to be included in the local optimization via modification of the local cost function. This framework will be used to show how some of the inherent sub-optimality of MPC can be alleviated. Also, we will show that different objective schedules found by the outer loop optimizer yield identical performance while exhibiting different trajectories.

1.2.2 Experimental Data

The second phase of this research explores experimental data of two drivers that can achieve identical lap times while exhibiting different styles. There are a few key problems that arise in dealing with measurement; specifically, in preparing measurements to compare to simulation. First, modeling the track features are explored by using optimal control to fit Global Positioning System (GPS) data of a vehicle driving the boundaries of the track [20]. This track model will be used later in the modeling efforts.

In general, onboard vehicle measurements consist of a limited set of sensors. GPS data was not available on our measurements of the professional drivers and such, a method of reconstructing the racing line needed to be developed. In this work, we propose a novel optimal control strategy of reconstructing the racing line from a limited set of sensor data

and the previously derived track model. This racing line reconstruction technique also provides a method to change the basis of the data from the time domain to the path distance traveled domain which is used in our vehicle dynamic simulation. In this phase, we also explore the results of the reconstructed racing line to compare and contrast the driving styles of the two professional drivers.

1.2.3 Modeling Driving Style

The final phase of this research puts the previous two phases together. We will use the cascaded optimization framework previously explored to create a mathematical model of the different driving styles seen in the experimental data. The cascaded optimization finds the schedule of objectives weights (used in each MPC horizon) that best matches the simulation to the onboard vehicle data. We will show that this framework can model key driving style differences between the two drivers. The final step of this work is to use these driver models to optimize vehicle parameters to suit each style. We will then use another cascaded optimization with each driver model to optimize tire parameters. We will show how each drivers' optimal parameters differ; thus, motivating how mathematical modeling driving style is critical to optimizing the human/machine system.

1.2.4 Key Contributions of this Dissertation

The following summarizes the key contributions of this dissertation and will be discussed in detail in the subsequent chapters:

- Proposed cascaded optimization framework to model driving style
- Alleviated inherent MPC sub-optimality by globally optimizing local MPC objectives
- Demonstrated local minima in the solution space for minimum-time vehicle maneuvering
- Attributed these local minima to driving style differences

- Proposed novel optimal control based racing line reconstruction using limited onboard vehicle measurements
- Used cascaded optimization to fit onboard vehicle measurements and model individual driving style
- Optimized vehicle parameters to suit a particular driving style

1.3 Outline

The remainder of this dissertation is organized as follows. Chapter 2 will present a literature review of solution techniques for minimum-time vehicle maneuvering. In Chapter 3 the mathematical framework that will be used to model driving style is detailed. Our work in this chapter was published in [21, 22]. Chapter 4 presents our method for recreating the racing line from a limited set of onboard measurements and a track model and has been submitted for publication in [23]. Chapter 5 uses the cascaded optimization framework and the onboard measurements to create a model of two different professional drivers that are able to achieve identical maneuvering times. This chapter also explores using the previously identified driver models to optimize vehicle parameters to suit each driving style. This work has been submitted for publication in [24]. Finally, Chapter 6 will offer conclusions and possible directions of future work.

Chapter 2

Literature Review

While racing began nearly at the same time as the inception of the automobile, it took some time before engineering principals were applied to investigate vehicle performance. According to [25], Mercedes-Benz is credited with the first applications of engineering principals on the performance of race cars as early as the 1930's with formal publications beginning in the 1950's. The work presented in [26] gives a glimpse into the early days of race car engineering. At this point in racing, vehicles were relatively independent of aerodynamic forces which makes the vehicle performance envelope independent of speed. Because of this, the minimum-time problem over the race circuit can be broken down into a series of straight segments connected by constant radius turns. If the maximum lateral acceleration is known, then the speed in these constant radius turns is: $V_x = \sqrt{Ay_{max}R}$. Finally using the maximum tractive and braking accelerations of the vehicle, the optimum speed profile between turns can be calculated. This estimate of vehicle velocity around the track can be integrated over the path distance to derive the lap time. This method is referred to in the literature as the steady state method of determining lap time. As time progressed, so did the solution methods.

Today solutions of minimum-time vehicle maneuvering problems can be broken down into four general classifications. The first type of solutions are the performance envelope methods (also called quasi-steady-state methods) which solve for a series of steady-state

conditions that minimize vehicle maneuvering time over a predefined racing line. The second classification of problems is the two-step, path planning/path following solutions. In this formulation, a full transient vehicle model is controlled to negotiate a fixed-path in minimum time. The third class of solutions, which will be referred to as the optimal control methods, use optimal control theory to find an optimal set of vehicle inputs to negotiated a track in minimum time. In this method, the racing line is free to vary within the track width boundaries. In addition to these three main classes, machine learning techniques have also been applied to model driving.

The remainder of this chapter is organized as follows. First, Section 2.1 discusses the performance envelope methods. Section 2.2 discusses the path following portion of the two-step path planning/path following solution. Because path planning techniques are used in both of the previous classes of problems, they are discussed as a whole in Section 2.3. The optimal control solution techniques are discussed in Section 2.4. Finally, examples of machine learning application to minimum-time vehicle maneuvering can be seen in Section 2.5.

2.1 Performance Envelope Methods

These are the earliest examples of solving minimum maneuvering time problems and as discussed above have been around since the 1950's. A good description of this method and history is described in [25]. In these early days of the work, aerodynamic downforce on race cars was negligible. That is to say that the coupling between the performance envelop of the vehicle was relatively independent of speed. Because of this, the solution to the minimum-time problem is relatively straightforward and could be calculated analytically. As discussed above, the racing circuit can be broken down into a series of constant radius curves connected by straight lines. By assuming cornering limits the vehicle speed in the turns, the velocity in the turns can be calculated. The remainder of the problem is to identify the optimal longitudinal speed profile that connects the two turns. With the full

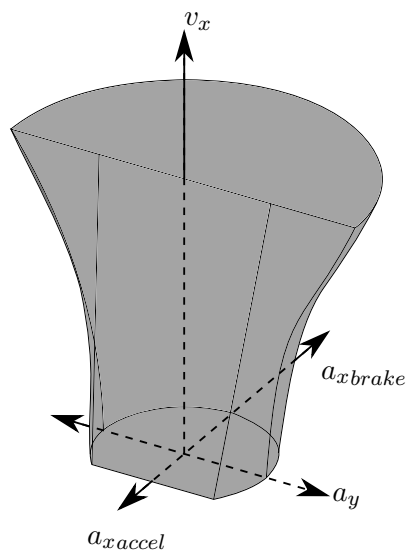

Figure 2.1: Performance envelope, g-g-speed diagram. Based on [1].

velocity profile determined around the track, it can be integrated over the track distance and a measure of lap time can be extracted.

As time progressed, the solution methods were advanced to include the combined lateral and longitudinal cornering case. Also, methods of treating aerodynamics were introduced as the performance envelopes on modern race cars are highly dependent on speed [1]. A general speed-dependent performance envelope (g-g-speed diagram) can be seen in Figure 2.1. Full ground effect cars introduced in the late 1970's have substantially increased tire loading to the point that the cornering performance achieved is many times greater than by mass alone. Now, that the performance envelope is directly coupled with speed, solving the problem requires an iterative solution.

These solution techniques first require identifying the performance envelope of the vehicle (g-g-speed) diagram and a model of the racing line (curvature versus distance $C(s)$). Identifying the performance envelop problem will be discussed in the next subsection and the subject of fitting the racing line will be discussed later in Section 2.3 as this subproblem

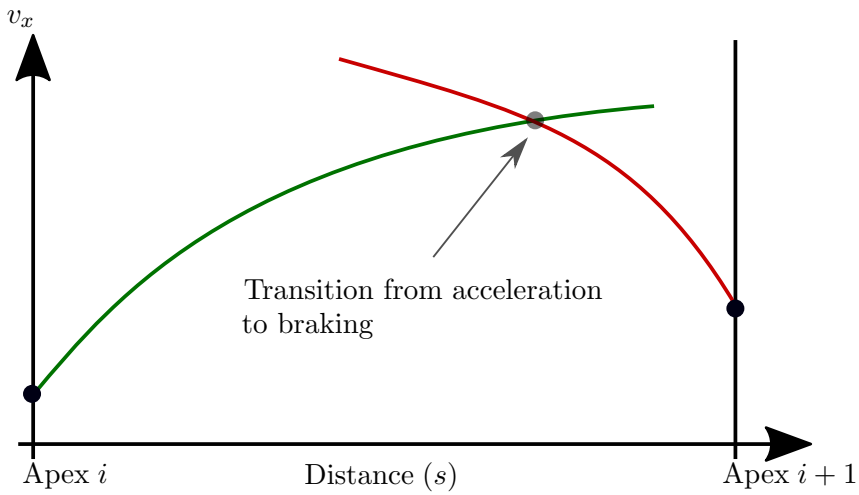

Figure 2.2: Method for calculating optimal velocity profile. Based on [2].

is shared with other methods of solving minimum-time vehicle maneuvering problems. With these two items, the racing line can be discretized into a series of points and steady-state conditions can be found at each point that minimizes the vehicle's maneuvering time. The solution is found by identifying the apexes at each corner; this is the location where peak lateral acceleration occurs, and this governs the maximum speed in the turn. Moving forward from the apex location a profile of the maximum longitudinal acceleration possible is calculated. In addition to this, the maximum deceleration from the next apex backward is calculated. The point where they intersect is the switching point between an accelerating and braking strategy. See Figure 2.2 for a illustration of this. This process is then repeated around the entire race circuit. Some examples of this work can be seen in [27, 28, 29].

2.1.1 Performance Envelope

The performance envelope can be found a few different ways from optimization of mathematical models to fitting onboard vehicle measurements. We will concentrate on the mathematical framework route that uses a vehicle model (we will denote this as $f(\mathbf{x}, \mathbf{u}, t)$).

The works in [2, 30, 31] use optimization to find steady state conditions that make up the full performance envelope. They discretize the space into a cloud of points and optimize for these steady state conditions. The process is started by finding the vehicle's maximum speed (presumed to be in a straight line) by solving the following optimization.

$$\begin{aligned} \min_{\mathbf{u}} \quad & J = -v_x \\ s.t. \quad & \dot{\mathbf{x}} - f(\mathbf{x}, \mathbf{u}, t) = 0 \end{aligned} \tag{2.1}$$

where the goal is to find the vehicle inputs $\mathbf{u}$ that maximizes velocity (v_x) subject to the vehicle dynamics $f(\cdot)$. Next, the vehicle maximum longitudinal acceleration ($\dot{v}_x$) is found at several discrete intervals of the vehicle's maximum speed.

$$\begin{aligned} \min_{\mathbf{u}} \quad & J = \pm\dot{v}_x \\ s.t. \quad & \dot{\mathbf{x}} - f(\mathbf{x}, \mathbf{u}, t) = 0 \end{aligned} \tag{2.2}$$

We now have a shape of vehicle longitudinal potential versus speed. The remainder of the problem is to fill in the lateral potential (peak $\dot{v}_y$) of the vehicle at discretized points along the peak longitudinal acceleration at each speed increment.

$$\begin{aligned} \min_{\mathbf{u}} \quad & J = \pm\dot{v}_y \\ s.t. \quad & \dot{\mathbf{x}} - f(\mathbf{x}, \mathbf{u}, t) = 0 \end{aligned} \tag{2.3}$$

For symmetric vehicles, one side of the envelope is sufficient (i.e., $J = +\dot{v}_y$ only) to characterize the full envelope.

There are many works utilizing this method, and due to the relatively small computational burden, they are widely used to this day; especially for a large design of experiment studies. The remainder of this section will summarize many of the works that utilize this method. Dominy wrote a series of fascinating papers utilizing performance envelope methods to study general aerodynamic effects [32]. His later work even incorporated aerodynamic yaw effects derived from wind tunnel testing [33]. Aerodynamic effects on lap times were

also studied in [34]. Trade-offs of weight, power, and even hybrid powertrains were explored in [35]. In [36] multi-objective optimization was used to examine the tradeoff that different vehicle setup strategies had in a small and large radius corner. Kurt et al. used parallel computing and steady-state cornering simulations in [37] to examine the trade-offs between key vehicle parameters for two different radius turns via a multi-objective Pareto analysis. In 2000, Siegler compared a quasi-steady-state simulation method with steady-state methods (which treats longitudinal and lateral controls separately) and a full transient method on a short maneuver [38]. In this article, it was recommended to use a full transient solution because it takes into account factors that are not accounted via the other methods thus would allow greater tuning. These performance envelope methods were used by Kapania et al. to efficiently compute the optimal velocity profile of a fixed path in [39]. Also, [40] planned the optimal velocity profile considering three-dimensional road effects for an autonomous vehicle near the vehicle's performance limits. In [41] a simple quasi-steady-state lap time simulation tool was discussed that utilized a backward/forwards integration scheme and a simple friction ellipse constraint to optimize gear ratios of a racing vehicle from a discrete set of possibilities. Both optimization and exhaustive search of the discrete points were considered. Results of the vehicle simulations were compared to onboard vehicle data. These methods have been successfully used to study sensitivities of key vehicle parameters and evaluate different active technologies [42, 2]. Some tools using this simulation technique were even commercialized [43]. More recently, the work in [44] introduced a method for including transient effects into quasi-steady state solution methods via iteratively updating quasi-steady state solutions at a particular location on the track to obey a fully transient vehicle model. This alleviates the lack of ability to model transient vehicle effects that these solutions suffer from.

2.2 Path Following

The previous solution type provides a quick, computationally inexpensive solution to the minimum-time maneuvering problem that has shown to have good correlation with actual vehicle data with distinct overprediction of performance during heavy braking phases on a race track [30, 31]. However, this approach neglects the effect of the human driver altogether which has been shown to have a significant effect on this problem [45, 46]. Even very early work showed the importance of preview in human control. The work in [47] shows how very early experiments of "drivers" were used to correlate optimal tracking control models of drivers. In contrast to the performance envelope methods of the automotive industry, the aviation industry took a different path in the 1950's. Their approach was to study and model how pilots interact with aircraft. This early work was extended to the man-machine interface of the automobile as shown in [48] and one of the first driver models of note is the crossover model [49]. This model utilizes a simple experimentally derived transfer function to model a driver's control actions during regulation tasks such as negotiating a straight section of highway. While this type of driver model is inadequate for modeling minimum-time vehicle maneuvering problems, it is noteworthy because even modern optimal preview control techniques reduce to the crossover model for regulation tasks [50, 51]. While the complete history of driver modeling is out of the scope of this chapter, several good literature review papers exist that could be consulted [52, 53, 54]. Much of the work in minimum-time vehicle maneuvering is typically deeply rooted in MacAdam's optimal preview control work [55]. Again, this method assumes a fixed racing line to follow. Planning the path to be followed is discussed in Section 2.3. Despite this shortcoming, this method is extremely relevant and useful. It can be implemented with relatively low computational cost and can be fairly robust while including the important effects of transient vehicle behavior and a way to model the driver.

This method is the method typically used by commercial software (for example CarSim [56]). The driver model in Tesis Dynaware (Vedyna) is explained in [57]. In this

software they use a two-step approach where the initial racing line is planned a priori [58] and then tracked via the driver model. The racing line calculation includes the ability to modify the acceleration limits (g-g-v diagram) so that the model can be adjusted to model different levels of driver skills. They use a nonlinear controller to steer the vehicle model.

Many academic works utilize this solution method also. In [59], IPG's CarMaker was used to simulate lap time around two different tracks. A design of experiment was created using Taguchi's approach, and key suspension parameters were examined on their relative effects on the total performance. A series of papers from Velenis and Tsiotras gave a very formal framework for a solution of the velocity profile generation of a vehicle with a fixed friction envelope. In their first paper [60], the optimal velocity profile was derived for a particle motion model constrained to a fixed path with a fixed friction ellipse. They derived the adjoint system of equations and enforced first order necessary condition of optimality to achieve a solution. They looked at several cases of path primitives (i.e., constant radius, decreasing radius, and increasing radius turn) and were able to concatenate a series of solutions to achieve the optimal velocity profile for an arbitrary path. They then extended the work in this paper to include a bicycle model vehicle and a simple Pacejka tire model [61]. To mitigate stability issues, constraints were added at critical vehicle slip angles. Their work in [62] gave analytical solutions of the minimum-time problem for a vehicle bound by a friction ellipse on a prescribed path. In this work, they also proposed a receding horizon method for calculating the optimal velocity profile that could be implemented in an online control strategy. The work in [63] proposed a quadratic minimization approach to identify the driver input to best match the reference path and reference trajectory computed a priori using a performance envelope method. In [64], a reference trajectory was found using approaches discussed in Section 2.4 for a simple motorcycle model. Those trajectories were then tracked via Proportional Integral Derivative (PID) control on a higher fidelity vehicle model. In [65], Sharp used a linearized motorcycle model, LQR theory and an iterative approach to learn the ideal speed profile for a fixed path. This technique was applied to race cars in [66]. The work in [67] also considered controlling motorcycles and concentrated

on creating a nonlinear tracking control to follow the desired trajectory. They applied their controller to a high fidelity multi-body motorcycle model in ADAMS. In [68], lap simulation was conducted by using a linearized and discretized vehicle model. The time-varying parameters of the model captured the nonlinear vehicle effects and this model compared favorably to a high-fidelity ADAMS vehicle model. A reference simulation was used as the reference path to follow, and two control strategies were examined: predictive control and finite-time control strategies which showed reasonable results. The main contribution of this work is showing how a strictly linear system could be used in a highly nonlinear vehicle model with good results. Experimental results of a nonlinear tracking controller considering three-dimensional road effects were presented in [40] at Thunderhill Raceway. In [69], Dynamic Programming (DP) was utilized to solve for the optimal velocity profile of the vehicle given a fixed path and identify an optimal hybrid powertrain policy (split between an internal combustion engine and electric motors). Experimental data of autonomous vehicles using tracking controllers to achieve near limit handling performance have been demonstrated in [70] using their Audi test vehicle [16]. In this work, they concentrated on tracking a racing line modeled with a series of constant radius, straight, and clothoid connector segments which they have shown to be a suitable method for modeling and fitting a racing line [71, 72, 73]. Real-time control has been investigated in [74] where Nonlinear Model Predictive Control (NMPC) was used to track a predefined trajectory. In this work, they showed experimental results implemented on scale remote control vehicles where the autonomous algorithm was able to beat a human controller.

A significant contribution in this method came from Boyd et al. [75] where they applied the work in [76] to transform a fixed path time-optimal vehicle maneuvering problem to a convex optimization via a novel transformation. This convexification has implications for real-time critical control where computational cost is critical.

2.3 Path Planning

Both the performance envelop methods, and the two-step path planning/path following methods require a path to follow. There are several methods for identifying the racing line, and they can be broken into three broad categories, racing lines derived from onboard vehicle measurements, geometric optimization, and vehicle simulation. They will be discussed in the subsequent subsections.

2.3.1 Path Planning from Onboard Measurements

From onboard measurements, the racing line model can be determined one of two ways, either directly from the geometry of the measured path (GPS or estimated local coordinates x, y points, or from simple kinematic relationships of the vehicle measurements; i.e., $C = \dot{\psi}/v_x$. GPS measurements can directly be used to estimate the racing line [77], although, care must be taken when converting these measurements into paths used to follow as they contain noise, satellite dropouts, and other measurement issues that must be treated to achieve a reasonable model of the path to be followed. The work in [41] discusses reconstructing the path curvature from the x, y coordinates of the measured path after filtering. In [78, 72], a racing line was fit from measurement data by a series of straights constant radius curves, and clothoid segments. In [5], the racing line ($C(s)$) was fit using simple kinematic relationships of the measured vehicle states. In this work, an ad-hoc method of compensating integration errors at each integration step with a kinematic vehicle model is discussed resulting in a closed curve model of the racing line around a full race circuit. Rather than using the previous ad-hoc methods of correcting integration errors, the work in [23] uses a model of the track itself and a simple particle motion model to find the racing line that best matches onboard data while remaining within the track width boundaries.

2.3.2 Path Planning via Geometric Optimization

In several works, the racing line is derived from geometrical properties rather than based on measurement or simulation. The work in [63] derives two racing lines; one of minimum curvature and one of minimum distance. They manipulate control points of splines and constrain them such that they remain within the track boundaries. Then, they combine these two racing lines via a combination factor, ϵ. They use a performance envelop method to determine the optimized ϵ that minimized the vehicle maneuvering time. This approach operates on the theory that when selecting a racing line, the driver is balancing two objectives, going as fast as possible and traveling the shortest distance. The work in [79] extends [63] to racing video games and decomposes the track in to several segments where combination factor ϵ can be modified. Simulations show results for a large variety of tracks.

2.3.3 Path Planning via Simulation

Using the previously discussed performance envelope methods of lap simulation is another method of finding the racing line. The racing line can be modeled as a general curve via a set of basis functions such as splines or Bézier curves [80]. The parameterized curves can be manipulated from a set of control points. An optimization routine can manipulate these control points and then a performance envelope method provides a measure of lap time of the current iterate. The work presented in [81, 82] uses genetic algorithms to move spline control points at track waylines (lines perpendicular to the track) to optimize lap times. The control points can be constrained to remain within the track width boundaries. In [82], the optimal racing line at the Circuit de la Sarthe (Le Mans) was found and compared to measurements from onboard vehicle data. The work in [71] moves control points of a set of straight lines, clothoid segments, and constant radius turns to optimize lap times.

While these three classes capture the majority of the methods, a few others noteworthy works do not fit into these general classification. The work in [27] discusses how the "groove" (racing line) can be modeled with piecewise fifth order spiral functions. Other

methods are also discussed in the literature. In [83], a computationally inexpensive framework for finding a suitable racing line using a linearized vehicle model and quadratic programming is discussed. In [74], rapid exploration of random trees (RRT) was used as means of path planning. Finally, the results from the one step trajectory optimization (discussed later in Section 2.4) can be used as the racing line to be followed by these two step algorithms. This is explored in [84, 85, 15] for the application of providing a reference trajectories for real-time control.

2.4 Optimal Control

The final class of problems is the optimal control approach. Optimal control theory is used to find the vehicle control inputs (i.e. steering, brake, throttle, etc.) subject to constraints such as the vehicle dynamics and road boundary. For general background in optimal control theory, the reader is referred to [86, 87]. These problem can be posed in a general form such as:

$$\begin{aligned} \min_{\mathbf{u}} \quad & J = \int_{s_o}^{s_f} \tfrac{1}{\dot{s}} ds \\ s.t. \quad & \tfrac{d\mathbf{x}}{ds} - f(\mathbf{x}, \mathbf{u}, s) = 0 \\ & h(s, \mathbf{x}(s), \mathbf{u}(s)) \leq 0 \\ & g(s, \mathbf{x}(s), \mathbf{u}(s)) = 0 \\ & g_b(\mathbf{x}(s_0), \mathbf{x}(s_f), \mathbf{u}(s_o), \mathbf{u}(s_f)) = 0 \end{aligned} \tag{2.4}$$

where the vehicle dynamics are written as $f(\mathbf{x}, \mathbf{u}, s)$. In this case, the independent variable is distance traveled s. The general set of vehicle states are $\mathbf{x}$ and vehicle controls are $\mathbf{u}$. Inequality constraints are placed on the problem ($h(\cdot)$) and are typically used to constrain the vehicle to remain within the track width boundaries and limit the the longitudinal control to remain within the peak engine power. Equality constraints are modeled by $g(\cdot)$. Boundary conditions are denoted in $g_b(\cdot)$.

In this problem, the racing line is an outcome of the optimal control inputs to the

vehicle and is free to vary as necessary. This line of work began in the early 1990s [88] and [89] which may be considered the first significant formulation of these problems [90]. Shortly after Hendrix et al., Da Lio published a very similar work for motorcycles [91]. The work in [92] provides an excellent background on this topic.

The remainder of this section is organized as follows. First, solutions of optimal control problems are discussed in Section 2.4.1. Then, specific sub-problems and applications within minimum-time vehicle maneuvering are discussed in Section 2.4.2.

2.4.1 Solving The Optimal Control Problem

Once the optimal control problem is posed, there are several methods for solving these problems. The solutions are well reviewed in [3, 93]. Solutions of optimal control problems are classified into three categories: indirect methods, direct method, and dynamic programming. Indirect methods utilize calculus of variations to derive first-order necessary conditions of optimality. Direct methods discretize the optimal control problem and solve the discretized problem via nonlinear programming problem (NLP) techniques. Dynamic programming is rooted in solving the Hamilton-Jacobi-Bellman equation and is an attractive optimal control technique as it can yield a state feedback control law and it is guaranteed to be a globally optimal policy. However, It suffers from the curse of dimensionality and these problems quickly become intractable for all but the simplest vehicle models [94]. Despite the fact this solution method is not currently widely used (and will not be discussed further here), recent development in the field such as Differential Dynamic Programming looks promising as a way to alleviate some of the computational burden [95].

2.4.1.1 Indirect Methods

Indirect methods aim at deriving the first-order necessary conditions of optimality via application of Pontryagin's Minimum Principle. The problem resulting from these indirect methods is a Hamiltonian boundary value problem which in general is quite arduous to solve. Still, there are many works offering examples utilizing indirect methods [89, 91, 96].

They have also been applied to many sub-problems in this field: extensive study of differentials [97], gear ratios [98, 99], racing karts [100], varying model fidelity [101] and vehicle layouts [102].

While not strictly vehicular optimal control, a substantial piece of work was released in 2004, in the form of a software package, *MBSymbia*. This software provides the ability to generate symbolic equations of motion for multibody systems automatically. This software has been heavily utilized in recent works that use indirect methods. In [103], the software package is demonstrated by deriving the equations of motion for a motorcycle. An interesting feature of this work is the automatic ability to linearize the system which can then be used to perform classic control techniques as demonstrated in this work. In [96, 104] this technique was applied to minimum-time vehicle maneuvering. The result of these derivations is a two-point boundary value problem. They were able to solve this problem numerically, and the optimal solution was presented on a full race track (Adria circuit). In a later work, real-time control was addressed [105] (for other applications besides minimum-time vehicle maneuvering).

2.4.1.2 Direct Methods

The second class of solution methods is direct methods which aim at solving the posed optimal control problem instead of deriving the necessary conditions. This is generally done by transforming the optimal control problem into a Nonlinear Programming Problem (NLP) via discretization [106, 107]. This method has been used since the late 1990s to solve minimum-time vehicle maneuvering problems [108] and much of the modern work is rooted in [90]. Direct methods have been utilized to research many problems in minimum-time vehicle maneuvering. Sensitivity studies were examined in [109] and showed good correlation between practical observations to simulation.

Direct methods can generally be divided into two classes: methods that parameterize the control input only and methods that parameterize both the state and control input. They are typically referred to as shooting methods and collocation methods, respectively.

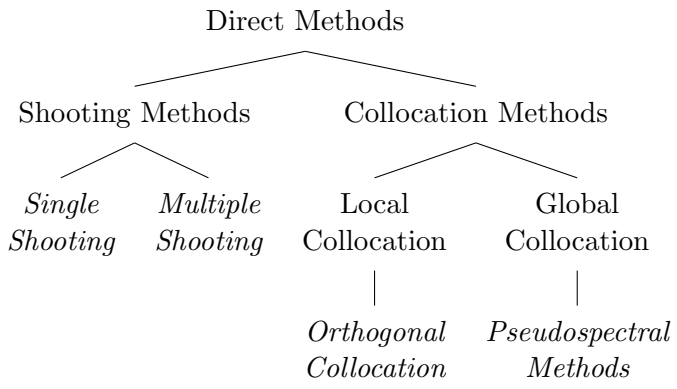

Figure 2.3: Classification of direct methods. Based on work in [3].

This classification can be seen in Figure 2.3. While the intricacies of all of the different methods are outside of the scope of this document, a brief overview is written for single shooting, multiple shooting, and collocation methods below. The reader is referred to one of the many excellent resources on this topic for the full details [3, 93, 107, 106, 4].

2.4.1.3 Shooting Methods

The *single shooting method* is the simplest place to begin. This method's name got its origins from shooting a projectile at a target. As the name implies, a cannon is aimed at a target and shot. The difference between the projectile and intended target is assessed, the cannon re-aimed, and the process is recursively repeated until the target is hit. In this method, the control input is parameterized across the solution space. This parameterization can be anything from a zero-order hold scheme which holds the current control value constant until the next discrete point, spline interpolation, or another basis function. The user provides an initial guess of the discretized set of control points, and the process begins. The system dynamics are then integrated given the control signal. Next, a sensitivity of the cost function with respect to each discrete control point is established. These gradients are used to construct the search direction. A step is taken along the identified search direction to reduce the cost of the optimization. The new control inputs are then retested, and the process continues until a local optimum is found. Unfortunately,

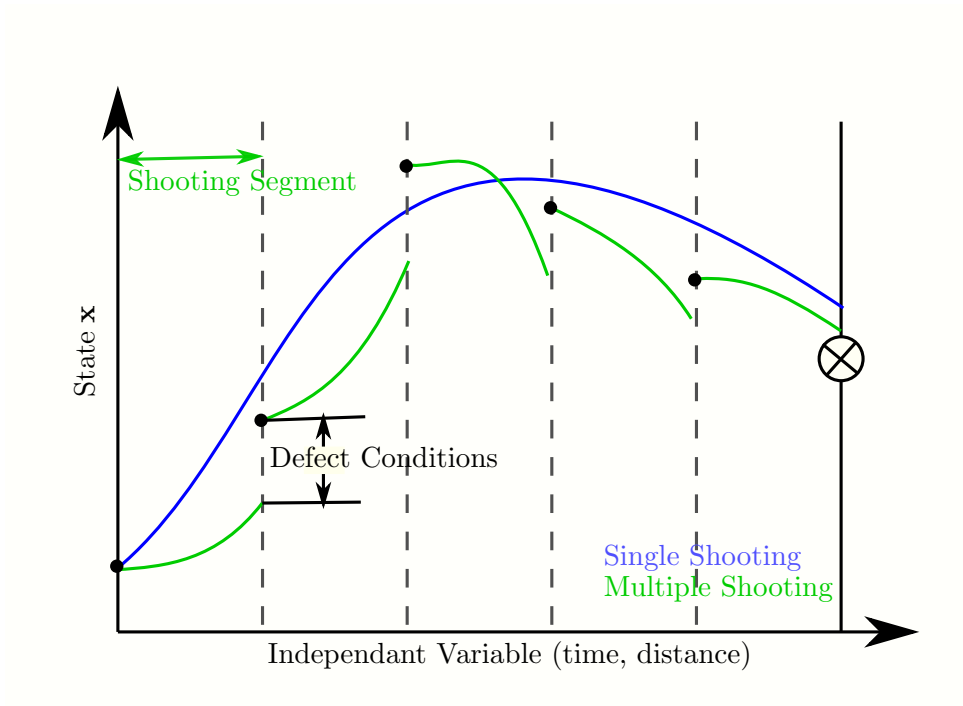

Figure 2.4: Illustration of single versus multiple shooting methods. Based on the work in [4].

this method is highly sensitive to the initial guess as the guess is propagated through the entire system dynamics. Issues like numerical stability make this method difficult to achieve robust solutions. The user must be fairly close to the solution to ensure convergence.

Multiple shooting methods aim to address the problems of single shooting methods. The solution space is divided into multiple single shooting segments. At the interface between segments defect equality constraints are introduced to constrain the solution to be continuous across the segments. While these methods introduce additional constraints in the optimization, they generate sparse NLP problems that are computationally easier to work with. They are also much less sensitive to the initial guess than single shooting method, and many successful optimal control codes use this method for solving the optimal control problem. One such example is ACADO [110]. Figure 2.4 illustrates both single shooting and multiple shooting methods.

2.4.1.4 Collocation Methods

In these methods, both the state and control inputs are described by a set of basis functions, and the solution is constrained to satisfy the dynamic constraints only at collocation points in the trajectory. Depending on the parameterization procedure and type of collocation used, these solutions are further subdivided into several methods, and the reader is referred to [3, 4] for the full details. A common parameterization is to use Lagrange polynomials to globally parameterize the solutions space (this parameterization is classified as a *pseudospectral* or a *global orthogonal collocation* method). This is the method employed by the solver GPOPS-II which is used extensively throughout this dissertation [111].

2.4.1.5 Comparison of the Two Methods

There is a discussion on which method is more suited to this problem [92]; however, both methods have yielded excellent results [112, 95]. Moreover, the work in [113] shows that the Lagrange multipliers used in direct methods are discrete approximations of the co-state variables found in the indirect methods and with either method, numerical methods are required (for all but very simple systems) to solve the problem.

2.4.2 Specific Sub-Problems

The subsequent subsection will be divided into different subproblems and application areas for these optimal control solution.

2.4.2.1 Early Solutions

As previously discussed, this method has been applied since the 1990's. In [88], a transient vehicle model was used to minimize maneuvering time for a hairpin turn. The boundary conditions were chosen such that additional constraints were not necessary to keep the vehicle on the track. The work presented in [89] can be considered the first significant formulation of the optimal approach to solving minimum-time problems. In this paper, they solved the problem for simple short maneuvers utilizing optimal control theory and

Pontryagin's Minimum Principle. In [114], a simple linearized vehicle dynamic model and a quasi-Newton penalty method was used to solve for the optimal trajectories.

A very extensive set of papers from authors Lot, Da Lio, et al. was presented in literature dating back to the mid-1990's where they were at the forefront of this work. In [91], it is claimed that Da Lio independently and nearly simultaneously to [89] formulated the optimal control approach for motorcycle handling [115, 116]. In [91] they concentrated on utilizing indirect methods to solve the problem for motorcycles. Rather than minimizing time, the distance over a fixed time was maximized. The boundary constraints of the vehicle were placed into the cost function via penalty functions. The underlying two-point boundary value problem was numerically solved in this work. Good correlation between data on a section of the Mugello racing circuit in Italy and the optimal control solution was shown.

Sharp et al. has also produced a series of important works starting in the late 1990's that help lay the foundation for modern minimum-time vehicle maneuvering problem. Allen's master's thesis [108] shows how Sequential Quadratic Programming (SQP) could be used to solve for the optimal vehicle inputs subject to vehicle dynamics and road constraints for a short maneuver. Casanova in his dissertation [5] later extended these solutions to a full track.

In addition to the previously mentioned works, Siegler et al. also worked on some of the early publications. In [38], they compared and contrasted these optimal control solutions to performance envelope methods. They later refine their trajectory optimization on a short segment and showed a correlation to experimental data [117, 118].

2.4.2.2 Extending Solutions Over Short Segment To Arbitrarily Long Track

Solving an arbitrarily long track is significantly more difficult than a short segment, and many works looked at ways to extend short segment solutions to arbitrarily long tracks. Casanova utilized a multiple shooting algorithm to facilitate the solution of an entire race track [5]. In this work, he used automatic differentiation to speed up computations [119].

Kelly took the research in a different direction and used a receding horizon approach to extend a short segment solution to an arbitrarily long track [120, 45]. This work had the added focus of dealing with a black-box vehicle model. Therefore, he relied on finite-differencing techniques to obtain derivative information and a Feasible Sequential Quadratic Programming (FSQP) optimization algorithm [121] to guide solvers away from exploring non-feasible regions of the solution space.

Today, state-of-the-art solvers have been able to realize optimal control solutions of minimum-time vehicle maneuvering over a full track [20].

2.4.2.3 Modeling Human Drivers

At the heart of this work is modeling the human element of driving. There have been several works that concentrate on modeling this in various ways. While not strictly minimum-time maneuvering, [122] showed how different driving styles (comfort-oriented driving, aggressive driving, etc.) could be modeled via different cost functions in an MPC framework. The work in [120] considered the control grid spacing (in direct methods) as analogous to the human driver control bandwidth and studied its effect on maneuvering time. The work presented in [123, 124], aimed to recreate specific advanced driver maneuvers such as trail-braking via modifying the optimal control formulation. A robust, tube-based MPC was also explored in [46] to model drivers in the presence of disturbances.

2.4.2.4 Vehicle Optimization

A typical goal after modeling a driver is optimizing the closed-loop system. Several works used these optimal control techniques to analyze and optimize vehicle setup. In [90], a four-wheel vehicle model with a differential and a simple aerodynamic model was used to solve the minimum-time vehicle maneuvering problem for a double lane change maneuver. This was solved via direct methods and an SQP solver. This solution was used to evaluate the effect of yaw inertia on maneuvering time. In [109], the sensitivity of maneuvering time to vehicle mass was explored, and the optimal location of the vehicle center of gravity was

explored in [125].

The work in [20] presented a very compact and efficient vehicle model (three degrees of freedom for the sprung mass motion and treated loads, slip ratios, and steering as inputs to the system). In this work, extensive modeling of the situation where a tire loses contact with the ground was treated. Track modeling using optimal control and GPS data on the Barcelona Formula One circuit was discussed. They then were able to include vehicle setup parameters in the optimal control formulation and solve for them simultaneously with the state and control trajectories. They optimized the following vehicle parameters: center of gravity location, aerodynamic center of pressure, roll stiffness distribution, and differential constant. In this work, they relied on direct methods implemented in the ILOCS software package [126]. A stability analysis with respect to the longitudinal aerodynamic center of pressure was also presented. The work in [97] extensively explores optimizing differentials for minimum-time maneuvering situations. They use an indirect method to solve optimal control problem for a double lane change and investigate the ideal coupling between drive tires on a rear wheel vehicle. The trade-offs between lap time, tire wear, and controllability are also discussed.

2.4.2.5 Powertrains

Both direct and indirect methods were used to solve for the optimal control on a full course of vehicles equipped with hybrid powertrains [127] (indirect) and [128] (direct). In [128], energy recovery system on modern Formula One race cars were modeled. In this work, they also considered variable aerodynamic properties that were functions of longitudinal velocity in the formulation. This work uitalized the GPOPS-II software [111] which implements an adaptive direct collocation method of solving the optimal control problem. This work [128] was also presented in [93] along with a fantastic review of numerical methods for solving optimal control problems.

While not minimum-time maneuvering, [129, 130] offers a fascinating paper looking at minimum fuel, just-in-time optimal control problems of a hybrid race car. They showed

the importance of three-dimensional road features in the control strategy when studying a circuit with significant elevation features. This work stands out also as it gives a very practical insight into formulating the numerical solution to the optimal control problem including how they arrive at the initial guess.

In both works [131, 132] torque vectoring was explored by using an optimal control formulation. A causal torque vectoring strategy is explored an compared to the 'ideal' optimal control trajectory through the maneuver.

2.4.2.6 Modeling the Dynamics

In [133] reduction in the computational effort was researched by using a linearized vehicle model with an MPC approach. Berntrop et al. explored different vehicle and tire modeling techniques and compared and contrasted solutions in [134, 135, 136]. In [136], a single track, double track, and double track with load transfer were modeled for a 90° and a double lane change. In [101], a compelling argument is made for including higher order vehicle dynamic effects in lap time simulations. Specifically neglecting suspension dynamics can lead to different conclusions of primary vehicle parameters such as weight distribution. The work in [137] showed how a projection operator based Newton method could be applied to generate computationally efficient solutions to these types of problems. The analogy between the iteration steps and the human learning process was made in this work. A rigid body vehicle model was solved and lap time results compared favorably to results generated using the commercial software: VI-CarRealTime. In [138, 19, 139], Maniowski uses a piecewise linear approximation of the driver control inputs to drive a high fidelity vehicle model. He then uses a genetic algorithm to optimize the driver inputs and vehicle parameters for a simple maneuver. He also uses a multi-objective optimization to explore the Pareto-optimal solutions of minimizing time over the short maneuver and maximizing exit velocity.

Suspension effects were modeled and incorporated into the vehicle simulation as described in [140, 130]. In, [141] a very detailed vehicle model with suspension dynamics

was considered to show that a quasi-static tire load assumption is not the best. They delivered an excellent simulation to measurement correlation on a qualifying lap of a GP2 race car.

Three-dimensional track modeling was discussed in [142] and optimal control lap time simulation on these 3D tracks was presented in [143]. Much of this is discussed further in [144]. The work in [145] also considered three-dimensional track effects for optimizing a motorcycle's maneuvering time.

2.4.2.7 Thermal Tires

The thermal properties of tires have a significant effect on vehicle performance during these high-performance maneuvers. The work in [146] provides a great review of material physics that cause this phenomenon. In [147, 45], Kelly derives a thermally sensitive tire model and incorporates it into the lap time simulation. He provides insight on the effect of a tire's thermal state on lap times. Recently the work in [19] used a high fidelity vehicle model coupled with a thermally sensitive tire model. The tire model appropriately modified the global friction of a Pacejka tire model as a function of operating temperature. Tire temperature was calculated using a one-dimensional heat transfer equation accounting for heat generation due to slip as well as heat transfer to the environment. Driver controls were discretized and optimized using genetic algorithms. For this short segment, a Pareto analysis was carried out to examine the tradeoff between optimizing maneuvering time and exit velocity (which is sometimes advantageous over a short track when entering a long straight section after a corner) for a variety of tire conditions. Measurements were presented showing good correlation with the simulation. In [148] the interaction between tire wear and driving was studied. In this work, a thermally sensitive tire model was derived, and three scenarios were optimized. First, a tire warming strategy was developed which even showed the common practice of a driver weaving on a long straight to keep the tires up to temperature. Second, a tire saving strategy was examined where maximum tire wear limits were imposed on the lap optimization yielding slightly slower lap time while obeying

the wear constraints. Finally, the effect of vehicle set-up on tire wear was also studied by looking at several cases of differentials.

2.4.2.8 Real-Time Control

Verschureren et al. put out a series of papers working on real-time NMPC time-optimal control and this was even applied to scale remote control vehicles [149]. The real-time NMPC algorithm [110] required a least squares cost function form, and in this work, the cost was adjusted such that the least squares cost mimicked a true time optimal cost. This was implemented experimentally on a scale race track. In a later paper, [150], an alternate algorithm, the exact Hessian-based approach, was utilized for solving the NMPC problem. The results were compared to a true OPC solution obtained off-line with cyclic boundary constraints. In this paper, true real-time optimal control was realized. The authors cite the deteriorated performance (MPC solution compared to the OPC) due to the constraint of a fixed preview horizon.

2.4.2.9 Powertrain Gearing

Insight into vehicle setup, specifically gear choices, was shown in [98] using an optimal control framework. In this work, the authors performed an analysis of the traction potential of the vehicle and examined the room for improvement with respect to gear choice. Lap time improvement was shown with the updated gearing, and it was also shown that the "optimal" driver would change the control inputs in response to a different gearing choice. Colsalter et al. continued their work in the area of optimizing motorcycles for minimum-time maneuvering. In [99], they added an optimization routine to the algorithm to select the optimal gearing for a particular race circuit.

Optimal control approaches for solving problems of this type are extremely interesting and challenging because of the mixed-integer states that gears involved in the solutions. The work in [151] uses a branch and bound technique to deal with the integer constraints, and a direct method was used to solve the optimal control problem. The work presented

in [152] furthered the previous by looking at alternative solution techniques that take advantage of the natural bang-bang control found in optimal control problems to relax the integer constraints and find an optimal set of gear shifts on an elliptical track with a simple nonlinear bicycle model. The work in [153] solves this problem with direct multiple shooting techniques implemented in the MUSCOD-II software packaged [154] and compared to alternative solution techniques presented in [152].

2.4.2.10 Alternate Vehicle Types

Several works in literature have used these methods for optimizing motorcycles for minimum-time vehicle maneuvering some examples are [91, 103, 155] where the center of gravity location was optimized and [99] where optimal gearing was discussed. The work in [145] looked at time-optimal control of motorcycle dynamics with a hybrid powertrain and three-dimensional road for the annual Isle of Man TT Zero Challenge. In this work, they were able to show excellent computational efficiencies with indirect methods implemented in their solver described in [96]. In addition to motorcycles, racing karts were discussed in [100].

2.4.2.11 Large slip angle maneuvers

This subproblem of the vehicle minimum-time maneuvering has been studied by many authors. The work in [156] derived an unstable equilibrium point at high vehicle slip angles. This is a common maneuver in 'drifting' competitions where drivers control vehicles in very large sideslip conditions for extended periods of time. In [156], they were also able to experimentally demonstrate a vehicle tracking this equilibrium point using a controller. The work in [102] provides a fascinating look into the relationship between the minimum-time problems and driving at large vehicle slip angles. Here, several vehicle configurations were explored on several road surfaces (via modified tire characteristics). For the cases of off-road coupled with rear wheel and all wheel drive, large vehicle slip angles were observed when solving the minimum-time problem. In this paper, a single-track vehicle

model was utilized with a Pacejka tire model coupled with lags on the force response of the tire. In another publication [157], they used a similar vehicle model to specifically analyze a cornering technique where the driver will apply a handbrake (acting on the rear wheels only) in order to saturate the rear tires and increase the yaw velocity of the vehicle. To facilitate this, the controls were augmented to include a term for the application of the handbrake. Also, the optimal control cost function was augmented to include a time minimization as a means to drive the car to the inside of the track. They showed excellent correlation to experimental results of a professional driver performing this maneuver on an off-road course. Moreover, they also showed that increasing the friction characteristics to that similar to dry pavement did not affect the ability to reproduce the handbrake maneuver (with this mixed cost function) and concluded that this driving technique is more a function of road geometry than vehicle dynamics. The work in [158] showed how vehicle setup parameters could be optimized for maximizing vehicle slip angles for 'drift' competitions.

2.5 Machine Learning Methods

In the mid 90's MacAdam showed how neural networks could be applied to modeling driver behavior (albeit, this was not minimum-time driving) [159]. In this work, he showed how a simple neural network could be effectively trained and give good results compared to experimental validation data of drivers driving in a virtual environment. Casanova makes the connection in his work, between his control structure and neural networks operating in the same manner to model driving behavior [51]. Some works have applied these techniques to limit handling maneuvers. For instance, [160] uses an online racing simulator as a test bed and trains neural networks based on human driving telemetry. The goal is a controller that was capable of mimicking a human driver. Although there were cited issues such as the case when a driver enters into an unstable regime, a real driver can enter a recovery period; however, the neural network struggles. They propose that this strengthens the hypothesis that a real driver has a control hierarchy and different operating levels. The gaming industry

has put out a good number of works that use these methods. A good number of these are based around an online race car game, TORCS (The Open Racing Car Simulator) [161], and developing controllers to compete for the best lap times. The work in [162] is another example of applying neural networks to control the vehicles.

2.6 Conclusions

In this chapter, four classifications of solutions to the minimum-time vehicle maneuvering problem were detailed. These included performance envelope methods which used a quasi-steady-state assumption to find a series of steady-state conditions that optimizes lap time. Next, the two-step method of following a fixed racing line in minimum time was discussed. As the previous two methods needed a racing line to follow, methods for path planning were also detailed. Optimal control solutions as will be used in the remainder of this dissertation were then detailed. Their main contribution is removing the assumption that the racing line is fixed. In this section, methods for solving the optimal control problem were discussed, and application areas of these solution methods were detailed. Finally, machine learning techniques were also discussed as a means of solving the minimum-time vehicle maneuvering problem.

Chapter 3

Modeling Minimum-Time Maneuvering with Global Optimization of Local Receding Horizon Control

Abstract

In this chapter[1], we explore the notion that a human driver uses a receding horizon model predictive control (MPC) scheme for minimum-time maneuvering. However, MPC is an inherently sub-optimal control scheme because not all future information is incorporated into its finite preview horizon. In many practical applications, this sub-optimality is tolerated as the solution is sufficiently close to optimal. However, it is known that professional

[1]This chapter is compiled from:
J. R. Anderson and B. Ayalew. Modelling minimum-time manoeuvering wit a global optimisation of local receding horizon control. Vehicle System Dynamics, pages 1-24, 2018.
J. R. Anderson and B. Ayalew. Global optimization of local weights in mixed-cost MPC for minimum time vehicle maneuvering. In 2017 IEEE Conference on Control Technology and Applications (CCTA), pages 560-565, Kohala Coast, Hawaii, USA, August 2017. IEEE.

drivers have the ability to learn driving circuits and exploit their features to minimize their global maneuvering time. In this chapter, we will model their process with a cascaded optimization structure. Therein, the inner-loop features a local MPC scheme tasked with finding the control inputs that achieve a blended objective of minimizing time and maximizing velocity in each preview horizon/distance. The outer-loop of this cascaded structure computes the best set of weights for the two components of the local objectives in order to minimize the global maneuvering time. The proposed cascaded optimization and control approach is compared against a straight-forward fixed-cost time optimal MPC applied to minimum-time maneuvering over two well-known race courses. The chapter also includes an extended literature review and details of the computational formulation of the model approach.

3.1 Introduction

Minimum-time vehicle maneuvering is an important sub-set of studies in vehicle dynamics and has a very direct influence on the motorsports industry [1]. It also influences other aspects of the automotive sector especially for modern high performance automobiles. Moreover, knowledge gained here indirectly affects a much larger aspect of vehicle design such as safety and driver assistance systems. The modeling and understanding of how high-performance human drivers manage to operate efficiently despite the very nonlinear dynamics involved in minimum-time maneuvers can provide useful insights for future implementations of autonomous vehicle controllers as well.

This chapter presents a cascaded optimization structure which is intended to model a professional driver learning a new driving circuit to minimize maneuvering time. The inner loop of this structure features a blended cost receding horizon model predictive control (MPC) that is capable of weighting different objectives in each horizon. MPC is chosen as the control strategy for the inner loop based on the some recent justifications for how it closely represents human-driver actions. Casanova [5] makes the case that a human driver

behaves more like a MPC (in a moving horizon manner) than an optimal controller acting on the full maneuver. He states, if a driver were indeed a true optimal controller acting over the entire circuit then, he or she will choose his initial control inputs on the start line based on how he or she intends on crossing the finish line. Since a driver is clearly not using the full racing circuit to that extent in order make control decisions, a different mechanism must be in place. Moreover, it was stated in [92], 'there comes a point where the track ahead has diminishing importance for control decisions affecting the present time.' In other words, a human is not considering the full circuit when making local control decisions but rather utilizing a preview horizon. While we conjecture that a human driver behaves more like MPC than optimal control, we also know that a human can learn new race tracks to best exploit their features and minimize the global maneuvering time. In order to accomplish modeling of this learning, we expand the local MPC cost function to have two objectives: minimizing time and maximizing velocity at the end of the horizon. These two objectives were motivated by literature where [19] states, it can be advantageous in a short segment to drive with one or the other objective (minimizing time or maximizing velocity) depending on the future track configuration. For example, on a track with a curve followed by a long straight section, it can sometime be advantageous to the global maneuvering time to take more time in the current curve and maximize velocity of corner exit to achieve more speed through the following straight section. The outer loop in our algorithm does just that. It acts on the full track to find the best set of weights that trade-off the two objectives on each MPC horizon for minimal global time. In this direction, our previous work [163] has shown advantages for a hybrid (switching) cost function using a very simple vehicle model and a short section of track. However, the discontinuous switching may be unrealistic. The present work incorporates the ability to more naturally and smoothly blend two local objectives, a more detailed vehicle dynamics model, and much longer driving circuits.

In addition to more closely representing a human driver, MPC has another key computational benefit: the initial guess. Nonlinear optimization in general relies on an initial guess as a starting point to begin searching. The initial guess of the solution is

paramount to performance of the computational framework. If this initial guess is too far from the actual solution, the optimization could become computationally very expensive, or worse, fail to converge. With MPC, the only initial guess required is that of the first preview horizon and not the full maneuver as each subsequent horizon can be seeded with the initial guess of the solution to the previous. Therefore, if the first segment is in a location where we know what the driver is doing, for instance, a long straightway where full throttle is applied, then the initial guess should be sufficiently close to the solution in that horizon. This is much easier than guessing a good solution around a full track. The work in [120] originally used this feature of MPC to extend solutions over a short segment to an arbitrarily long track.

In summary, in this chapter, we formulate and detail a cascaded optimization scheme of local MPC costs to represent a human learning how to drive a new driving circuit to globally minimize maneuvering time. We will discuss how this cascaded control structure compares with the traditional fixed-cost time-optimal MPC applied around the track. The rest of the chapter is organized as follows. Section 3.2 details the vehicle model used and cascaded optimization framework. Section 3.3 presents results on a full race track while section 3.4 offers conclusions and an outlook on our future work.

3.2 Mathematical Framework

This section will detail both the vehicle model used for this work and the cascaded optimization structure. The vehicle model consists of a four wheel vehicle model including effects of load transfer, nonlinear tires, aerodynamics, and a differential. The vehicle model will be presented in section 3.2.1. The cascaded optimization structure consists of an inner loop MPC controller which drives the vehicle around the track while minimizing its local cost function while the outer loop finds the best cost function for each horizon. This will be further detailed in section 3.2.2. Finally, we briefly describe a time-optimal MPC controller in section 3.2.3 to compare the cascaded optimization to.

3.2.1 Vehicle Model

This work utilizes a four wheel vehicle model. The sprung mass has three degrees for longitudinal velocity (v_x), lateral velocity (v_y), and rotation about the yaw axis ($\dot{\psi}$). The wheel dynamics are modeled with four individual differential equations. The following subscripts are used to denote wheel position: $(\cdot)_p$ where $p \in \{fl, fr, rl, rr\}$ denotes front left, front right, rear left, rear right wheel position respectively. Much of the vehicle modeling is similar to those used in previous works [45, 20, 97]:

$$\dot{v_x} = v_y\dot{\psi} + \frac{F_x}{m} \tag{3.1}$$

$$\dot{v_y} = -v_x\dot{\psi} + \frac{F_y}{m} \tag{3.2}$$

$$\begin{aligned} I_{zz}\ddot{\psi} = a(\cos(\delta)(F_{y_{fr}} + F_{y_{fl}}) + \sin(\delta)(F_{xfr} + F_{xfl}))+ \\ w_f(F_{y_{fr}}\sin(\delta) - F_{xfr}\cos(\delta))+ \\ w_f(F_{xfl}\cos(\delta) - F_{y_{fl}}\sin(\delta))+ \\ w_rF_{xrl} - b(F_{y_{rr}} + F_{y_{rl}}) - w_rF_{xrr} \end{aligned} \tag{3.3}$$

where F_x and F_y denote the total lateral and longitudinal forces acting at the Center of Gravity (Cg):

$$\begin{aligned} F_x = \cos(\delta)(F_{xfl} + F_{xfr}) - \sin(\delta)(F_{y_{fl}} + F_{y_{fr}}) \\ +F_{xrl} + F_{xrr} + Fax \\ F_y = \cos(\delta)(F_{y_{fl}} + F_{y_{fr}}) + \sin(\delta)(F_{xfl} + F_{xfr}) \\ +F_{y_{rl}} + F_{y_{rr}} \end{aligned} \tag{3.4}$$

and the individual tire lateral and longitudinal forces are denoted by F_{xp} and F_{y_p}. The distance from the Cg to front and rear axle are a and b respectively, half the front and rear track width are w_f and w_r, and the front steering angle is δ as seen in Figure 3.1. Aerodynamic drag is F_{ax} and discussed below.

The remaining four degrees of freedom are comprised of the individual wheel dy-

namics.

$$\dot{\omega_{fl}} = \frac{(-T_{fl} + R_f F_{xfl})}{Jr_f} \tag{3.5}$$

$$\dot{\omega_{fr}} = \frac{(-T_{fr} + R_f F_{xfr})}{Jr_f} \tag{3.6}$$

$$\dot{\omega_{rl}} = \frac{(-T_{rl} + R_r F_{xrl})}{Jr_r} \tag{3.7}$$

$$\dot{\omega_{rr}} = \frac{(-T_{rr} + R_r F_{xrr})}{Jr_r} \tag{3.8}$$

3.2.1.1 Vehicle Controls

The lateral and longitudinal dynamics are controlled through inputs: u_1, u_2 which is the steering rate and torque demand rate on the chassis. This allows for a convenient mechanism of placing state constraints representing the human bandwidth of control and vehicle limitations. The steering angle and torque demand quantities satisfy:

$$\dot{\delta} = u_1 \tag{3.9}$$

$$\dot{T} = u_2 \tag{3.10}$$

The vehicle is assumed to have only front wheel steering. In other words, $\delta_{fl} = \delta_{fr} = \delta$ and $\delta_{rl} = \delta_{rr} = 0$. The torque allocation between the four wheels is modeled based on the work in [164] and depends on whether or not the vehicle is braking or accelerating. While driving, this vehicle is rear-wheel drive only; however, under braking, the brake forces are distributed among all four wheels. Because of this, the torque allocation (T) is separated into positive components: T^+, T^-. For our purposes, the following separation method was used.

$$T^+ = \frac{1}{2} + \frac{1}{2}\sin(\arctan(100 \cdot T)) \tag{3.11}$$

$$T^- = \frac{1}{2} - \frac{1}{2}\sin(\arctan(100 \cdot T)) \tag{3.12}$$

When it is known whether the vehicle is braking or driving, the torque distribution (k_t) can be determined via:

$$k_t = T^+ kt_{driving} + T^- kt_{braking} \tag{3.13}$$

where the parameters $kt_{driving}$,$kt_{braking}$ are fixed vehicle parameters. Finally, the wheel torques can be found:

$$T_{fl} = \frac{1 - k_t}{2} T \tag{3.14}$$

$$T_{fr} = \frac{1 - k_t}{2} T \tag{3.15}$$

$$T_{rl} = \frac{k_t}{2} T + k_d \Delta_\omega \tag{3.16}$$

$$T_{rr} = \frac{k_t}{2} T - k_d \Delta_\omega \tag{3.17}$$

where k_d is the viscous differential constant and Δ_ω is difference in rear wheel speed; i.e., $\Delta_\omega = \omega_{rl} - \omega_{rr}$.

3.2.1.2 Aerodynamics

A simple aerodynamic model is used to capture the speed dependent down force (F_{az}) and drag (F_{ax}) quantities acting on the vehicle. These forces are applied to the vehicle center of pressure shown in Figure 3.1. Other aerodynamic affects such as yaw and pitch coupling are neglected for the purposes of this work. The aerodynamic forces are described by:

$$F_{az} = \frac{1}{2} C_L \rho A v_x^2 \tag{3.18}$$

$$F_{ax} = \frac{1}{2} C_D \rho A v_x^2 \tag{3.19}$$

The constants C_L, and C_D are the downforce and drag coefficients, respectively. The vehicle's frontal area is denoted with A and the air density is denoted with ρ.

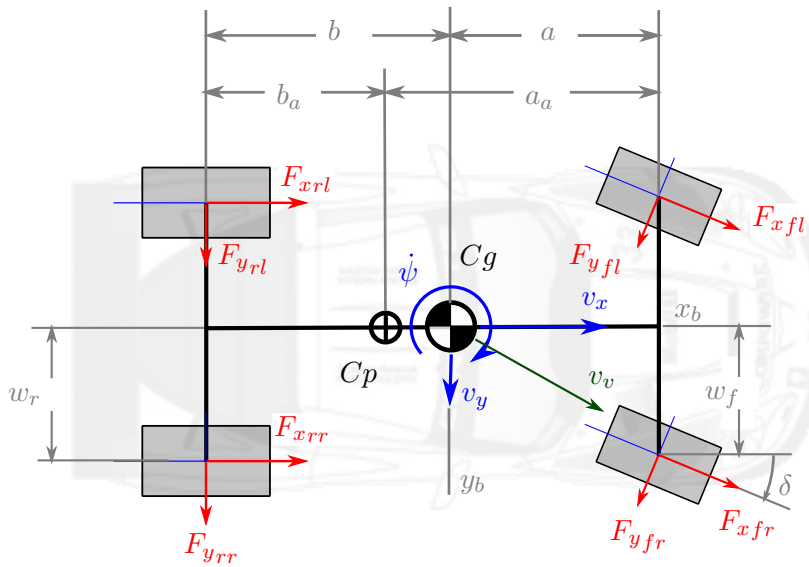

Figure 3.1: Vehicle top view. Note: body-fixed coordinates x_b and y_b are located vertically at the ground plane.

3.2.1.3 Load Transfer

The normal tire load is calculated by summing the forces and moments about the body fixed-coordinates seen in Figure 3.1 and enforcing a roll stiffness distribution $D \in [0, 1]$ such that the front axle load transfer is a fixed proportion of the total load transfer. This yields the following linear system to be solved:

$$\begin{bmatrix} 1 & 1 & 1 & 1 \\ -w_f & w_f & -w_r & w_r \\ -a & -a & b & b \\ D-1 & 1-D & D & -D \end{bmatrix} \begin{bmatrix} Fz_{fl} \\ Fz_{rl} \\ Fz_{rl} \\ Fz_{rr} \end{bmatrix} = \begin{bmatrix} -mg - F_{az} \\ -hF_y \\ (a_a - a)F_{az} + hF_x \\ 0 \end{bmatrix} \tag{3.20}$$

3.2.1.4 Tires

The tire's friction forces are calculated via an empirical formula that responds to changes in loads, lateral slip angle, and longitudinal slip. It is based on the simplified Pacejka

tire model presented in [45, 20]. The slip ratio (κ) and slip angle (α) are calculated:

$$\kappa = -\left(1 + \frac{R\omega}{v_{xtire}}\right) \tag{3.21}$$

and,

$$\alpha = -\arctan\left(\frac{v_{ytire}}{v_{xtire}}\right) \tag{3.22}$$

where R is the effective rolling radius of the tire and v_{xtire}, v_{ytire} are the longitudinal and lateral velocities of the tire accounting for vehicle rotation. A detail description of the adopted tire model can be found in Appendix B.

3.2.1.5 Path Intrinsic Coordinate System

In order to facilitate a convenient mechanism for constraining the vehicle to stay within the track bounds, path intrinsic coordinates will be used. This coordinate system models the vehicle trajectory with respect to the road centerline. It is depicted in Figure 3.2. The heading angle deviation (e_ψ) represents the difference between the path heading and the vehicle heading angle while the lateral deviation (e_y) refers to the vehicle lateral deviation from the path centerline. The vehicle speed in the path reference frame is denoted as $\dot{s}$. The quantities $\dot{s}$, e_ψ, and e_y are calculated as follows:

$$\dot{s} = \frac{v_x \cos(e_\psi) - v_y \sin(e_\psi)}{1 - e_y C} \tag{3.23}$$

where C is the path curvature and a known function of path distance i.e., $C = C(s)$.

$$\dot{e}_\psi = \dot{\psi} - C\dot{s} \tag{3.24}$$

$$\dot{e}_y = v_x \sin(e_\psi) + v_y \cos(e_\psi) \tag{3.25}$$

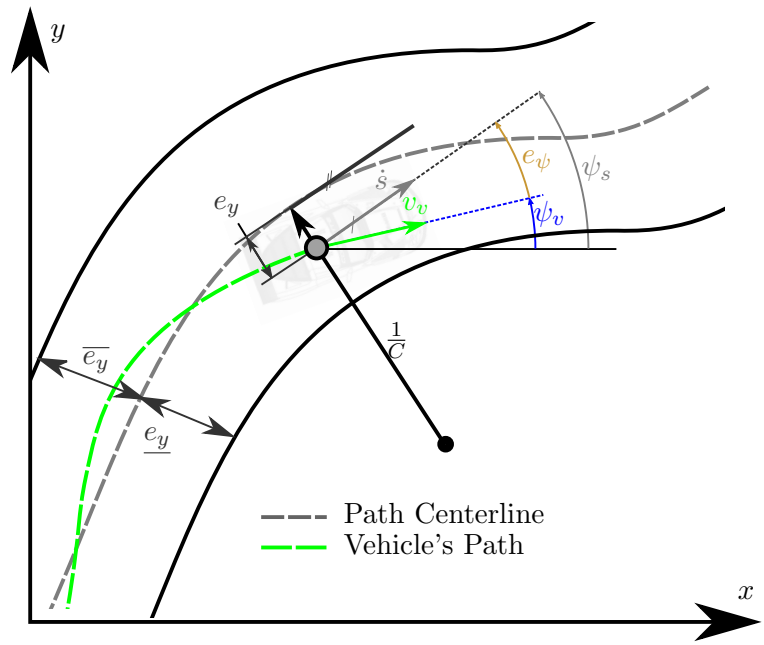

Figure 3.2: Path intrinsic coordinate description. Note subscripts s and v refer to the path and vehicle frame respectively.

3.2.1.6 Distance Based Description

The full system description can now be written as:

$$\dot{\mathbf{x}} = f(\mathbf{x}, \mathbf{u}, t) \tag{3.26}$$

where,

$$\mathbf{x} = \begin{bmatrix} e_\psi & e_y & v_x & v_y & \dot{\psi} & \omega_p & \delta & T \end{bmatrix}^T \tag{3.27}$$

The last step is to convert the independent variable from time to space. This is done to eliminate the free final time boundary condition that arises if the system is posed in the time domain. Once converted, the final distance is fixed; thus, the free final boundary condition is eliminated. This transformation is achieved via application of the chain rule of

differentiation to the system dynamics in: (3.26).

$$\frac{d\mathbf{x}}{dt}\frac{dt}{ds} = \frac{d\mathbf{x}}{ds} = \frac{\dot{\mathbf{x}}}{\dot{s}} \tag{3.28}$$

3.2.2 Cascaded Optimization

In this section, the proposed cascaded optimization approach will be detailed. This optimization structure is comprised of a lower level controller which utilizes a variable cost MPC to drive the vehicle around the track while minimizing the cost function at each MPC preview horizon. The variable cost allows the controller in a local horizon to blend two different objectives: minimizing time or maximizing exit velocity at the end of the horizon.

3.2.2.1 Inner Loop MPC

This loop is responsible for solving the optimal set of vehicle controls u_1 and u_2 over the prescribed maneuver while minimizing a cost function in each preview horizon. This Model Predictive Control (MPC) strategy utilizes a moving horizon where a portion of the track is previewed and an optimal control problem is solved over this portion. The horizon then moves forward and the process repeats around the track. Within in each horizon the optimal control problem can be posed as:

$$\begin{aligned} \min_{u} \quad & J(x, x(s), u(s), w_k) = J_{MPC} \\ s.t. \quad & \tfrac{d\mathbf{x}}{ds} - f(s, x(s), u(s)) = 0 \\ & h(s, x(s), u(s)) \leq 0 \\ & g_b(x(s_0), x(s_f), u(s_o), u(s_f)) = 0 \end{aligned} \tag{3.29}$$

where J is a general cost-functional that will be further clarified in the proceeding discussion. The function $f(\cdot) \in \mathbb{R}^n$ represents the system dynamics described by (3.28). The function $g(\cdot) \in \mathbb{R}^{n_g}$ is used to constrain the lateral deviation of the vehicle to stay within the track width boundaries ($\underline{e_y} \leq e_y \leq \overline{e_y}$) and to limit the maximum engine power ($P_{eng} = T\omega_{rear} \leq P_{eng}^{max}$). The function $g_b(\cdot) \in \mathbb{R}^{n_{g_b}}$ captures boundary conditions of the problem.

In the cascaded optimization formulation, a mixed-cost function capable of blending the objectives of minimizing the local segment maneuvering time and exit velocity will be used. The two objectives are balanced via the weighting terms w_k, where the subscript $k \in \{t, v_x\}$ denotes either time or longitudinal velocity. Therefore, the local MPC cost function used in each horizon can be written as:

$$J^i_{MPC}(Z^i) = \underbrace{w^i_t \left(\frac{t(s^i_{horizon})}{s_t} \right)^2}_{\text{Minimize Time}} - \underbrace{w^i_{v_x} \left(\frac{v_x(s^i_{horizon})}{s_{v_x}} \right)^2}_{\text{Maximize Exit Velocity}} \tag{3.30}$$

In this cost structure, proper scaling between the objectives is handled via the scaling (normalization) terms. These are denoted s_t and s_{v_x} and are, respectively, the maximum values of time and velocity found in the reference time-optimal MPC solution (see section 3.2.3). Their values are fixed throughout the whole maneuver.

The computation process given a global set of weights $\mathbf{Z}$ is depicted in Figure 3.3. First, the problem domain $s \in [s_0, s_f]$ is divided in to $i = 1, 2, ..., N$ segments. These segments define the MPC update interval: $s_{MPC} = (s_f - s_0)/N$. Next, the first MPC horizon ⓐ is posed over the horizon $s^1 \in [s^1_0 = s_0,\ s^1_0 + s_{horizon}]$ with initial conditions $x^1_0 = x_0$. The preview horizon ($s_{horizon}$) is a chosen parameter and can be seen in Table 3.2. Now, the optimal control problem (3.29) can be solved over this horizon using the local cost $J^1(Z^1) =$ (3.30). Where the weights $Z^1 = [w^1_t\ w^1_{vx}]$ blend the objectives minimizing time and maximizing velocity over this horizon. Once this optimal control problem is solved, the global solution is then updated over the MPC update interval ⓑ. Next, the problem advances forward by the MPC update interval and the next MPC horizon is formed ⓓ. This next segment starts at $s^2_0 = s^1_0 + s_{MPC}$ and has the initial conditions $x^2_0 = x^1(s^2_0)$ are found from the previous horizon ⓒ. The second horizon is then solved and the process is repeated around the entire racing circuit for all $i = 1, 2, ..., N - 1$ MPC horizons. To allow the vehicle to come up to operating speed, the maneuver timing is started a distance after the initial simulation distance s_0 which is denoted as s_{start}. This simulates the 'out lap' a human driver performs when first going on a racing circuit and comes up to speed before

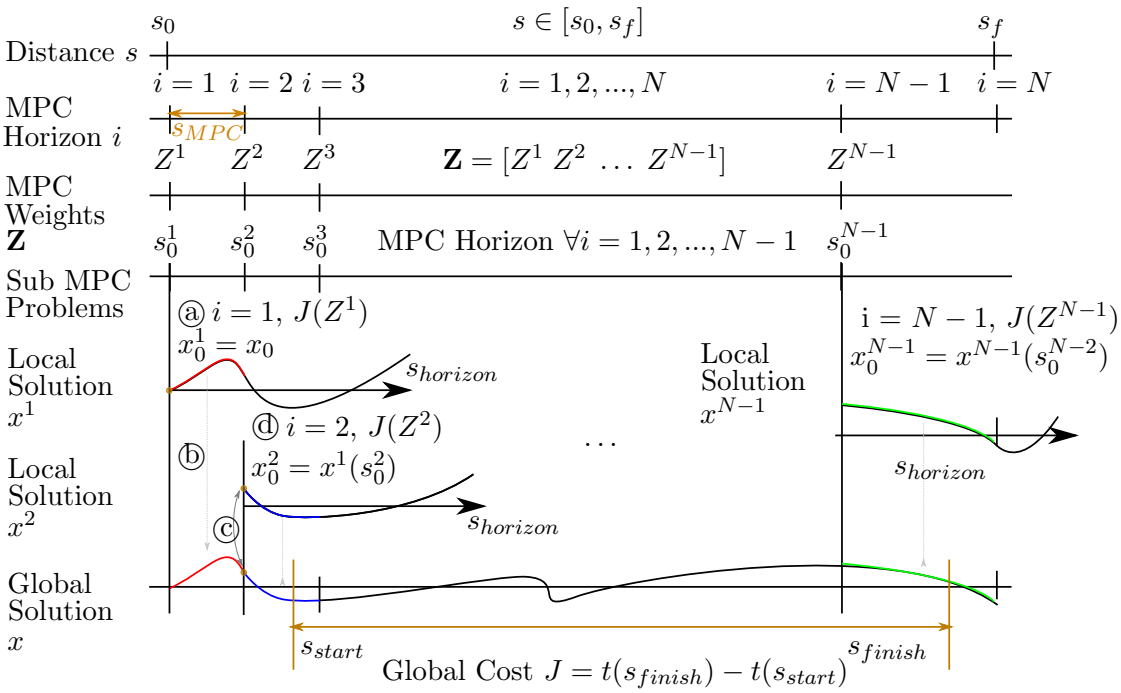

Figure 3.3: MPC Lap Simulation.

the timed maneuver begins. Similarly, an 'in lap' is also simulated as the timed portion of the maneuver ($s_{finish} - s_{start}$) occurs before the simulation is complete at distance s_f. Therefore, the global performance index is: $J = t(s_{finish}) - t(s_{start})$.

3.2.2.2 Outer Loop Optimization

The objective of the outer loop optimization is to find the optimal set of weights that the inner loop controller will use in each local MPC horizon such that the global maneuvering time ($t(s_{end}) - t(s_{start})$) is minimized. The cascaded optimization can be

written as:

$$
\begin{array}{ll}
\min\limits_{\mathbf{Z}} & J = t(s_{end}) - t(s_{start}) \\
 & \boxed{\begin{array}{c} \text{Sub MPC Problem:} \quad for\ i = 1, 2, ..., N-1 \\ \hline \text{Optimal Control Problem(3.29)} \\ s^i \in \begin{bmatrix} s_o^i & (s_o^i + s_{horizon}) \end{bmatrix} \\ s^{i+1} = s_o^i + \frac{(s_f - s_0)}{N} \\ x_0^{i+1} = x(s^{i+1}) \end{array}} \\
s.t. & w_k^i \in [0, 1]
\end{array}
\tag{3.31}
$$

where $\mathbf{Z}$, the decision variable of the outer loop and contains the set of weights ($w_k^i,\ k \in \{t, v_x\}$) to be used over each local MPC horizon. In other words:

$$
\mathbf{Z} = \begin{bmatrix} Z^1 & Z^2 & \dots & Z^{N-1} \end{bmatrix}^T = \left[\begin{array}{cc|c|cc|c|cc} w_t^1 & w_{v_x}^1 & w_t^2 & w_{v_x}^2 & \dots & w_t^{N-1} & w_{v_x}^{N-1} \end{array}\right]^T \tag{3.32}
$$

where N-1 is the number of MPC segments on the track. Therefore, the global set of weights $\mathbf{Z} \in \mathbb{R}^{2(N-1)\times 1}$. Furthermore, each element of $\mathbf{Z}$ is constrained such that $w_k^i \in [0, 1]$.

Note that as will be highlighted below, the cascaded optimization is generally non-convex with substantial computational overhead. We applied genetic algorithms and used supercomputing clusters to arrive at the results presented below.

3.2.3 Reference Time-Optimal MPC Solution

To facilitate comparison between the cascaded optimization approach, we will consider a traditional fixed-cost time-optimal MPC applied over the whole maneuver. The local cost function for this time-optimal MPC is:

$$
J_t^i = \int_{s_0^i}^{s_{horizon}^i} \frac{1}{\dot{s}} ds \tag{3.33}
$$

Hereafter, we refer to the solution to this formulation as reference time-optimal

MPC solution.

3.3 Results and Discussion

In this section, the preceding control strategies are applied to a short chicane maneuver and two racing circuits: Hockenheim and Nürburgring. On each track, the globally optimized MPC will be compared to the traditional fixed-cost time-optimal MPC. The vehicle used in this work is representative of a Formula 1 racing car and was presented in [20, 45]. The parameters used can be found in Table 3.1. To solve the problem posed in (3.31), two solvers were utilized. For the outer-loop MATLAB's global optimization tool box [165] was employed to find the global set of weights $\mathbf{Z}$ that minimized global maneuvering time. A genetic algorithm was chosen as there are many local optima in the solution set (which will be discussed further later). The cascaded optimization is generally non-convex with substantial computational overhead; thus, supercomputing clusters were used to arrive at the results presented below. The inner loop performs the MPC procedure outlined in Figure 3.3 and recursively solves the optimal control problem described in (3.29). The solution for this optimal control problem is found via an orthogonal collocation method (implemented in the software package GPOPS-II [111]). The vehicle model used is a four wheel vehicle model with seven degrees of freedom. Three degrees of freedom for rigid body motions: (v_x) longitudinal velocity, (v_y) lateral velocity, and yaw rate ($\dot{\psi}$). Four differential equations are used to calculate the wheel dynamics. The MPC algorithm and simulation parameters can be seen in Table 3.2.

Split channels will be used below and provide a convenient means for comparing these two solutions and are defined here as the difference between the two simulations at each distance on the track. Formally written:

$$\Delta y = y(s)|_{timeOpt} - y(s)|_{locallyOptMPC} \tag{3.34}$$

where y can be any measured state, control input, or calculated channel.

Parameter	Description	Units	Value
m	Mass	kg	660
I_{zz}	Yaw inertia	kgm^2	450
L	Wheelbase	m	3.4
a	Distance of Cg to front axle	m	1.8
b	Distance of Cg to rear axle	m	1.6
h_{cg}	Height of the Cg	m	0.3
w_f	Half front track width	m	0.73
w_r	Half rear track width	m	0.73
$kt_{driving}$	Rear axle torque distribution while driving	-	1
$kt_{braking}$	Rear axle torque distribution while braking	-	0.4
P_{eng}	Maximum engine power	kW	460
C_L	Coefficient of lift	-	3
C_D	Coefficient of drag	-	0.9
A	Vehicle frontal area	m^2	1.5
ρ	Air density	kg/m^3	1.2
a_a	Distance of Cp to front axle	m	1.9
b_a	Distance of Cp to rear axle	m	1.5
k_d	Differential coefficient	$Nm/(rad/s)$	10.47
D	Proportion of front axle load transfer	-	0.5
R	Effective rolling radius of the tire	m	0.33

Table 3.1: Vehicle parameters used for simulation.

Parameter	Description	Units	Value for Chicane	Value for Hockenheim	Value for Nürburgring
$s_{horizon}$	MPC horizon	m	150	200	250
s_{MPC}	MPC update rate $s_{MPC} = (s_f - s_0)/N$	m	10	10	10
s_0	Initial distance	m	-50	-200	-200
s_{start}	Timing start distance	m	0	0	0
s_{finish}	Timing stop distance	m	650	2640	4501

Table 3.2: Control scheme parameters used in simulation.

3.3.1 Chicane Maneuver

First, a chicane maneuver (this is a track feature found on many race circuits) was simulated and the two control strategies, globally optimized MPC and time-optimal MPC were compared. Note, the metric maneuvering time is calculated as $t(s_{finish}) - t(s_{start})$ were $s_{start} = 0m$ and $s_{finish} = 650m$. For the trajectories (Figure 3.4) in a macro view, the racing lines are extremely similar; however, looking at the difference in lateral deviation between the two solutions versus distance around the track (Figure 3.5) shows that they are indeed quite different with almost 0.7m deviation occurring just after point ②. This can be considered a substantially different racing line through this section of the maneuver.

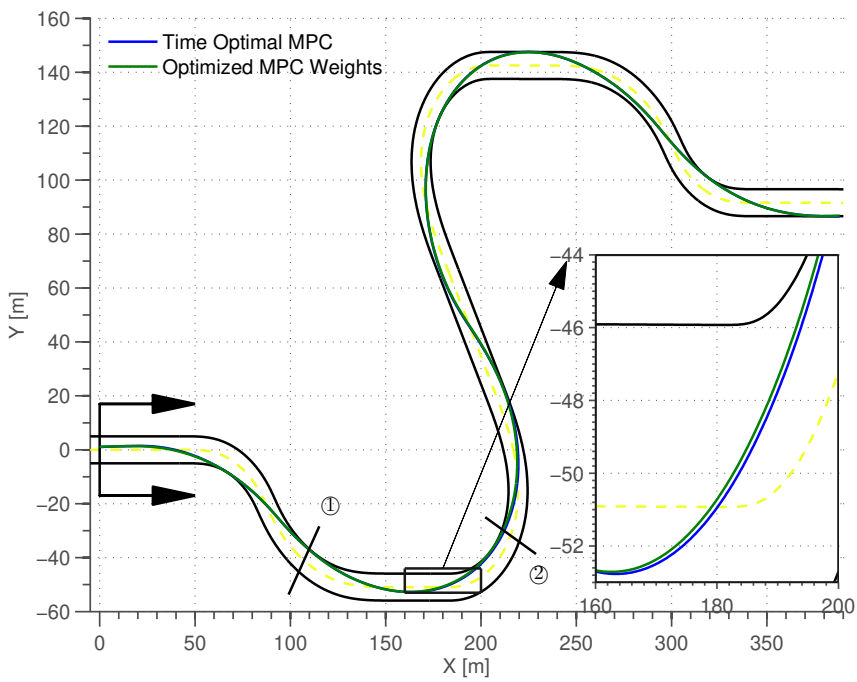

Figure 3.4: Vehicle trajectories.

The values of the weights themselves w around the track are quite noisy as seen in Figure 3.6; however, conclusions can still be drawn. If the contribution of the velocity weight, i.e., $w_{v_x}/(w_t + w_{v_x})$ is plotted along side the track curvature. Distinct spikes in w_{v_x} contributions can be seen when the curvature is changing (Figure 3.7). On the straight portions of track, the two objectives minimizing time and maximizing velocity are nearly

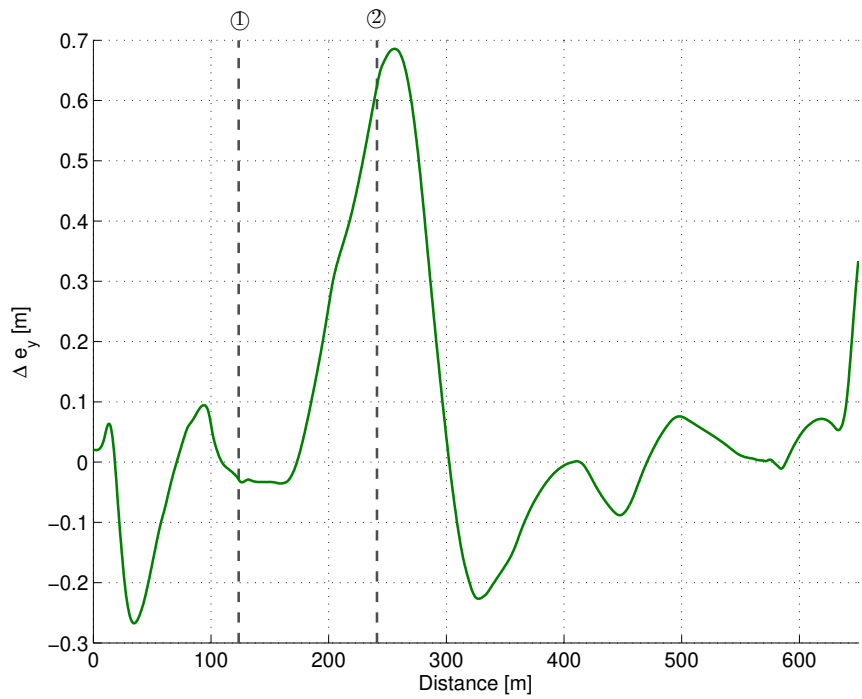

Figure 3.5: Difference in racing line versus track distance of the two solutions. Note: $\Delta e_y = e_y(s)|_{timeOpt} - e_y(s)|_{locallyOptMpc}$.

identical objectives (albeit some subtleties exist) and contribute to the noise seen in these weights; thus, the reason for the highlights in the plot.

The difference in these solutions manifest themselves mainly at two key points over the maneuver seen in Figure 3.8 (approximately ① $= 125m$ and ② $= 240m$). These two points demonstrate exactly what the algorithm is capable of doing. The outer loop sees a section of track where it is beneficial to sacrifice some speed at the local section of track ① to maintain a higher velocity later in the maneuver ② where it is more important to the global objective. In other words, some speed is sacrificed in the high speed section of the track to maintain higher speed through the low speed section of the track yielding a net improvement in performance over the entire maneuver. Figure 3.9 show a comparison of the vehicle steering and throttle differences in the two control strategies and Table 3.3 show the final maneuvering times and performance differences.

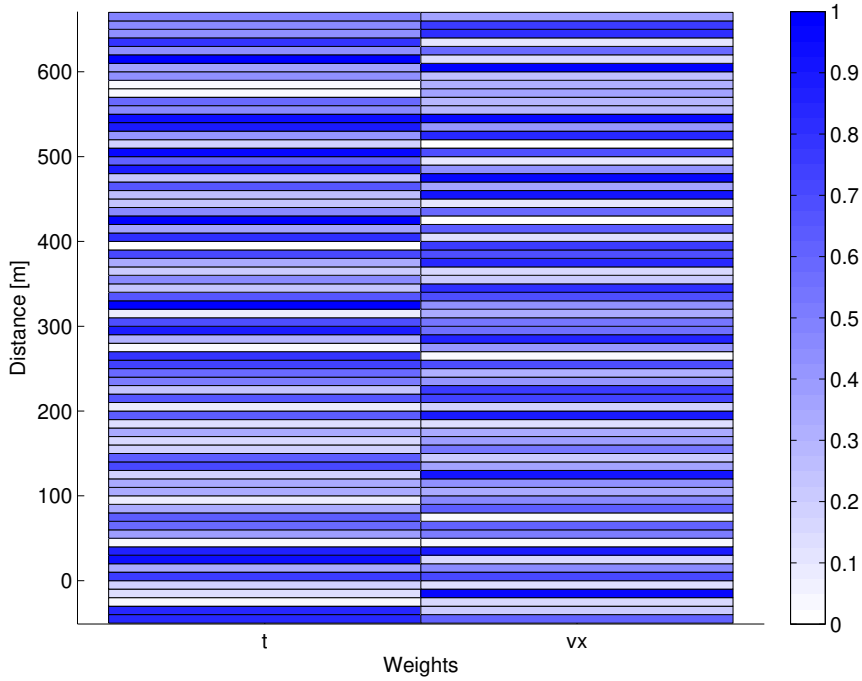

Figure 3.6: Optimized weights **W** around the chicane maneuver.

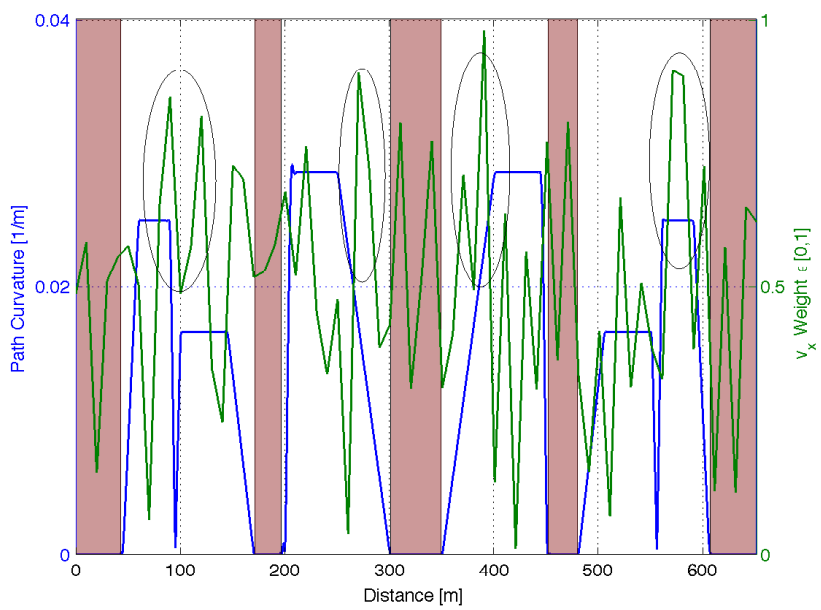

Figure 3.7: Contribution of weight of exit velocity $w_{v_x}/(w_t+w_{v_x})$ and track curvature. Note the circled spikes in section of the track where the curvature is changing. The highlighted region denotes a straight path segment.

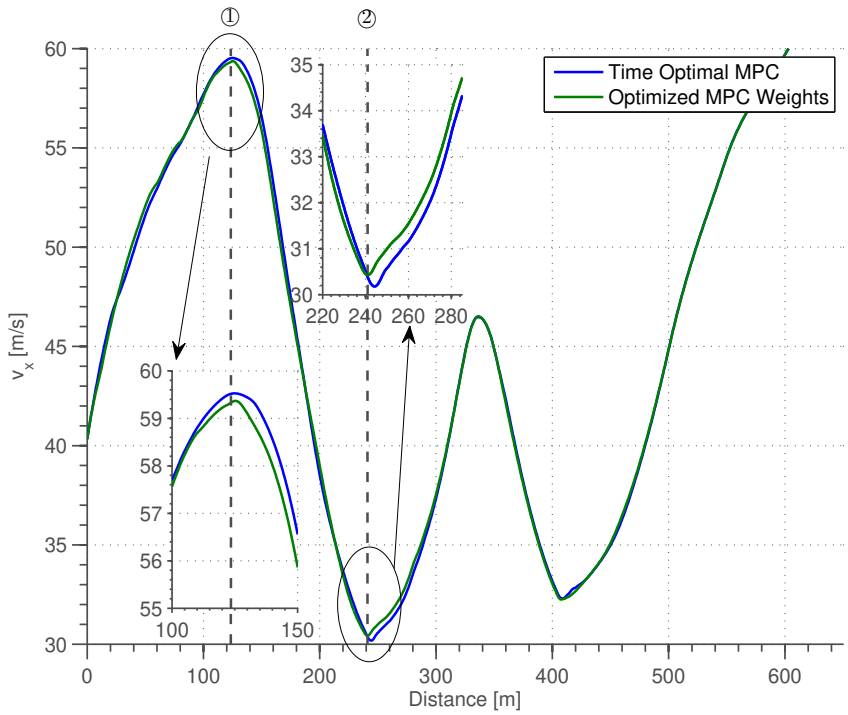

Figure 3.8: Velocity comparison.

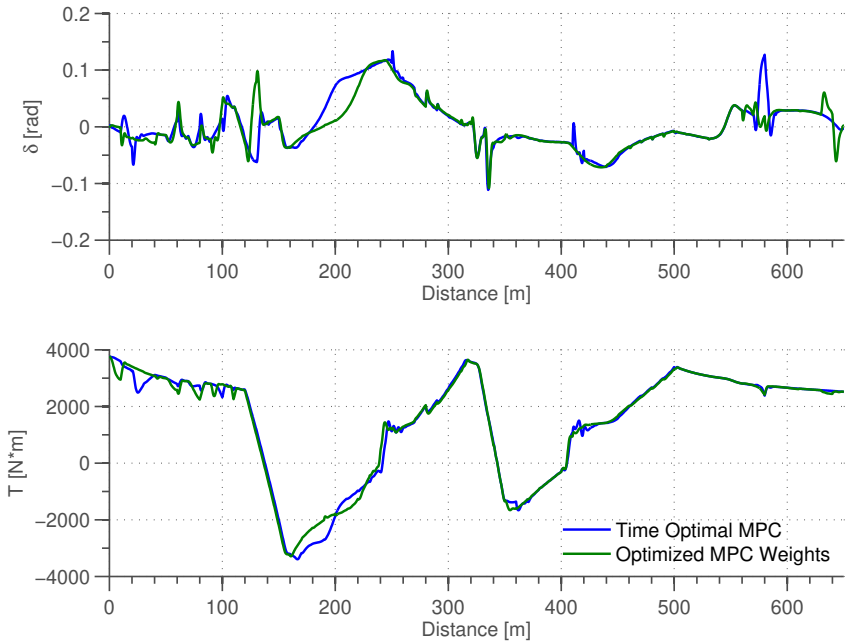

Figure 3.9: Steering and throttle demand.

3.3.2 Hockenheim

This race course is located in the town of Hockenheim, Germany and was open in 1932 [166]. In this research, the short configuration will be used which consists of a 2.6km closed road course with 10 various radii corners. The globally optimized MPC and traditional time-optimal MPC trajectories can be seen in Figure 3.10. The trajectories are quite similar over most of the race course with one very large difference occurring from the apex to exit of turn four. The key data channels from this simulation can be seen in Figure 3.11. The top plot in this figure is the vehicle's longitudinal velocity over the lap and right below is the split velocity. Split channels provide a convenient means for comparing these two solutions and are defined here as the difference between the two simulations at each distance on the track. Formally written:

$$\Delta y = y(s)|_{timeOpt} - y(s)|_{locallyOptMPC} \tag{3.35}$$

where y can be any measured state, control input, or calculated channel. The split velocity trace in Figure 3.11 shows that adjusting speed by just a few m/s in certain sections can have an impact on the final performance. The third plot of Figure 3.11 shows the split-time plot and is the key indicator for showing the advantage of the globally optimized MPC. The reader can see that right after the apex of turn four through corner exit and all the way to the entry of turn 6 (to a lesser degree) that the slope of the globally optimized MPC Δt is down; i.e., this solution is gaining time on the reference time-optimal MPC solution. Thus, at the same location on the track, there has been less elapsed time with the globally optimized MPC. Turn four is the key location on the circuit where the global weights were able to change the trajectory to yield a net benefit. The controller did this by sacrificing time right before the apex of turn four as can be seen on the same plot (where the Δt traces is increasing to a peak right past the turn four apex). This is the key point demonstrating how the globally optimized MPC mimics a human driver, it can learn to sacrifice time in a particular location of the track, in this case the entry of turn four through the apex,

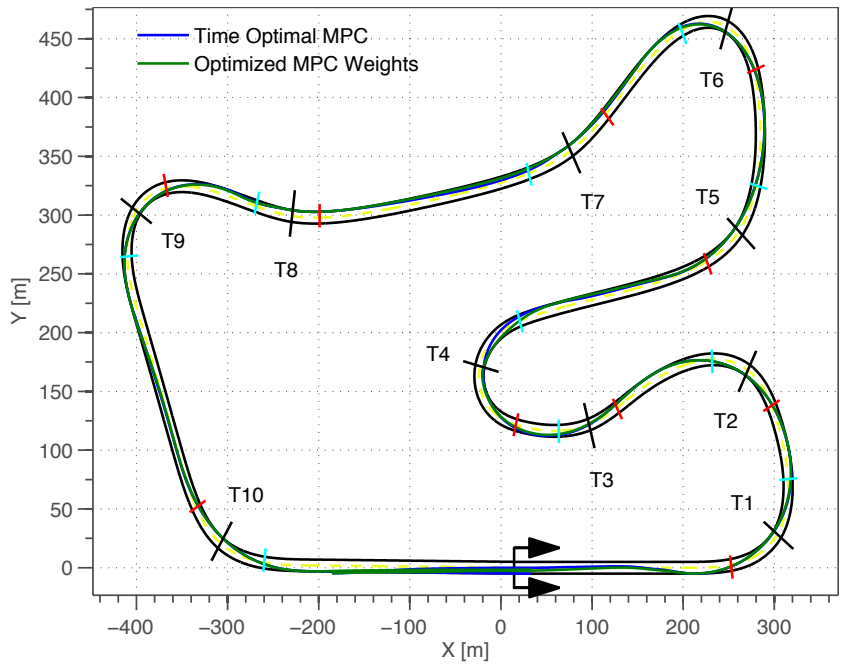

Figure 3.10: Trajectories on the Hockenheim racing circuit. Numbers with the prefix 'T' denote the 10 different turn apexes on the course. Red waylines denote corner entry locations and cyan lines denote corner exit lines.

in order to 'setup' the next section with higher velocity and ultimately achieve a better solution over entire maneuver. The fourth plot in this figure shows the split (Δe_y) racing line and again, the key difference between the two solutions is at turn four where the globally optimized MPC is able to apex the turn earlier, sacrificing some time early in the corner while achieving a higher velocity at corner exit.

The globally optimized weights themselves are quite noisy as can be seen in the last trace of Figure 3.11 and overlaid on the track map in Figure 3.12. Much of this noise comes from the fact that when traveling in a straight line, the objectives of maximizing velocity and minimizing time are nearly identical. This is demonstrated in the control quantities: steering (δ) and torque demand (T) shown in Figure 3.11. On the straight sections of track (section without highlights denoting the corners), the control quantities of the globally optimal MPC are nearly identical to the time-optimal MPC in spite of the

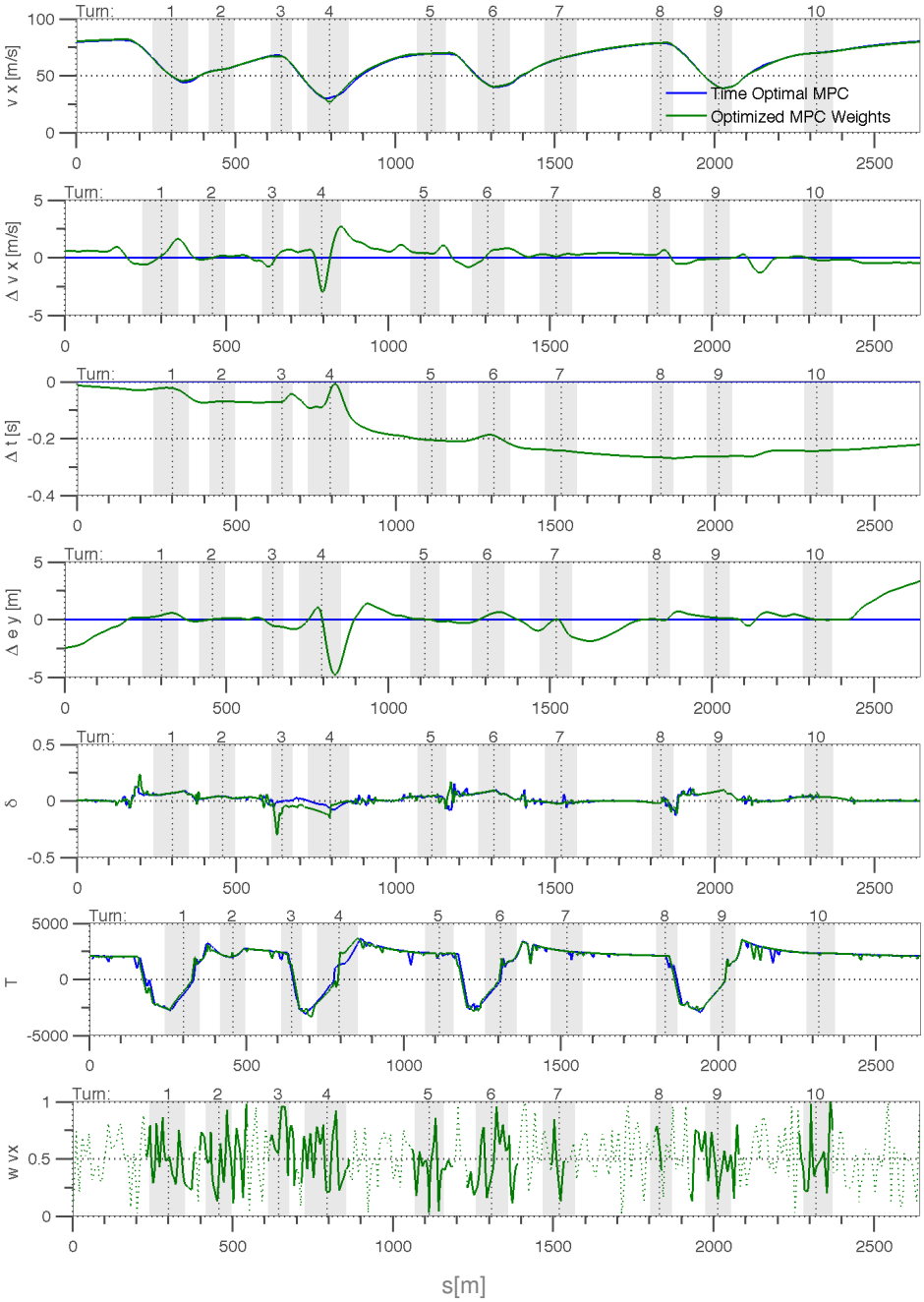

Figure 3.11: Hockenheim distance histories. Blue denotes the reference time optimal MPC and green is the optimized cascaded optimization. From top to bottom longitudinal velocity, split velocity, split time, split racing line, steering wheel angle, torque demand, and contribution of the exit velocity MPC weight in each local segment. The weight contribution is defined as: $w_{v_x}/(w_t + w_{v_x})$. Weights in straight portions of the track are dotted to emphasize results during corners. Note that each turn is denoted with a grey patch and corner entry and exit points correspond to those denoted in Figure 3.10. Corner apex location makeup the x grid location in these plot and corner number are located at the top of each channel.

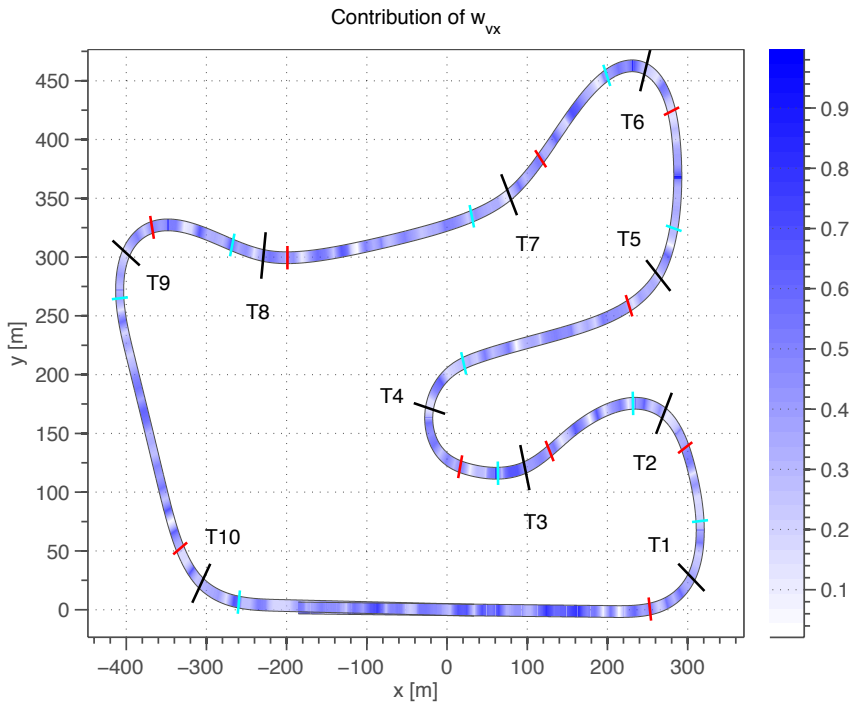

Figure 3.12: Contribution of the exit velocity MPC weight in each local segment. This contribution is defined as: $w_{v_x}/(w_t + w_{v_x})$.

fact that the globally optimal MPC is choosing different values for the contribution of exit velocity and maneuvering time at each local segment. The key benefit to this structure is that the weights can change in a corner to setup different trajectories that could impact global performance. There is a small section of track right after the apex of turn four where the globally optimal MPC more heavily weights the exit velocity (w_{v_x}) and the trajectory in that location is able to change enough to setup the next section of track yielding a better maneuvering time overall. The final results can be seen in Table 3.3.

3.3.3 Nürburgring

The two control strategies were also applied to the Nürburgring race course. This is a very historic track located in the town of Nurburg Germany and was constructed in the 1920s [167]. For the purposes of this work, the grand prix configuration consisting of

14 turns over a distance of 4.5km was used. The vehicle trajectories can bee seen in Figure 3.13. The results on this track were very similar to Hockenheim; there was one key location from the apex of turn six (T6) to corner exit that comprised much of the performance advantage of the globally optimized MPC. The distance histories of velocity, split velocity, split time, split racing line, steering wheel angle, torque demand, and contribution of exit velocity weight can be seen in Figure 3.14. Just as in the Hockenheim case, changing speed by just a few m/s in key locations around the course yields global performance benefits. Looking at the split time (Δt) plot shows that the majority of the performance advantage of the globally optimized MPC comes just after the apex of turn six to just after corner exit. The globally optimal trajectory sacrifices time just before the apex of turn six to take advantages of higher speed all the way to the entry of turn nine (T9) yielding a net improvement. The split racing line plot (Δe_y) shows that a very different racing line is used in this turn.

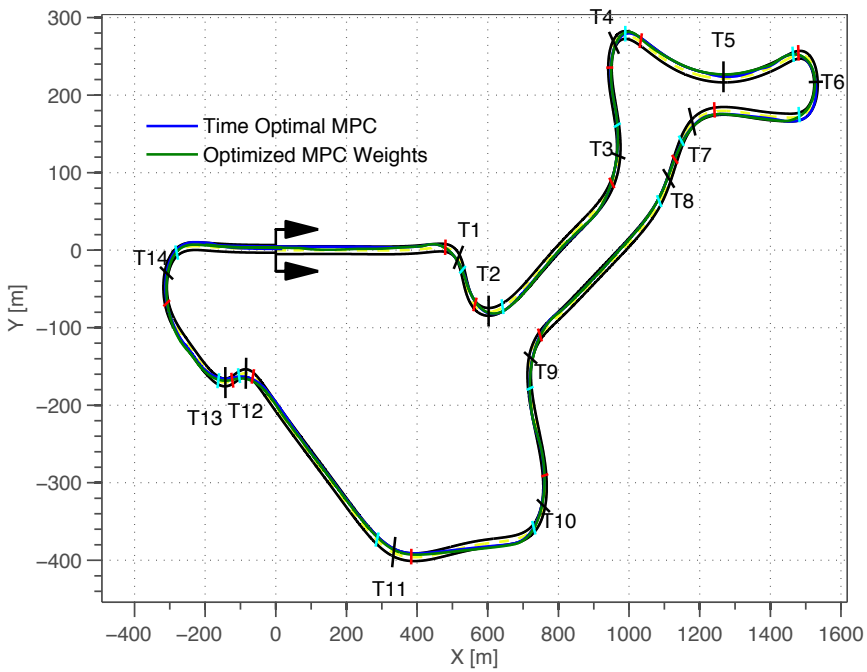

Figure 3.13: Trajectories on the Nürburgring racing circuit. Numbers with prefix 'T' denote corner apexes, red waylines denote corner entry locations and cyan lines denote corner exit lines.

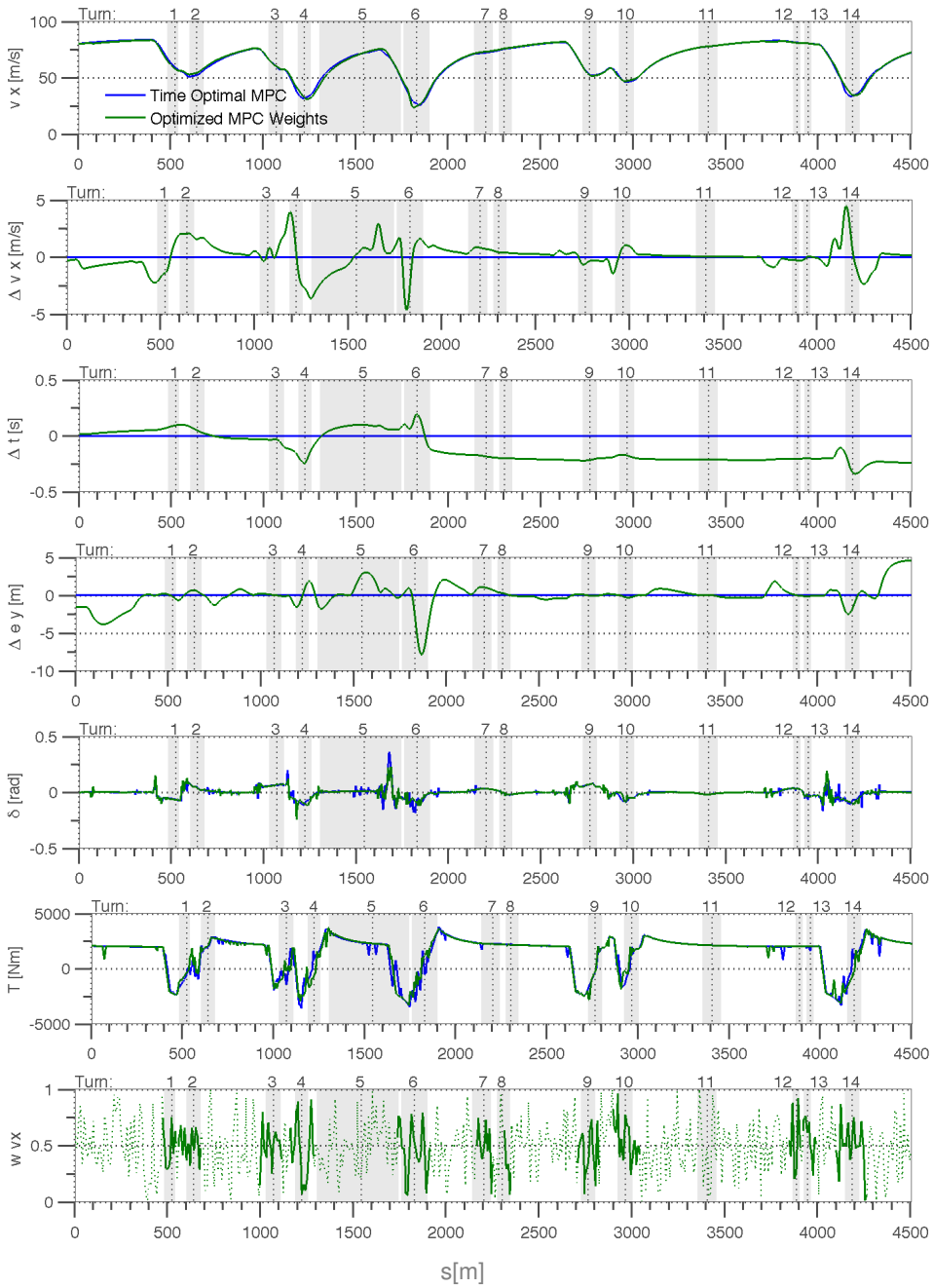

Figure 3.14: Nürburgring distance histories. Blue denotes the reference time optimal MPC and green is the optimized cascaded optimization. From top to bottom longitudinal velocity, split velocity, split time, split racing line, steering wheel angle, torque demand, and contribution of the exit velocity MPC weight in each local segment. The weight contribution is defined as: $w_{v_x}/(w_t + w_{v_x})$. Weights in straight portions of the track are dotted to emphasize results during corners. Note that each turn is denoted with a grey patch and corner entry and exit points correspond to those denoted in Figure 3.13. Corner apex location makeup the x grid location in these plot and corner number are located at the top of each channel.

3.3.4 Summary of Results and Discussion

The final performance of both controllers can be seen in Table 3.3. While these performance gains may seem small to the casual observer, in the context of motorsports these can be significant. In Formula 1 racing, teams spend millions of dollars for millisecond gains in lap time performance [93, 12]. Moreover, these small gains come with dramatic changes to the racing line. This corroborates the authors' experiences with professional drivers. Different drivers are able to achieve similar performance with a very different trajectory or driving style. Mathematically speaking, this demonstrates the existence of multiple local minima in the solution space, a point which has not been directly discussed in reviewed literature. It is the opinion of the authors that these local minima could be used to explain different driving styles that are exhibited by professional drivers. To further support this point, five other iterates of the genetic algorithm outputs for the global weight ($\mathbf{Z}$) search are plotted for the Hockenheim track in Figure 3.15. Their respective maneuvering times and improvement over the time-optimal MPC can be seen in Table 3.4. It is clear to see that this notion of globally optimizing the local MPC weights has advantage over the traditional fixed cost time optimal MPC and is able to outperform it repeatably. Moreover, there are many different sets of weights that all out perform the time optimal MPC and thus demonstrating the existence of multiple local minima in the solution space.

Course	Vehicle Model	Controller	Time [s]	Δ Time [s]	Δ [%]
Chicane	Particle Motion†	Time-optimal MPC †	22.787	-	-
		Blended-cost MPC †	22.349	-0.438	-1.92
Chicane	Four Wheel	Time-optimal MPC	14.493	-	-
		Blended-cost MPC	14.446	0.047	-0.324
Hockenheim	Four Wheel	Time-optimal MPC	44.471	-	-
		Blended-cost MPC	44.264	-0.207	-0.466
Nürburgring	Four Wheel	Time-optimal MPC	72.121	-	-
		Blended-cost MPC	71.866	-0.255	-0.354

† These results were published in [163].

Table 3.3: Results from the chicane, Hockenheim, and Nürburgring.

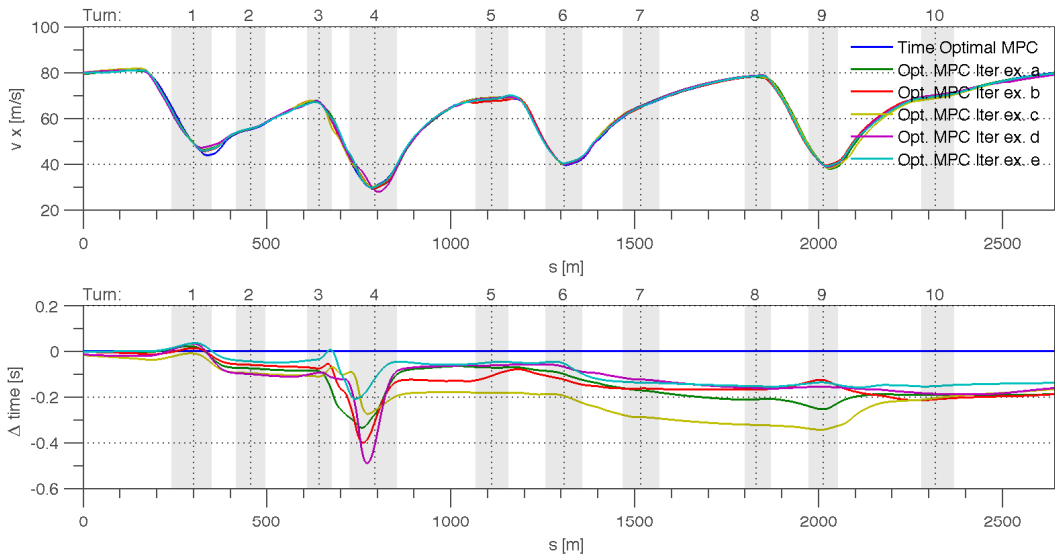

a.)

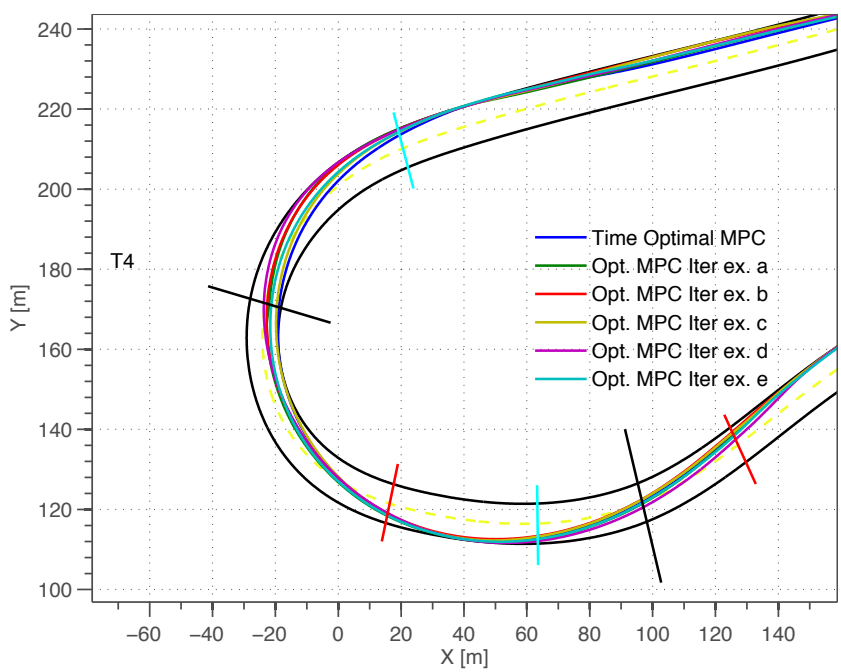

b.)

Figure 3.15: Five example iterate solutions show outperformance of the time optimal MPC. a.) Distance Histories b.) trajectory comparison.

Controller	Maneuvering Time [s]	Δ Time [s]	Performance Δ [%]
Time optimal MPC	44.471	-	-
Example iterate a	44.286	-0.185	-0.416
Example iterate b	44.286	-0.185	-0.415
Example iterate c	44.323	-0.148	-0.334
Example iterate d	44.325	-0.146	-0.328
Example iterate e	44.335	-0.136	-0.306

Table 3.4: Other iterates on Hockenheim showing globally optimized MPC outperforming time optimal MPC.

3.4 Conclusions

In this chapter, a cascaded optimization structure is formulated to model how a professional driver is able to optimize over local segments of race circuits to minimize maneuvering time over the whole track. An inner loop MPC with a variable cost function is used to set local control and an outer loop optimization searches to find the best set of weights that the inner loop will use in each horizon to optimally blend the objectives of minimizing time or maximizing velocity in each MPC horizon. This cascaded optimization structure is then used to simulate a Formula 1 car on a simple chicane and two well-known race courses: Hockenheim and Nürburgring. The results are compared to a traditional fixed-cost time-optimal MPC controller. In both cases, the cascaded optimization is able to outperform the time-optimal controller. Moreover, examining other iterates in the solution space demonstrates that there are several different solutions with similar performance; i.e., a demonstration of the existence of local minima in solution space. The later is a corroboration of the intuition and practical field observations that different driving styles may achieve very similar maneuvering times. Future work will look at exploiting this optimization structure to further analyze the driving style differences between different human drivers.

Chapter 4

An Optimal Control Approach to Race Line Reconstruction from Limited Onboard Data

Abstract

The racing line is a key response studied in minimum-time vehicle maneuvering problems. Different drivers have different driving styles and these differences can manifest themselves in the racing lines they take. By understanding these lines, one can gain insights into how different drivers achieve minimum-time performance. State of the art racing simulation techniques use time optimal control formulations wherein the racing line is free to move within the boundaries of the track. It is often of interest to be able to compare results from these simulation techniques with onboard measurements taken during racing events or controlled tests. Vehicles are often tested with a limited set of sensors and traditional methods of estimating the racing line from onboard measurements accumulate too much error to provide useful comparisons. In this chatper[1], we will present a novel method of

[1]This chapter has been submitted for publication: J. R. Anderson and B. Ayalew. An optimal control approach to race line reconstruction from limited onboard data. Vehicle System Dynamics (Submitted, under review), 2018.

reconstructing the racing line using optimal control formulations in order to fit onboard measurements to a reference track model. The reference track model is generated from GPS measurements collected a priori and serves as a method of grounding the onboard measurements that are prone to drift and error accumulation. The details of the proposed method are demonstrated with a case study using measurements conducted at Sebring International Raceway.

4.1 Introduction

The racing line is the path taken by the vehicle on a given driving/racing circuit resulting from the driver's control actions (i.e., throttle, steering, braking, etc.) which are applied to achieve the goal of minimizing the vehicle's maneuvering time. This line must lie within the track boundaries. The line itself is a compromise between the ability of the vehicle to travel as fast as possible (i.e., minimizing curvature of the racing line) and traveling the shortest distance. Generally, a professional driver blends these two objectives in some fashion to achieve the goal of minimizing overall time, given his/her knowledge of the vehicle's performance envelop and the track configuration [63]. Professional human drivers are still considered the benchmark for minimum-time vehicle maneuvering performance. Gaining insights on how they are able to accomplish this performance is important to motorsports [1], the high-performance vehicle segment of the automotive industry, and even the gaming industry [80]. These racing lines are not unique to a particular vehicle/track combination and can change based on vehicle setup [20]. Also, as will be shown in this chapter, different human drivers have different driving styles and they can achieve similar performance while adopting different driving lines [11]. Being able to understand different driving styles by identifying the differences in racing lines will aid in understanding how the system can be solicited in different ways to achieve time optimal performance. By understanding these solicitations, tunings of the vehicle can be tailored to specific drivers resulting in an optimized vehicle/driver system. Our recent research is in the area of

mathematically modeling driving styles [21, 22] and a key consideration being the ability to capture the effect of the differences in racing lines.

In addition, vehicle measurement is not often acquired relative to the road traveled which makes a comparison to simulation difficult. At best, test vehicles are instrumented with Global Positioning System (GPS) sensors and a relative comparison of the racing lines in cartesian or GPS coordinates is possible; however, sensor error such as bias and resolution still prevents a good comparison to simulation. Moreover, racing and high-performance vehicles, in general, are instrumented with a very limited set of sensors that capture the global chassis motion (e.g., accelerometer, gyroscopes, and optical slip angle sensors). Estimating the racing line from these limited set of sensors is not straightforward as noise and sensor drift affect the estimation. One work that investigated the issue is that of Casanova [5] which presented a method for compensating integration errors to estimate the path taken by the driver; however, his corrections still accumulate too much error to compare to optimal control based simulations as will be shown in our results.

Modern methods of simulating minimum-time vehicle maneuvering problems are generally formulated as the following optimal control problem:

$$\begin{aligned} \min_{\mathbf{u}} \quad & J = \int_{s_o}^{s_f} \tfrac{1}{\dot{s}} ds \\ s.t. \quad & \tfrac{d\mathbf{x}}{ds} - f(\mathbf{x}, \mathbf{u}, s) = 0 \\ & \underline{\mathbf{x}} \leq \mathbf{x} \leq \overline{\mathbf{x}}, \ \underline{\mathbf{u}} \leq \mathbf{u} \leq \overline{\mathbf{u}} \end{aligned} \tag{4.1}$$

where the independent variable s is the distance traveled along the track centerline, $\mathbf{u}$ is a general set of controls to the vehicle (e.g., throttle/brake, steering), and $\mathbf{x}$ is a general set of vehicle states (e.g., acceleration and velocity components). The states and control inputs are bounded. These techniques date back to the work presented in [88, 89, 91] and the topic is also reviewed well in [92]. The vehicle dynamics are typically written in path intrinsic coordinates and bounded such that lateral deviation of the vehicle from the center of the path remains within the track width limits. This formulation allows the racing line

to naturally vary within the track boundaries.

The model of the track is often expressed in a path intrinsic coordinate system. In its simplest form (as will be used in this chapter), the model can be a general function of track curvature versus distance ($c(s)$). In this chapter, we will use spline interpolation of curvature data versus path centerline distance. Recent works have extended track modeling to three-dimensional tracks by using the differential geometry of ribbons or strips to describe the track via a generalized Frenet Serret description of the path [168, 142]. Once the track model is chosen, then the next step is fitting these models to an existing racing circuit. The work in [169] models the track by fitting a series of straight, constant radius, and clothoid segments. More generally, [20] uses an optimal control fitting method for modeling the track curvatures as a function of distance from just GPS data. We will adopt this approach in the subsequent section to fit a track model of Sebring International Raceway as an intermediate step towards reconstructing the racing line.

An alternate method for solving minimum-time vehicle maneuvering problems is to treat the path planning and path following hierarchically as separate problems. The path planning phase of the problem relies on constructing the desired path to follow. One method that is typically employed to optimally select this line, is geometric optimization. With this method, the racing line is constructed from a parameterized curve such as a spline and its geometry is optimized to either minimize curvature, minimize distance traveled, or blend these two objectives while remaining within the track boundaries. The work presented in [63, 80, 79, 170] provides good examples of this technique. Alternatively, onboard vehicle data can be used to reconstruct the reference path. This is another application of the work presented in this chapter. With a reference path identified, the remainder of the problem is to follow the path in minimum time. The work presented in [51] gives an excellent overview of this technique. Solving a fixed-path minimum-time vehicle maneuvering problem has been shown to be a convex optimization problem in [75]. This work extends the fixed-path time optimal problem for robots [76] to vehicles.

In this chapter, we aim to accomplish the following: first, we give an example of

fitting the track model from GPS data acquired on the boundaries of the track. Second, we present a novel method of optimally fusing onboard vehicle measurement with a model of the racing circuit itself. To outline our proposed approach, we use data collected on Sebring International Raceway [171]. Lastly, we will further motivate the importance of studying the racing line and will show how different lines around the same track can yield nearly identical lap times.

The remainder of the chapter is organized as follows. Section 4.2 describes fitting of the reference track model from GPS data. Section 4.3 details our method for optimally reconstructing the racing line. We apply this methodology to actual vehicle data on Sebring International Raceway in Section 4.4. In this section, we will also compare driving styles of two drivers that are able to achieve identical performance while using different racing lines. Section 4.5 offers conclusions and outlines some directions for future work.

4.2 Track Modeling

To outline our proposed approach, we shall use actual data collected on Sebring International Raceway [171]; however, the formulation and approach are general and can be applied to other similarly configured race tracks. The basis of the track model is GPS measurement of the track itself. To that effect, a vehicle equipped with an accurate GPS sensor was driven at low speed around the inner and outer boundaries of the circuit. This data will serve as the basis to fit the track model. Because of the low elevation change and banking angle around this circuit, a planar track model is sufficient to capture the pertinent features. In this chapter, the track model is defined as the track curvature as a function of path distance $c(s)$.

Before fitting of the track model ($c(s)$) is possible, the centerline of the track should be estimated from the data collected on the inner and outer boundaries. First, the cartesian coordinates are calculated from the GPS measurements of the inner and outer boundaries. The data recorded is then split into two data sets that represent the inner and outer track

boundaries respectively. Because the data is measured in the time domain with a constant sampling rate, it is spatially nonuniform as seen in Figure 4.1. The data is then resampled to a spatially uniform grid using a one-dimensional spline-based interpolation.

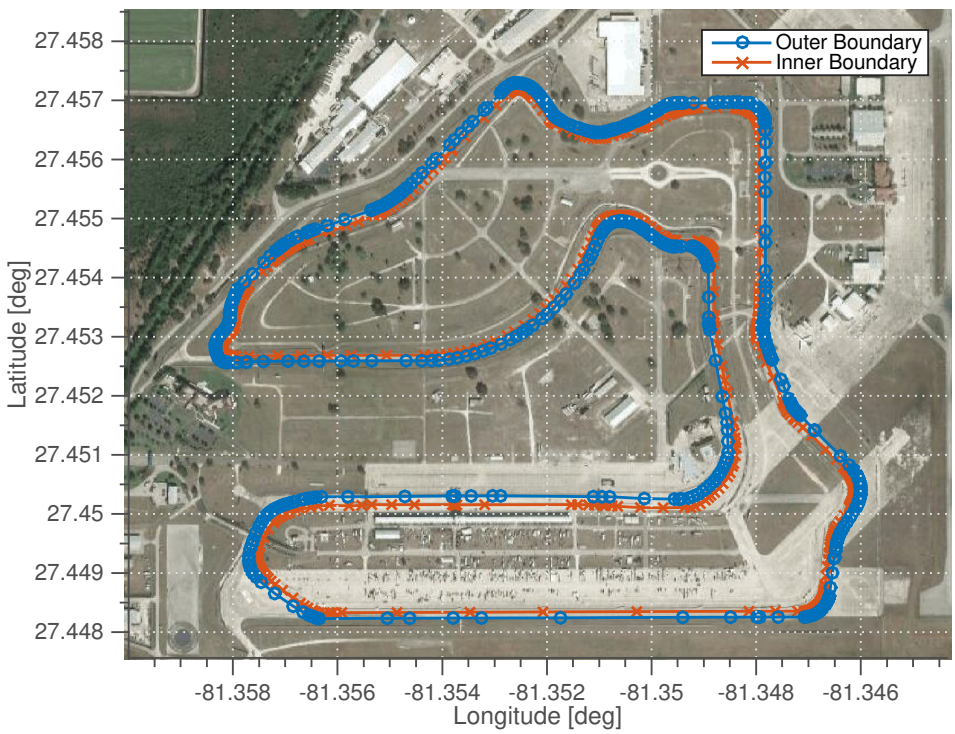

Figure 4.1: GPS data of the boundaries of Sebring.

The centerline of the track can now be reconstructed from the x, y coordinates of the inner and outer boundaries. Similar to the approach presented in [142], a nearest neighbors approach is used. Each discrete data point along the outer boundary $(x_o^j, y_o^j,\ j = 1, 2, ..., N)$ is looped over and the following four-step algorithm is performed. In the first step, we construct a perpendicular line $(y_\perp)$ from the outer boundary at the point x_o^j, y_o^j:

$$y_\perp^j(x_o^j) = m_\perp^j(x_o^j) + b_\perp^j \tag{4.2a}$$

$$m_\perp^j = (y_o^{j+1} - y_o^j)/(x_o^{j+1} - x_o^j) \tag{4.2b}$$

$$b_{\perp}^{j} = y_o^j - m_{\perp}^{j} x_o^j \tag{4.2c}$$

This perpendicular line is projected from the outer boundary toward the inner boundary. In step two, the nearest neighbors (to the projected perpendicular line $y_{\perp}$) on the inner boundary (x_i^j, y_i^j) are found. A spline is fit through the nearest three neighbors. In step three, we find the intersection between the nearest neighbors spline on the inner boundary and the projected perpendicular line $(y_{\perp})$. Finally, in step four, we find the midpoint between the original outer boundary data point (x_o^j, y_o^j) and the calculated intersection point from the previous step. The result is an estimated center point on the track $(\hat{x}_j, \hat{y}_j)$. This procedure is repeated for all $j = 1, 2, ..., N$ points along the outer boundary to give the reference path centerline coordinates. Figure 4.2 gives a graphical representation of this procedure.

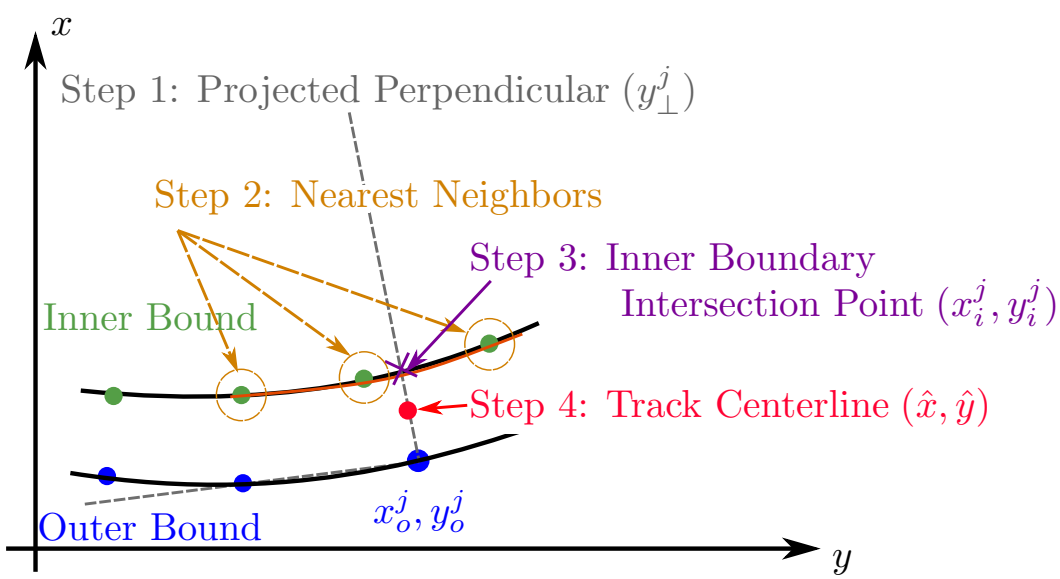

Figure 4.2: Nearest neighbors method of interpolating track centerline from boundaries.

To fit the track model $(c(s))$ to the data representing the track centerline $(\hat{x}, \hat{y})$ previously calculated, we adopt the optimal control formulation suggested in [20]. A simple

kinematic mapping of the path curvature to Cartesian coordinates is written as:

$$c' = u \tag{4.3a}$$

$$\psi' = c \tag{4.3b}$$

$$x' = \cos(\psi) \tag{4.3c}$$

$$y' = \sin(\psi) \tag{4.3d}$$

The system states ($\mathbf{x}$) are the track curvature (c), path heading angle (ψ), and x y Cartesian coordinates. Note that the $(\cdot)'$ operator denotes spatial derivatives ($\frac{d(\cdot)}{ds}$). The system input is u which is the spatial rate of change of curvature. With $\mathbf{x} = \begin{bmatrix} c & \psi & x & y \end{bmatrix}^T$, the above system (4.3) can be written compactly as:

$$\frac{d\mathbf{x}}{ds} = f(\mathbf{x}, u, s) \tag{4.4}$$

Next, the optimal control problem can be written to fit the track model to the measured data:

$$\begin{aligned} \min_{u} \quad & J = \int_{s_o}^{s_f} w_u u^2 + (\hat{x} - x)^2 + (\hat{y} - y)^2 ds \\ s.t. \quad & \mathbf{x}' - f(\mathbf{x}, u, s) = 0 \\ & \int_{s_o}^{s_f} c\, ds = 2\pi \\ & x_0 = x_f,\ y_0 = y_f,\ c_0 = c_f \end{aligned} \tag{4.5}$$

where $\hat{x}, \hat{y}$ denotes cartesian coordinates of the centerline of the track derived from the GPS data. The function $f(\mathbf{x}, u, s)$ represents the system dynamics, and the remaining equations enforces the track closure conditions. The weighting term w_u in the cost function is used to filter the track model and obtain a smooth estimate of the track curvature ($c(s)$).

Having found good estimates of the centerline of the track $(\hat{x}, \hat{y})$, we solve the nonlinear optimal control problem (4.5) to obtain the optimal track model $(c(s))$ subject to the imposed constraints with a suitable solver. For our purposes, we found the orthogonal collocation methods implemented in the software GPOPS-II [111] sufficient; however, any nonlinear optimal control solution techniques could be applied to solve this problem. The final fit of the track model from GPS data can be seen in Figure 4.3. It can be seen that the optimal control approach very closely fits the estimated (from GPS measurements) centerline while retaining sufficient smoothness.

In order to quantify performance of the track fitting, the distance normal to the fit $c(x)$ (blue curve in Figure 4.3) and each estimated centerline point (red 'x' in Figure 4.3) is calculated. Using this approach, the mean distance is calculated to be 5.98m with a standard deviation of 2.82m. Considering the track spans 1000m in the x and y coordinate, this error can be considered small. Note that this error is due to the smoothing performed by weighting on the rate of change of curvature (w_u) and closure conditions enforced in the optimal control formulation. We found these results to be a sufficient balance of accuracy of fit and a sufficiently smooth track model. The fit curvature versus distance $(c(s))$ will be used as the track model in our racing line reconstruction method detailed in the next section.

4.3 Race Line Reconstruction

In this section, the algorithm for reconstructing the race line from vehicle measurement and the fit track model (discussed in Section 4.2) will be detailed. As previously mentioned, measurements from typical sensors found on a racing car can be quite limited as in our case study. The vehicle was not equipped with a GPS sensor during the test, and as such, only the four sensors: lateral and longitudinal velocity $(v_x,\ v_y)$ and lateral and longitudinal acceleration $(a_x,\ a_y)$ will be used in this algorithm.

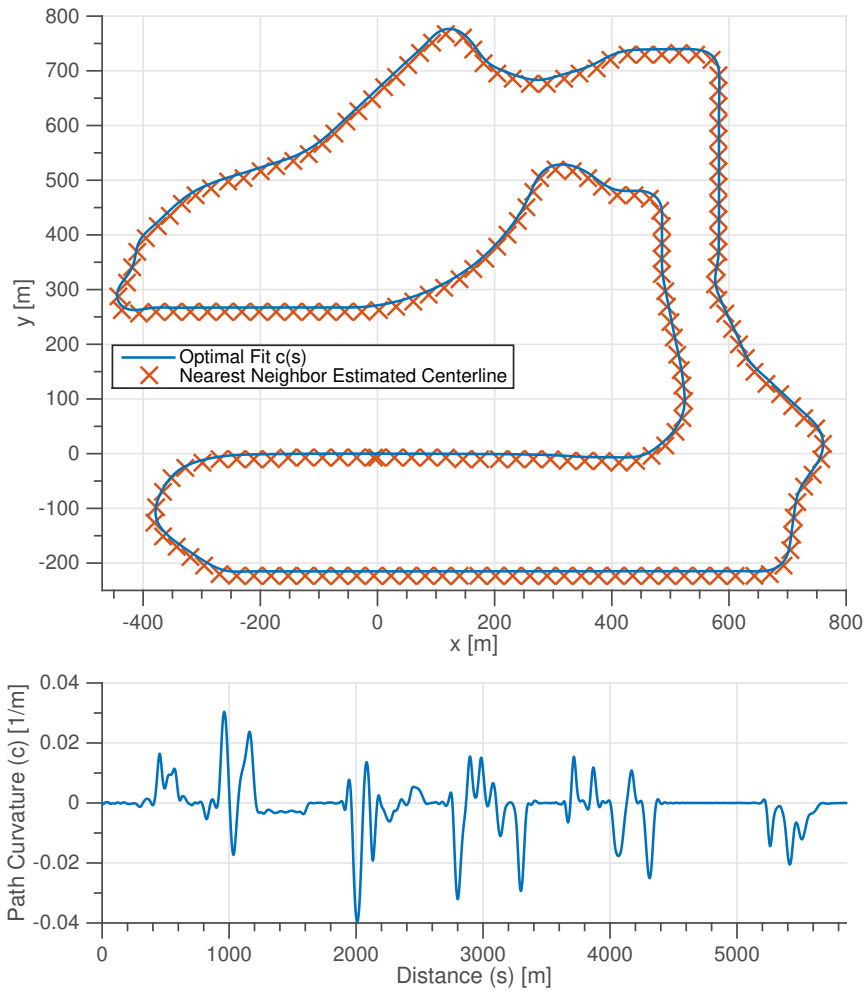

Figure 4.3: Fit of the track model ($c(s)$) from GPS data.

4.3.1 Motivation for Optimal Race Line Reconstruction

As previously mentioned, the work [5] is one of the few works to discuss reconstructing the racing line from onboard measurements. Therein, an ad-hoc method of compensating integration errors to enforce closure conditions was proposed. With this method, a simple kinematic model is used to estimate curvature from vehicle velocity and lateral acceleration (after appropriate data filtering):

$$c = \frac{a_y}{v_x^2} \tag{4.6}$$

Then, vehicle yaw is computed as:

$$\psi(t) = \int_{t_0}^{t_f} c(t) v_x(t) dt \tag{4.7}$$

The error accumulated in the vehicle yaw over one lap can be written as:

$$E_\psi = \psi(t_f) - 2\pi \tag{4.8}$$

where 2π assumes a closed lap with no overhead crossings. To enforce continuous track conditions at the start/finish line, a correction to the curvature (c) estimation is applied. This correction is written as: $\Delta_\psi = -E_\psi/s$; where s is the distance travelled. Thus the corrected yaw estimate ($\overline{\psi}$) is:

$$\overline{\psi}(t) = \int_{t_0}^{t_f} \left(c(t) + \Delta_\psi\right) v_x(t) dt \tag{4.9}$$

Yaw is then integrated yaw to find the x, y coordinates, a similar correction is applied to (4.9) such that the beginning and end x, y points are collocated.

$$\begin{aligned} E_x = x_0 - x_f, \quad E_y = y_o - y_f \\ \Delta_x = \tfrac{-E_x}{s}, \qquad \Delta_y = \tfrac{-E_y}{s} \end{aligned} \tag{4.10}$$

Finally, the corrected x and y coordinates $(\overline{x}, \overline{y})$ can be written as follows:

$$\overline{x}(t) = \int_{t_0}^{t_f} \left[cos(\psi(t)) + \Delta_x\right] v_x(t)dt \tag{4.11a}$$

$$\overline{y}(t) = \int_{t_0}^{t_f} \left[sin(\psi(t)) + \Delta_y\right] v_x(t)dt \tag{4.11b}$$

This method was applied to our data set and the result can be seen in Figure 4.4. It can be observed that there is a poor correlation between the reconstructed racing line and the reference track boundaries. This may be acceptable if the goal was relative comparisons between data sets; however, when trying to compare lap simulations to onboard measurement, the data needs to be represented in the same reference frame.

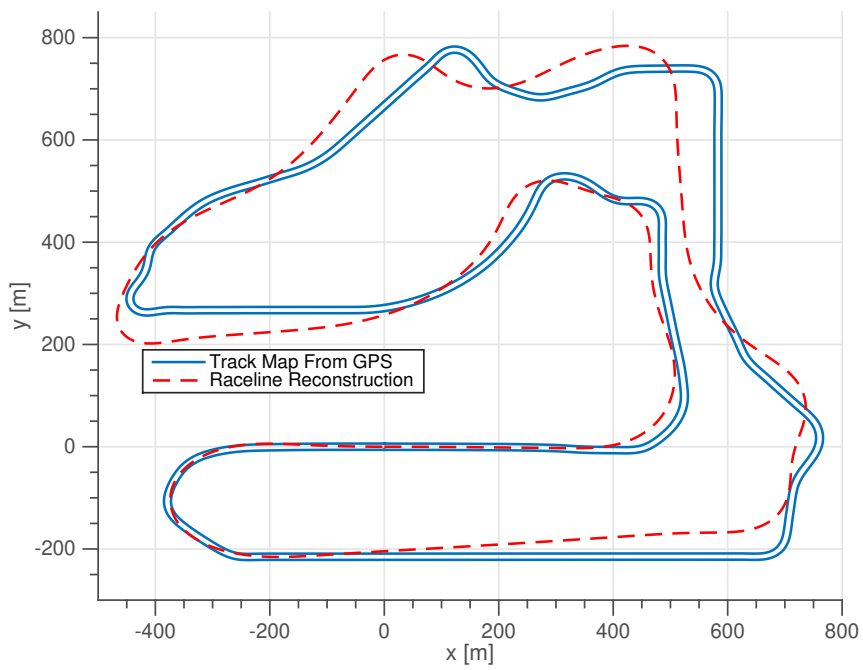

Figure 4.4: Comparison of racing line reconstruction [5] to track map derived from GPS.

4.3.2 Optimal Control Approach

In order to reconstruct a smooth racing line from measurement, a base vehicle model is used to ensure natural vehicle motion. The particle motion model is a good choice because of its simplicity while retaining the capability of modeling minimum-time vehicle maneuvering problems [163]. In fact, very few parameters are necessary to characterize a vehicle using this model. Simple dynamic lags are used that model the vehicle specific dynamics (powertrain, suspension, tires, etc.). As derived in [172], the particle (center of gravity of the vehicle) motion in path intrinsic coordinate can be written as:

$$\dot{s} = \frac{v_t \cos(e_\psi)}{1 - e_y\, c(s)} \tag{4.12a}$$

$$\dot{v_t} = a_t \tag{4.12b}$$

$$\dot{e}_\psi = \frac{a_n}{v_t} - v_t \cos(e_\psi) \frac{c(s)}{1 - e_y\, c(s)} \tag{4.12c}$$

$$\dot{e}_y = v_t \sin(e_\psi) \tag{4.12d}$$

$$\dot{a_t} = 1/\tau_t\,(u_1 - a_t) \tag{4.12e}$$

$$\dot{a_n} = 1/\tau_n\,(u_2 - a_n) \tag{4.12f}$$

Here, the subscripts $(\cdot)_t$ and $(\cdot)_n$ denote directions tangential and normal to the path. Velocity is represented by v and acceleration by a. The path intrinsic coordinates (which can be seen in Figure 4.5) describe the vehicle motion as a lateral deviation from the path centerline (e_y) and heading angle deviation (e_ψ). The heading angle deviation (e_ψ) is defined as the difference between the path heading angle (ψ_s) and the vehicle heading angle (ψ_v). The subscripts $(\cdot)_v$ and $(\cdot)_s$ are used to denote vehicle and path, respectively. The inputs ($\mathbf{u} = \begin{bmatrix} u_1 & u_2 \end{bmatrix}^T$) control tangential and normal vehicle motion and operate through lags τ which model the specific vehicle's transient behavior. The curvilinear distance along the path centerline is denoted as s. The models states are: $\mathbf{x} = \begin{bmatrix} s & v_t & e_\psi & e_y & a_t & a_n \end{bmatrix}^T$.

Finally, the above vehicle model can be written by:

$$\dot{\mathbf{x}} = g(\mathbf{x}, \mathbf{u}, t) \tag{4.13}$$

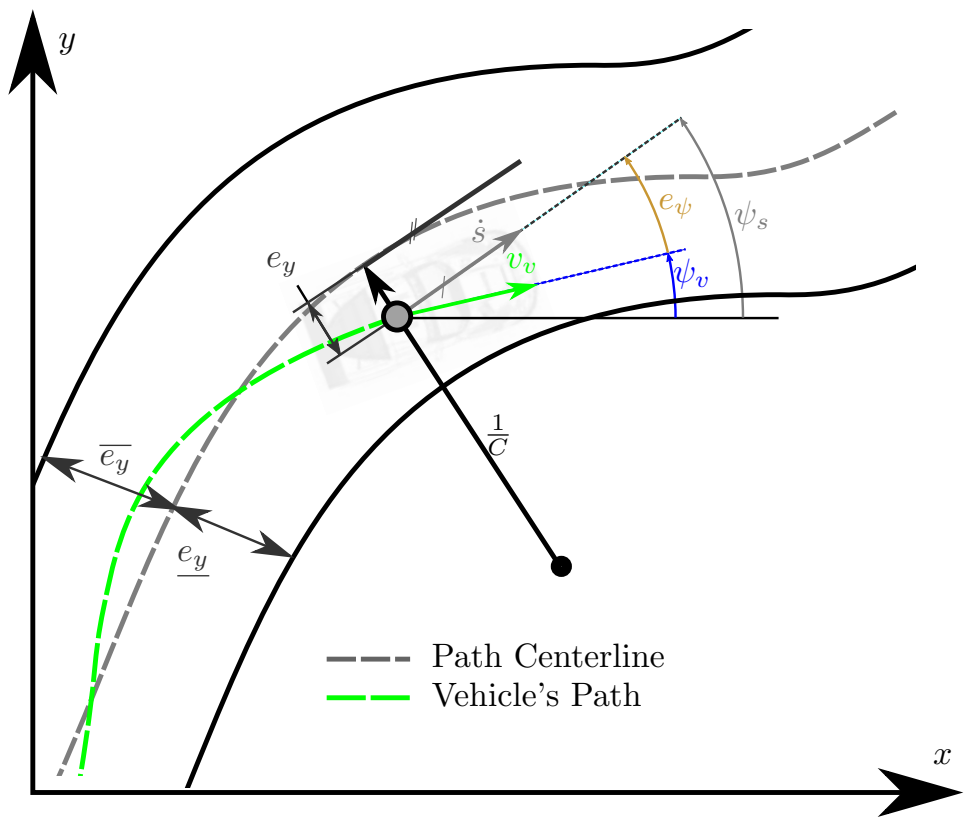

Figure 4.5: Path intrinsic coordinate description. Note subscripts s and v refer to the path and vehicle frame respectively.

With the above model of the vehicle motion, the racing line reconstruction can be

accomplished by solving the following optimal control problem:

$$
\begin{aligned}
\min_{\mathbf{u}} \quad & J = \int_{t_0}^{t_f} ||\hat{\mathbf{x}} - \mathbf{x}||_Q^2 + ||\mathbf{u}||_R^2 \, dt \\
s.t. \quad & g(\mathbf{x}, \mathbf{u}, t) - \dot{\mathbf{x}} = 0 \\
& |e_y| \leq \overline{e_y} \\
& t \in \hat{t} \\
& s \in s_{track} \\
& v_{t0} = v_{tf}, \; e_{y0} = e_{yf}, e_{\psi 0} = e_{\psi f}
\end{aligned}
\tag{4.14}
$$

The problem is written to find the optimal inputs $\mathbf{u}$ to the particle motion model that best fit our measured vehicle states ($\hat{\mathbf{x}}$), subject to the motion dynamics and the track width constraints ($\overline{e}_y$). The time duration for the problem should span the time from vehicle measurements and the curvilinear distance along the path should span the distance of the track from our reference track model ($c(s)$). Finally, the initial and final states of position and velocity are collocated to enforce a cyclic boundary condition found on a racing lap. The matrices Q and R are diagonal weighting matrices used to adjust the fit relative to the measured states and control effort, respectively.

4.4 Results and Discussion

4.4.1 Racing Line Reconstruction at Sebring

In this section, vehicle measurement taken during a test session at Sebring International Raceway will be used along with the reference track model fit in Section 4.2 to reconstruct the racing line taken during a test. First, the onboard vehicle measurements are preprocessed. Each signal is filtered with a Chebyshev type II filter [173] as described in the racing line reconstruction method offered in [5]. Next, the measurements are rotated from the body fixed x, y coordinates, to the particle's tangential and normal coordinates (t, n) via the vehicle slip angle $\beta = \arctan(v_y/v_x)$ [174]. Finally, the previously described optimal

Parameter	Description	Value
$Q_{2,2}$	Weight on v_t	1.00
$Q_{5,5}$	Weight on a_t	0.01
$Q_{6,6}$	Weight on a_n	0.01
$R_{1,1}$	Weight on u_1	0.01
$R_{2,2}$	Weight on u_2	0.01
τ_{an}	Normal acceleration lag	0.07s
τ_{at}	Tangential acceleration lag	0.07s

Table 4.1: Table of parameters used in the racing line reconstruction.

control algorithm (4.14) can be solved. As with the track model fitting problem, the racing line reconstruction optimal control problem (4.14) was solved using orthogonal collocation techniques implemented GPOPS-II [111]. This software does an efficient job of transcribing the optimal control problem into a finite dimensional nonlinear programming problem and includes built-in mesh refinement which helps approximate the continuous control signal. The parameters we used in our formulation of the problem are listed in Table 4.1.

Figure 4.6 shows the measured states of the vehicle compared to the adjusted values from the racing line reconstruction algorithm. It can be seen that minor corrections to the measurements are applied by our racing line reconstruction algorithm such that the trajectory does not violate the track width constraints. The reconstructed racing line overlaid on the track map can be seen in Figure 4.7 along with the racing line as a function of curvilinear distance along the track centerline ($e_y(s)$). It can be clearly seen that, compared to Figure 4.4, our racing line reconstruction gives an accurately reconstructed racing line that lies within the boundaries of the track.

4.4.2 Driver Comparison

While these results demonstrate the effectiveness of the algorithm, a comparison between drivers will further motivate the importance of reconstructing the racing line. From this test session, two experimental runs with identical vehicle setups but two *different* drivers are fed through our optimal control based racing line reconstruction algorithm and

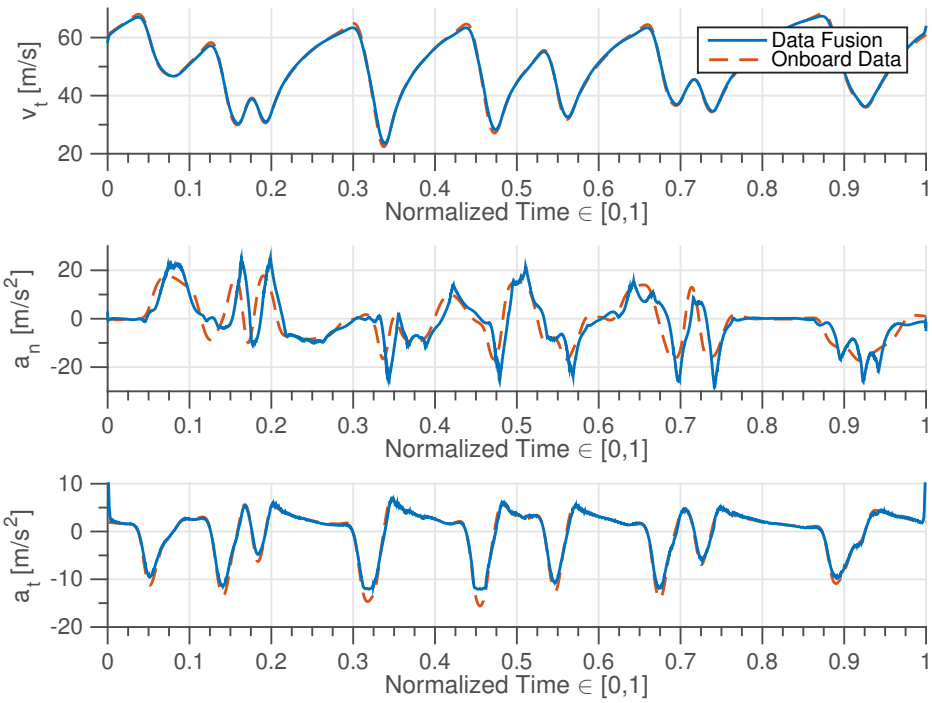

Figure 4.6: Results of the racing line reconstruction for Driver A.

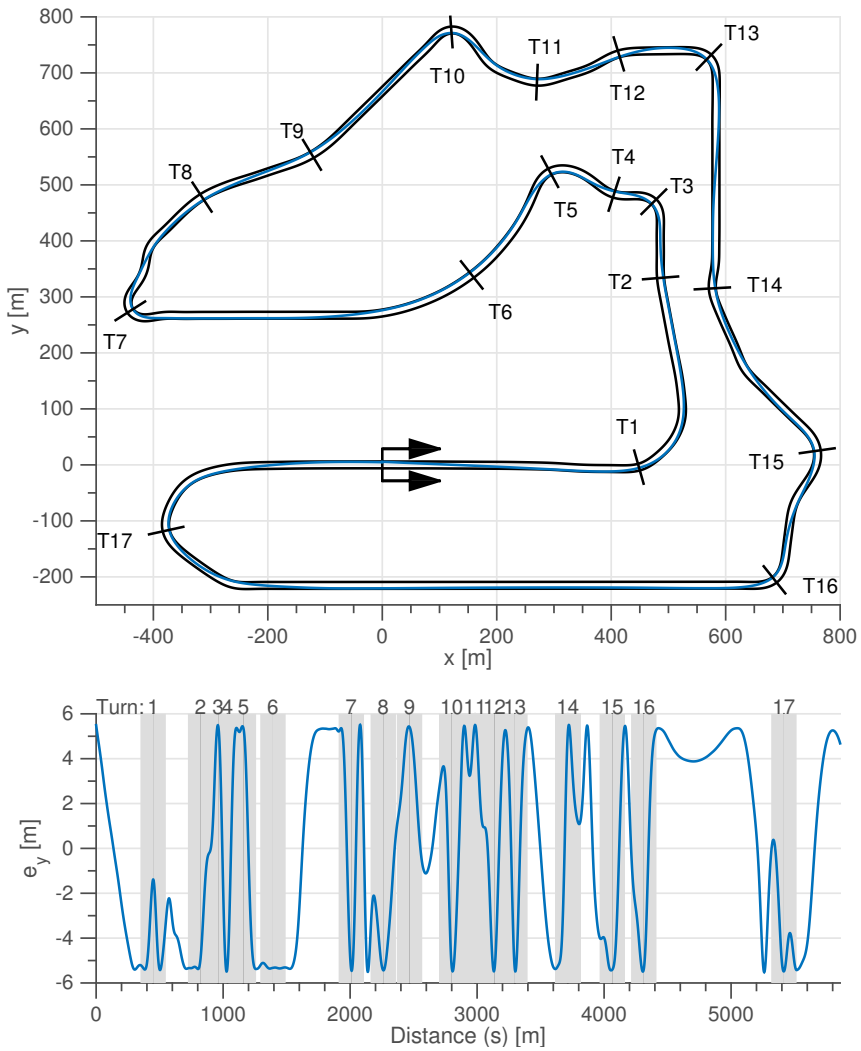

Figure 4.7: Results of racing line reconstruction on measurements from Driver A.

compared. The two lap times were separated by only 0.06%. This minor difference can easily be explained in experimental factors such as the different times of day that the two runs were conducted, ambient air and track temperature differences, differences in track friction evolution as other cars negotiate the circuit, etc. These factors considered, the two drivers were able to achieve nearly identical performance. While the maneuvering time performances were practically identical, the vehicle states and trajectory deviated considerably. To facilitate comparison, we will use split channels to compare the differences between the two runs. They provide a convenient mechanism for comparing two data sets and they are formally defined as:

$$\Delta y = y(s)|_{driverA} - y(s)|_{driverB} \tag{4.15}$$

where y can be any signal to compare.

Figure 4.8 shows the split velocity and split racing line taken by the two drivers. It can be seen that while the speed only varies a few m/s at key locations, the racing line varies by as much as 2m over the course of the lap which is significant (Note: Δe_y does reach over 4m between turns 16 and 17 and on the front straight; however, this was driver B returning to the center of the track and has little effect on the maneuvering time).

Key sections where a difference in driving style can be observed is turn 6 (denoted as T6 in Figure 4.7) through turn 7 (denoted as T7). The data traces of the split channels and trajectories during this section of the track can be seen in Figures 4.9 and 4.10. Driver B carries more speed through turn 6 but then slows more in the straight before turn 7 staying close to the center of the track, braking in a straight line, and 'setting up' turn 7 sooner rather than carrying more speed into the entrance of turn 7 as driver A does. The result is driver B has more speed at the apex through the exit of corner 7. The result is very similar maneuvering times through the segment ($\leq 0.04s$ difference) but the drivers accomplish the segment with two different styles. Driver A carries more speed into turn 7 while driver B apexes the turn earlier and exits at a faster velocity.

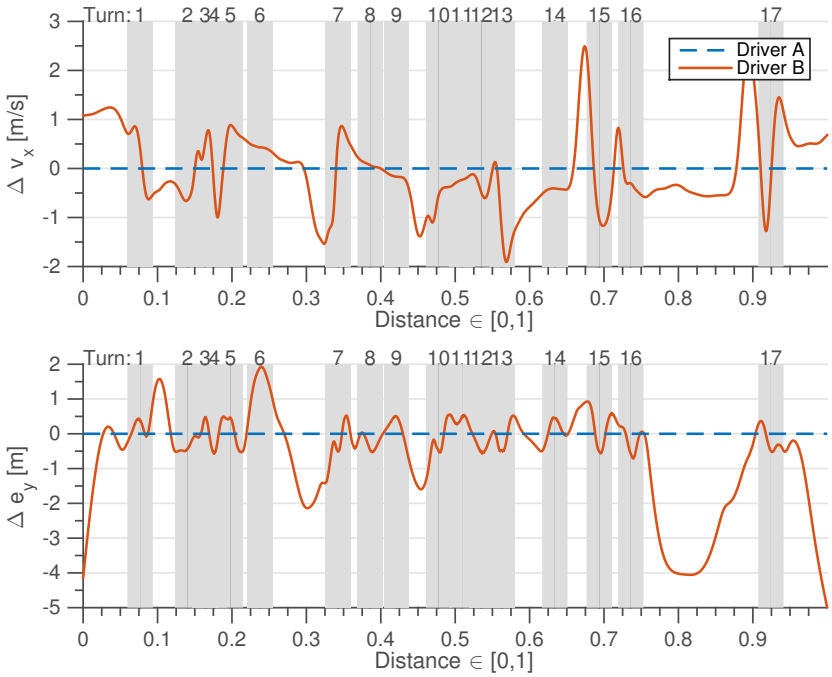

Figure 4.8: Comparison of the split velocity and split racing line between drivers A and B.

Different trajectories with identical performance demonstrate there are multiple local minima with respect to global maneuvering time. Using our reconstruction technique, we are able to compare the racing line taken by each driver and gain insights on different actions taken by the two drivers.

Local minima are discussed in our previous work [22], where a hybrid Model Predictive Control (MPC) cost was used to more closely model the inherent sub-optimality of the minimum-time maneuvering problem. In this work, we are able to see that multiple controllers achieved identical maneuvering times while taking different trajectories. As evidenced in Figures 4.8-4.10, different driving styles are able to demonstrate nearly equivalent performance thereby corroborating our previous work [22].

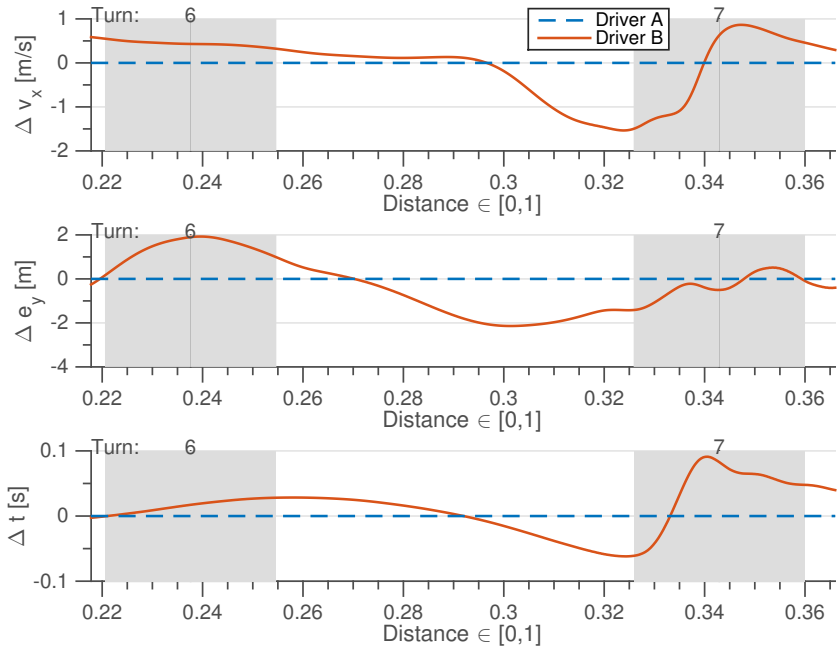

Figure 4.9: Comparison of the split velocity and split racing line between drivers A and B.

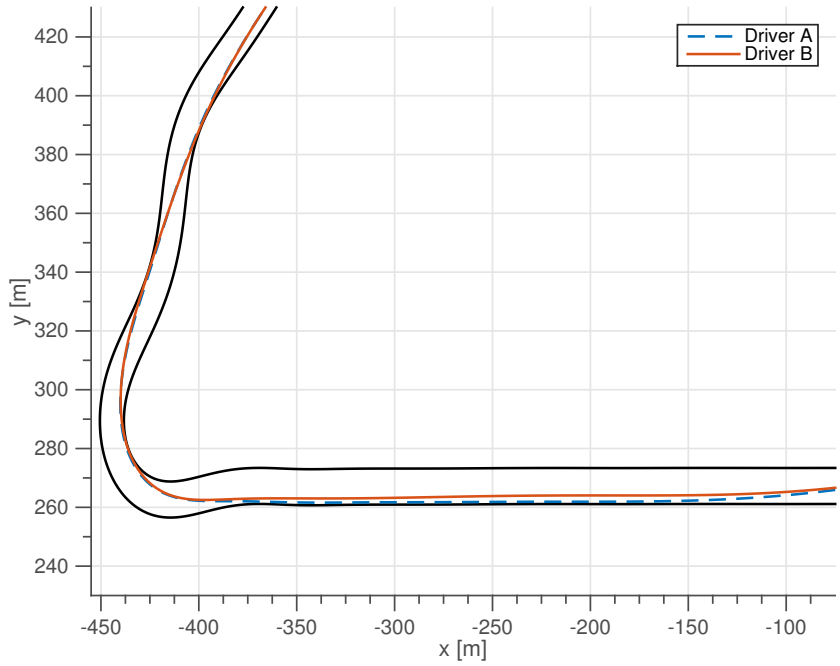

Figure 4.10: Comparison of the driving lines of drivers A and B between at turn 7.

4.5 Conclusions

Typical methods of racing line reconstruction prevent a close comparison of simulation to actual measurements. Since modeling and simulations are conducted with respect to a track model and the onboard inertial data is measured without this reference, it is often difficult to make accurate comparisons. In this chapter, we first fit a reference track model from GPS data using optimal control techniques. We then used this track model ($c(s)$) along with onboard vehicle measurements and a particle motion model to reconstruct the driven racing line. This estimate of the racing line is the line that best fits the measured data while obeying the track width constraints of the track model. This reconstruction scheme was exercised for the case study of two drivers on the same vehicle setup at Sebring International Raceway. Both data sets were used with a track model of Sebring to reconstruct the drivers' racing lines.

With both tests' racing lines reconstructed using the Sebring track model, a comparison of the driving styles between drivers was possible. The two drivers achieved identical performance (albeit small difference exist in the data; but, can be accounted for with minor environmental changes that occur during the experiment) while utilizing a fairly different driving style. A difference in racing lines of 2m can be observed in key locations of the circuit. These differences in driving styles help corroborate the conclusion that there are indeed multiple local minima that exist in the minimum-time solutions space. Understanding of the driving style differences can help with tuning and design of the vehicle systems (e.g. tires, suspensions, etc.) to suit a particular driver or driving style.

Future work aims at using the proposed technique for racing line reconstruction towards developing mathematical/computational models that explain the driving styles of high-performance drivers.

Chapter 5

A Cascaded Optimization Approach for Modeling a Professional Driver's Unique Driving Style

Abstract

In the context of minimum-time vehicle maneuvering, previous works have shown that different professional drivers drive differently while achieving nearly identical performance. These differences are typically attributed to the driving style of the individual driver. In this chapter[1], we present a cascaded optimization framework for modeling individual driving styles. Therein, an inner loop Model Predictive Controller (MPC) finds the optimal vehicle inputs that minimize a blended-cost function over each receding horizon. The outer loop of this framework is an optimization computation which finds the optimal weights for each local MPC horizon that best fit data obtained from onboard vehicle mea-

[1]This chapter has been submitted for publication: J. R. Anderson and B. Ayalew. A cascaded optimization approach for modeling a professional drivers unique driving style. Vehicle System Dynamics (Submitted, under review), 2018.

surements to the simulation of the maneuver. This cascaded optimization is exercised for a case study on Sebring International Raceway where two different professional drivers were able to achieve nearly identical lap times while adopting different driving styles. It will be shown that this framework is able to model key differences in style between the two drivers during a particular corner. The models of the individual drivers are then fixed, and a final optimization is used to tune tire parameters to suit each driving style and illustrate the importance of modeling the individual driver.

5.1 Introduction

Modeling the human component of ultra-high-performance driving is of key interest to the motorsports and high-performance automobile industry. In the motorsports industry, the vehicle is tuned, and in some cases designed, with a particular driver or small set of drivers in mind. The same situation occurs with automakers of high-performance vehicles. Typically, they employ a small team, ranging from one to just a few key engineers, to lead the vehicle tuning efforts and sign-off on the final design. In both situations, the individual driving preferences and driving styles of these drivers are imprinted on the basic feel and setup of these vehicles. In this chapter, we refer to driving style as the different control strategies that drivers tend to use to accomplish their goals. This can be seen in the different racing lines that they take. Some drivers will tend to brake early for a turn to set up the exit of the corner sooner than others while some execute the opposite, and carry much more speed into a turn and apex the corner later. Considering these differences in style, the ability to understand and mathematically model differences between professional drivers is essential to advancing simulation efforts.

Previous works have demonstrated that different human drivers are able to achieve equivalent performance using a very different set of control histories and vehicle trajectories. In [33], Dominy states: "it is the authors' experience that two top racing drivers may describe quite different techniques for driving the same car through a particular turn". The

works in [11] and [23] have demonstrated that two drivers with an identical vehicle are able to achieve equivalent performance while adopting different racing lines. These differences can be attributed to the individual driving styles among these professional drivers.

Literature suggests that Model Predictive Control (MPC) provides a good foundation for modeling the human driver's decision process [18, 5]. In this work, we will use a cascaded optimization structure where an inner loop utilizes a multi-objective or blended-cost MPC while an outer loop optimization varies the weights used on the multiple objectives in each MPC horizon. The local MPC cost function is capable of blending the objectives of minimizing time over the MPC horizon and maximizing velocity at the exit of the MPC horizon. This particular cost structure was motivated by the work in [175, 19], which states that over a short segment, it can be advantageous to global maneuvering time to maximize the exit velocity rather than minimize time over the segment. This is true especially when the track section consists of a curve followed by a long straight. In our previous work [22], we used the cascaded optimization strategy to show that by varying the objectives between key horizons, the blended-cost MPC could outperform a traditional time-optimal MPC. In traditional MPC, the global objective of minimizing time over the maneuver is approximated by minimizing time in every MPC horizon. Not only was the cascaded optimization able to outperform the traditional MPC, it was shown that identical lap time performance could be achieved while adopting different trajectories and control histories. We attributed these local minima in the solution space to different driving styles. In this chapter, we aim to expand on our previous work and use the cascaded optimization framework along with onboard vehicle measurements to model differences between actual drivers. Specifically, we will use the outer loop of our cascaded optimization to find the objectives used in each local MPC horizon that give the optimal match of the simulated response with the proposed driver model and the onboard vehicle measurements. After extracting models of different driving styles with this approach, we will then use these models to individually optimize tire parameters that best suit the individual driver's style.

The remainder of this chapter is organized as follows. The mathematical framework

we use to model driving style is explained in Section 5.2. Section 5.3 details a case study of this approach on experimental data collected at Sebring International Raceway with two professional drivers. In Section 5.4, we will use the identified models of the two drivers in a scenario where it is desired to optimize the tire parameters. Finally, Section 5.5 offers conclusions and directions for future work.

5.2 Cascaded Optimization Framework For Modeling Driving Style

To model different driving styles, we will adapt the cascaded optimization presented in Chapter 3 as outlined in Figure 5.1. The inner loop remains a Model Predictive Controller (MPC) with a blended-cost in each MPC horizon that is capable of minimizing time or maximizing velocity at the end of the horizon. This controller calculates the optimal vehicle inputs $\mathbf{u}$ that minimize a local cost function while the outer loop searches for the optimal weights for each local MPC horizon that best match onboard vehicle measurements. Each loop is detailed in the following subsections.

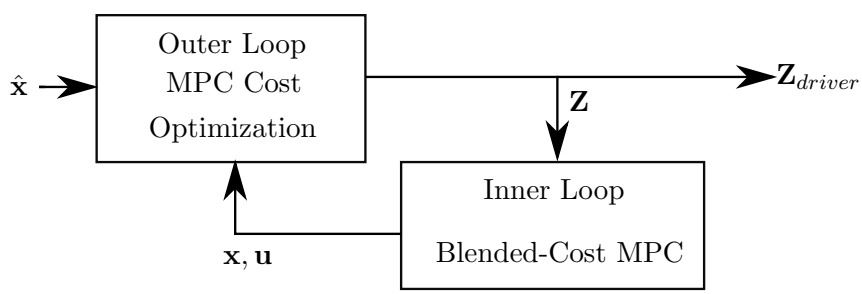

Figure 5.1: Overview of the cascaded optimization framework for modeling driving style. The reference measurements are denoted as $\hat{\mathbf{x}}$. The vehicle simulation state and control variables are $\mathbf{x}, \mathbf{u}$, respectively. The decision variables of the outer loop optimization are $\mathbf{Z}$. The output of the algorithm is the optimal set of weights that best fit the measurement $\mathbf{Z}_{driver}$.

5.2.1 Inner Loop MPC

As previously discussed, the cost function used in each MPC horizon (J_{MPC}) is a blended-cost function with two different performance objective terms. One term is used to minimize time over the MPC horizon and the other is used to maximize velocity at the end of the horizon. These terms are weighted via the weighting terms w_k, where the subscript $k \in \{t, v_x\}$ denotes either time or longitudinal velocity. The values of these terms are assigned from the outer loop optimizer for each horizon i and this is detailed in the next subsection. A regularization term is also added to the cost function that introduces 'small' penalties on each control input to avoid numerical issues that arise from singular arcs [143]. The cost function is written as:

$$J^i_{MPC}(\mathbf{Z}^i) = \underbrace{w^i_t\, t(s^i_f)}_{\text{Minimize Time}} - \underbrace{w^i_{v_x}\, v_x(s^i_f)}_{\text{Maximize Exit Velocity}} + \underbrace{\int_{s^i_o}^{s^i_f} \sum_{i=1}^{m} \epsilon_i u_i \, ds}_{\text{Regularization}} \tag{5.1}$$

where $\mathbf{Z}^i$ is the set of weights w^i_k used in each MPC horizon i. The distance at the end of the MPC horizon is denoted as s^i_f, which is $s^i_f = s^i_o + s_{horizon}$ where $s_{horizon}$ is the length of the MPC horizon and s^i_o is the initial distance of the horizon.

The MPC process itself is carried out as illustrated in Figure 5.2. The optimal control problem is solved over the first MPC horizon: $i = 1, s^1 \in \{s^1_o, s^1_f\}$, given the initial conditions $\mathbf{x}^1_o$. The problem is then advanced by the MPC update interval ($s_{MPC} = s/N$) where N is the number of MPC horizons that the full track distance (s) is divided into. The next MPC horizon ($i = 2$) is formed: $s^2 \in [s^2_o,\, s^2_f]$, $s^2_o = s^1_i + s_{MPC}$. The initial conditions for this MPC horizon are extracted from the previous horizon; i.e., $\mathbf{x}^2_o = \mathbf{x}^1(s^2_o)$. This process is then repeated recursively $N - 1$ times over the full maneuver.

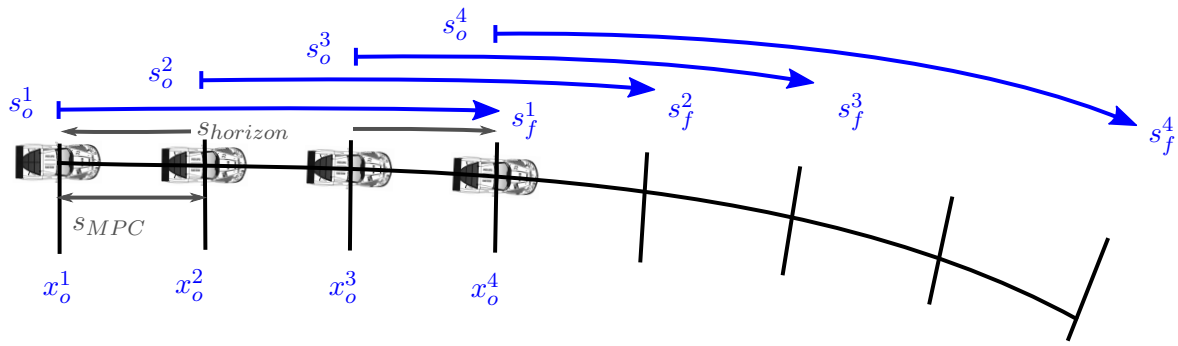

Figure 5.2: MPC Process.

5.2.2 Outer Loop MPC Weight Optimization

In this loop, the optimal weights for each MPC horizon $\mathbf{Z}_{driver}$ is found such that the simulation best matches the onboard vehicle measurements $\hat{\mathbf{x}}$. The outer loop can be written as:

$$\boxed{\begin{array}{ll} \min\limits_{\mathbf{Z}} & J_{global} = \int\limits_{s_{start}}^{s_{finish}} ||\mathbf{x}-\hat{\mathbf{x}}||^2_{\mathbf{Q}} + ||\mathbf{u}-\hat{\mathbf{u}}||^2_{\mathbf{R}}\, ds \\ & \boxed{\begin{array}{l} \text{Sub MPC Problem:} \quad for\ i = 1, 2, ..., N-1 \\ \hline \text{Optimal Control Problem (3.29)} \\ \\ s.t. \quad s_f^i = s_o^i + s_{horizon} \\ \qquad s^i \in \left[s_o^i, \quad s_f^i \right] \\ \qquad s_o^{i+1} = s_o^i + s_{MPC},\ s_{MPC} = s/N \\ \qquad \mathbf{x}_o^{i+1} = \mathbf{x}^i(s_o^{i+1}) \end{array}} \\ & w_k^i \in [0,1] \end{array}} \tag{5.2}$$

where $\mathbf{Z}$ is the decision variable of the outer loop and contains the set of weights ($w_k^i,\ k \in \{t, v_x\}$) to be used over each local MPC horizon. In other words:

$$\mathbf{Z} = \left[\begin{array}{cccc} Z^1 & Z^2 & \dots & Z^{N-1} \end{array} \right]^T = \left[\begin{array}{cc|cc|c|cc} w_t^1 & w_{v_x}^1 & w_t^2 & w_{v_x}^2 & \dots & w_t^{N-1} & w_{v_x}^{N-1} \end{array} \right]^T \tag{5.3}$$

where $i = 1, 2, ..., N-1$ is the index for the individual MPC horizon. Therefore, the global set of weights is $\mathbf{Z} \in \mathbb{R}^{2(N-1)}$. Furthermore, each element of $\mathbf{Z}$ is constrained such that $w_k^i \in [0, 1]$. The term $\mathbf{Q}$ is used to tune the outer loop optimization process and place emphasis on the key states to match between the vehicle simulation with the proposed driver model and the onboard measurement data. Note that the vector $\mathbf{Z}_{driver}$ represents the identified driver model corresponding to the onboard vehicle measurement data under consideration.

5.3 Results: Case Study on Sebring International Raceway

In this section, the mathematical framework previously presented will be applied to a case study at Sebring International Raceway [171]. The experimental setup is as follows: two different professional drivers drove a session on Sebring in a Grand Touring (GT) race car. After the tires warmed up, their lap times were separated by only 0.06%. This minor difference can easily be accounted for considering the two different times of day the vehicle was run, the change in ambient air temperature, change in track temperature, and grip evolution due to the other vehicles running on the circuit. Considering these things, the two lap times can be considered identical. There were locations on the circuit where the drivers exhibited different styles, and their trajectories varied considerably even though the maneuvering times were identical. One such key location is Turn 17 (T17) which can be seen in the track map in Figure 5.3. We chose to concentrate on this turn only in this chapter because the cascaded optimization with the adopted solution methods is highly computationally intensive to analyze the full track tractably. By concentrating on this section of track, we were able to achieve a tractable solution while modeling the differences between the two drivers. The section around Turn 17 was selected (as shown in Figure 5.3) because the two drivers were able to achieve identical maneuvering times over the section (see tabulated results in Table 5.3 in Section 5.4) and the selected section had nearly identical boundary conditions between the two drivers ($\mathbf{x}_{driverA}(s_{start}) \approx \mathbf{x}_{driverB}(s_{start})$, $\mathbf{x}_{driverA}(s_{finish}) \approx \mathbf{x}_{driverB}(s_{finish})$.

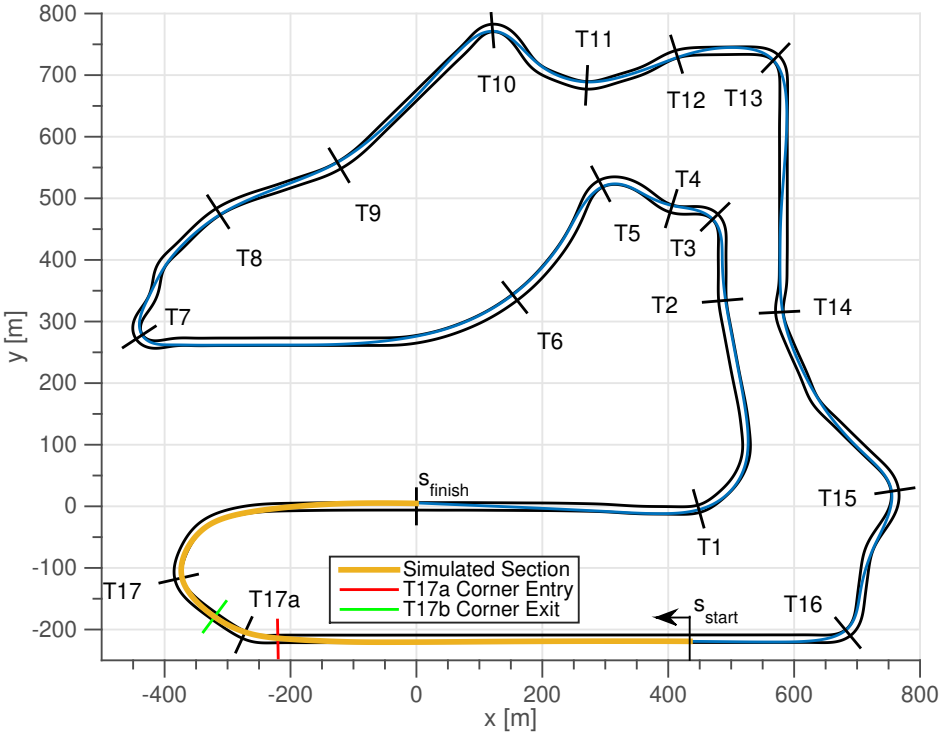

Figure 5.3: Map of Sebring International Raceway.

5.3.1 Problem Setup

The first step in the simulation process is estimating the vehicle state information from onboard measurements. These state and control estimates ($\hat{\mathbf{x}}$ and $\hat{\mathbf{u}}$) are to be used in the outer loop optimizations of (5.2). In this case study, the vehicle was equipped with a limited set of sensors; specifically, steering wheel angle, lateral and longitudinal acceleration, lateral and longitudinal velocity, and yaw rate; but, no GPS. In order to reconstruct the racing line ($e_y(s)$) and transform the measurements from the temporal domain into functions of the path distance traveled, the racing line reconstruction technique we outlined in our previous work [23] was used. The technique entailed fitting a track model (curvatures versus path distance, $C(s)$) using optimal control methods and measurements of the track boundaries. Then, the racing line was reconstructed using an optimal control problem that finds the optimal inputs to a particle motion model that best matches the particle motion to the onboard vehicle measurements subject to the track boundaries. By using this simple particle motion vehicle model, and a reference track model ($c(s)$) sensor noise and integration errors that typically make reconstructing the racing line problematic can be alleviated. The result of this step is the full reference measurements and inputs ($\hat{\mathbf{x}}$ and $\hat{\mathbf{u}}$) for each driver that we wish to model with the cascaded optimization framework.

The cascaded optimization structure outlined in Section 5.2 was then applied to the processed measurements obtained from each driver. For the inner loop, GPOPS-II was used to solve the optimal control problem in each horizon [111]. GPOPS-II is a general purpose optimal control software that uses a direct pseudospectral collocation method to transcribe the optimal control problem into a finite dimensional nonlinear programming problem (NLP). This software also features a mesh refinement scheme which better approximates the continuous nature of the dynamics studied. In setting up this solver, we chose to use automatic differentiation to generate derivative information (adigator was the specific software used [176]). IPOPT [177] was the general purpose NLP solver used by GPOPS-II. In the outer loop, we applied MATLAB's Genetic Algorithm (GA) implementation from their global optimization toolbox [165] to find the optimal cost function weights ($\mathbf{Z}$) used

in each MPC horizon. The nature of this problem is exploiting the local minima observed in the solution space to explain driving style differences, and as such, a global solver is necessary to explore the solution space.

Next, the weights in the matrix $\mathbf{Q}$ in (5.2) were adjusted to properly scale all cost function terms. The weighting matrix is a diagonal matrix where each diagonal entry can be factored into a weighting term and a scaling term; i.e.,

$$\mathbf{Q} = \begin{bmatrix} q_{1,1}/s_{1,1} & & 0 \\ & \ddots & \\ 0 & & q_{n,n}/s_{n,n} \end{bmatrix} \tag{5.4}$$

To properly scale each term in the cost function, a baseline time-optimal MPC simulation was used with all weights set to unity (i.e., $q_{j,j} = 1$) and the scaling factor $s_{j,j}$ were adjusted such that the state contribution of each state to the total costs is unity. In other words, we selected $s_{j,j}$ such that:

$$\int \frac{1}{s_{1,1}} ||\hat{v}_x - v_x||^2 \, ds = 1, \int \frac{1}{s_{2,2}} ||\hat{v}_y - v_y||^2 \, ds = 1, \ \ldots, \int \frac{1}{s_{5,5}} ||\hat{e}_\psi - e_\psi||^2 \, ds = 1 \tag{5.5}$$

With proper scaling between terms in the cost function, the weighting components $q_{j,j}$ can be used to place emphasis on the desired states in the cascaded optimization (5.2). The same strategy was taken for the control portion of the cost function, i.e., the weights in the matrix $\mathbf{R}$. The final weights used in our results are given in Table 5.1.

In order to compare detailed data between drivers, we use split channels (denoted by Δ) which provide a convenient mechanism to visualize differences. These channels can be formally defined as:

$$\Delta y = y(s)|_{driverA} - y(s)|_{driverB} \tag{5.6}$$

where y can be any signal we seek to compare for the two drivers, driver A and driver B.

Weight	State/Control	Value
$q_{1,1}$	v_x	12
$q_{2,2}$	v_y	0.1
$q_{3,3}$	$\dot{\psi}$	1
$q_{4,4}$	e_y	10
$q_{5,5}$	e_ψ	2
$q_{6,6}$	t	7
$r_{1,1}$	δ	1
$r_{2,2}$	κ_{fl}	0.25
$r_{3,3}$	κ_{fr}	0.25
$r_{4,4}$	κ_{rl}	0.25
$r_{5,5}$	κ_{rr}	0.25
$r_{6,6}$	F_{zfl}	0.25
$r_{7,7}$	F_{zfr}	0.25
$r_{8,8}$	F_{zrl}	0.25
$r_{8,9}$	F_{zrr}	0.25

Table 5.1: Table weights used in (5.2).

5.3.2 Results

The drivers' measured velocities, split velocity, and split time traces during Turn 17 (T17) are compared in Figure 5.4(a). While absolute correlation is not achieved between measurement and simulation (Figure 5.4(b)), the differences of driver B compared to driver A are preserved in the simulation. Absolute correlation is quite difficult especially considering the relatively simple vehicle model chosen; however, model simplicity was necessary to make this problem tractable. Also, the characterization of tire frictional properties is challenging as it can vary with everything from ambient conditions to the location on the track. Despite this, the relative differences between drivers observed in the measurements are also preserved in the simulations. It can be seen that driver B tends to brake later than driver A (i.e., retains a higher velocity longer than driver A, see $s \approx 5,225m$ in Figure 5.4(b)). Also, driver B tends to apex the corner earlier (i.e., the point of maximum curvature in the racing line which also occurs approximately where the drivers place their minimum speed for this turn, see $s \approx 5,445m$). The general shape of the split velocity curves is preserved well between the two drivers. Driver B gains a speed advantage right at the entrance of

Turn 17a (T17a), then loses some of that speed advantage at the exit of the corner before making up the difference afterward. The split time traces are very similar in shape as well.

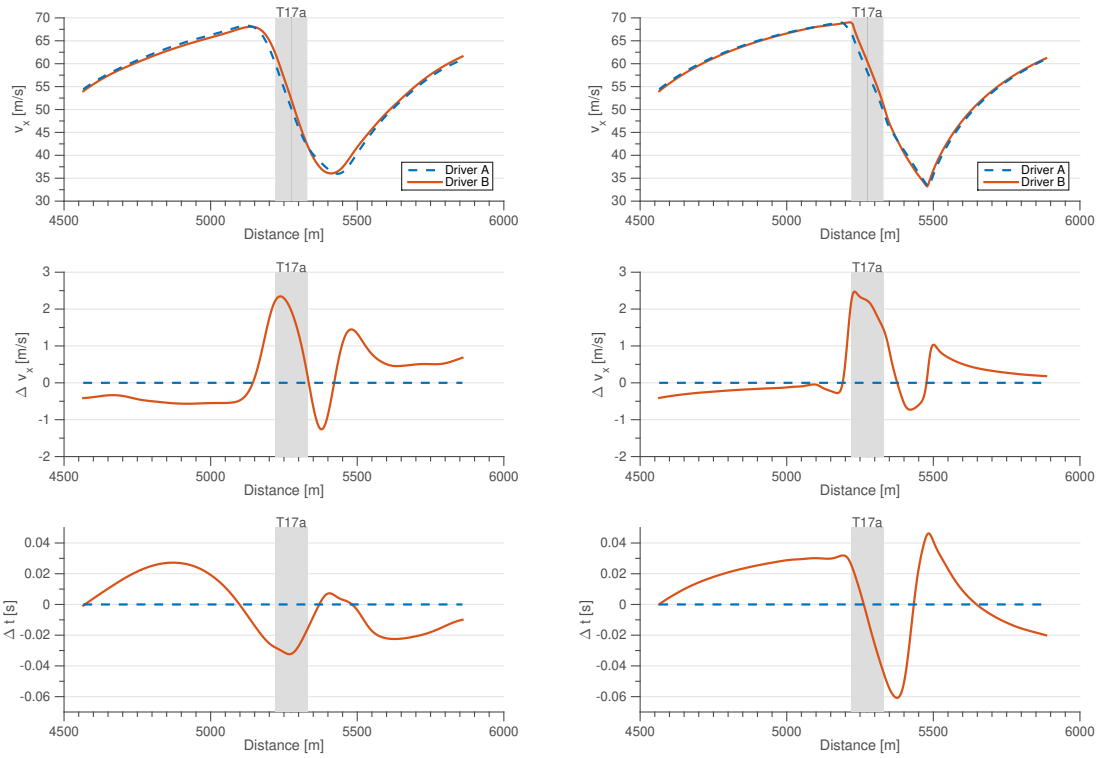

(a) (b)

Figure 5.4: Longitudinal velocities (v_x), split velocities (Δv_x), and split times (Δt) of Driver A and B for (a) measurement and (b) simulation.

While the key driving style differences (late braking and early apexing) observed for driver B were seen in both measurement and simulation, the racing line differences were not as clear. Figure 5.5 shows the split racing lines for the two drivers over this maneuver. Much of the differences are present in the straight sections of the maneuver where driver A would tend to return to the center of the track and driver B would not. This particular style difference has minimal impact on the global maneuvering time and is not able to be captured in our simulation. In order to capture this effect, the MPC inner loop would need

to be augmented to include a term to penalize lateral deviation of the vehicle. Alternatively, much more emphasis would need to be placed in matching the racing line in $\mathbf{Q}$. This was tried; however, matching racing line more closely comes at the expense of a good correlation in the velocity traces which we believe to be the most important feature to capture. The racing line that can be seen in the measurements and simulations lines up much better during Turn 17a and this can be seen in the trajectory plot of Figure 5.5. Driver A tends to stay more towards the outside of the corner than driver B.

The absolute correlation issue can also be observed in the trajectories during Turn 17a. While the simulated vehicles use all of the available track width, the vehicles in measurement do not. This is due to the nature of the physical corner that exists on this particular track, which is an old runway that exhibits a very rough vertical profile. In the measurements, the real drivers are able to negotiate the corner while avoiding vertical inputs that can disrupt the vehicle balance while we neglect this fidelity in our simulation. Again, absolute correlation was not the goal of our work; instead, we concentrated on a framework of representing style differences between the two drivers. Future work could look at increasing model fidelity to capture these effects (methods of incorporating this modeling detail have been researched in [45, 169]; however, the increased modeling detail has an increased computational cost, and this is traded-off with tractability of the problem.)

The mechanism that allows the vehicle simulation to capture these key differences in driving behavior is the variable MPC objectives that are allowed to change between horizons around the track. The optimal parameters for each driver are denoted as $\mathbf{Z}_{driver}$. Figure 5.6 shows how the optimal weights ($\mathbf{Z}_{driver}$) vary between the two drivers. It can be seen in a couple of key horizons that driver B chooses a heavily weighted velocity optimal cost just before the areas where he has a higher split velocity. These varying weights between driver A and B are able to capture the late braking behavior and early apex exhibited by driver B.

The results from these simulations are two distinctly different mathematical models (i.e., MPC with weights in $\mathbf{Z}_{driverA}$ and $\mathbf{Z}_{driverB}$) that capture the key differences between

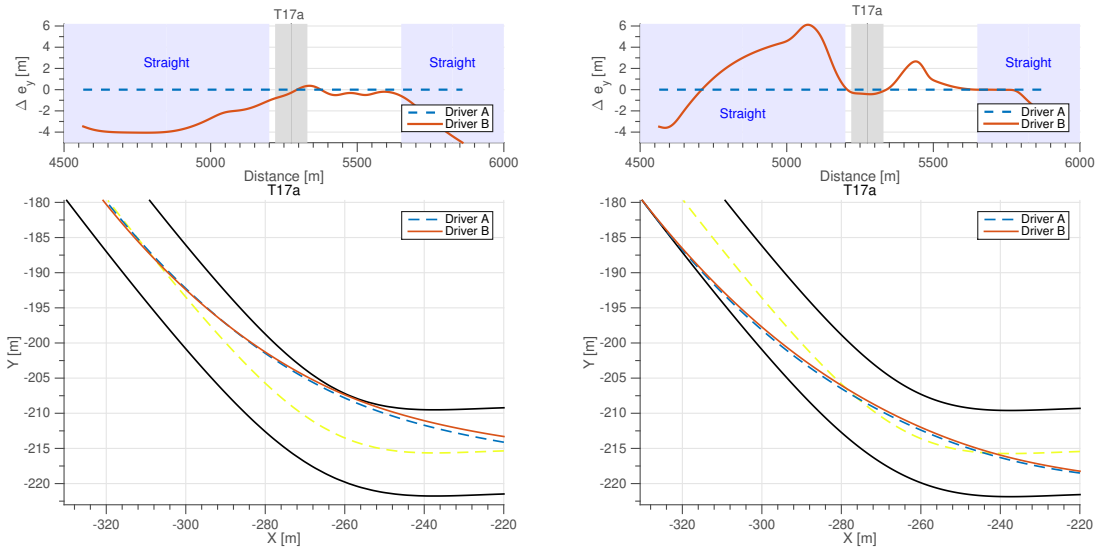

(a) (b)

Figure 5.5: Split racing line (Δe_y) and trajectories of Driver A and B for (a) measurement and (b) simulation in the turn 17a (T17a).

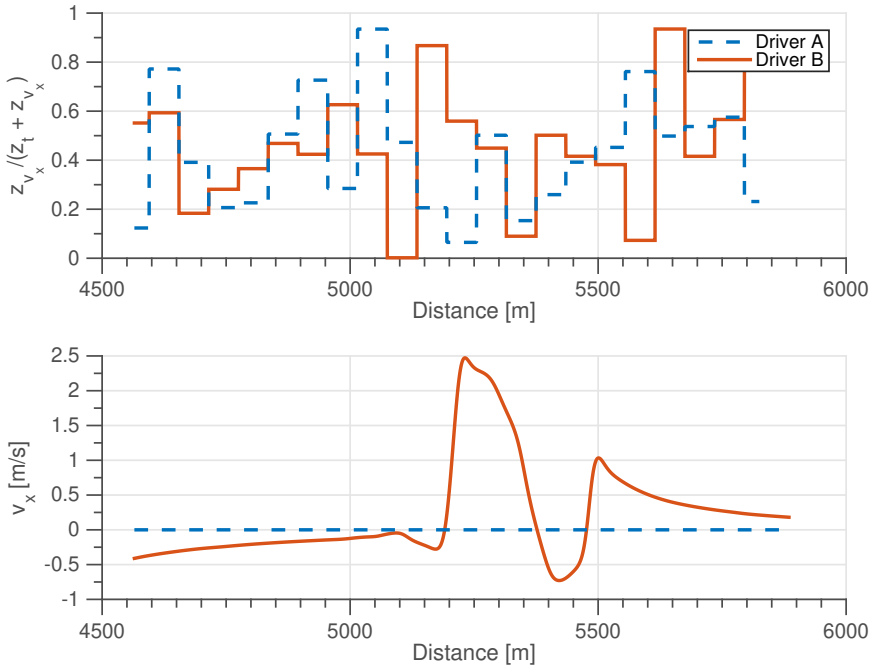

Figure 5.6: Contribution of exit velocity optimal weight ($w_{v_x}/(w_t + w_{v_x})$) for each driver and the split velocity trace (Δv_x).

these drivers while respecting nearly identical maneuvering times achieved in both simulation and measurement (see Table 5.3 in Section 5.4). In the subsequent section, we will use these models to perform virtual tire tuning for individual drivers.

5.4 Tire Optimization for a Given Driving Style

In a vehicle development program, there is an established supplier submission process, especially for tires. In this process, several tire variants are manufactured by the supplier and submitted to the vehicle manufacturer. A development test driver then subjects each variant to a battery of tests and each construction is then judged. In high-performance vehicle programs, lap time is a key metric used to sort tire variants. Armed with the conclusions from each construction, the tire designer then makes design decisions to prepare for the next submission. This iterative process is repeated until a final construction is then chosen that satisfies all of the vehicle manufacturer's requirements.

In this section, we will use the previously identified driver models ($\mathbf{Z}_{driverA},\ \mathbf{Z}_{driverB}$) for each of the drivers to virtually tune the tire to suit each driving style. To that end, we will construct a scenario that the tire friction balance can be shifted by 5% from the front to the rear axle, but the total frictional capability is constrained equivalent to the baseline case. The tire's longitudinal and lateral forces are modeled in the simplified Pacejka formulation as:

$$F_x(F_z, \alpha, \kappa) = \lambda_{1,2}\, F_z\, \mu_x(F_z)\, \sin\left(Q_x \arctan\left(S_x \sqrt{\alpha_n^2 + \kappa_n^2}\right)\right) \frac{\alpha_n}{\sqrt{\alpha_n^2 + \kappa_n^2}} \tag{5.7a}$$

$$F_y(F_z, \alpha, \kappa) = \lambda_{1,2}\, F_z\, \mu_y(F_z)\, \sin\left(Q_y \arctan\left(S_y \sqrt{\alpha_n^2 + \kappa_n^2}\right)\right) \frac{\alpha_n}{\sqrt{\alpha_n^2 + \kappa_n^2}} \tag{5.7b}$$

The friction coefficient is modeled as a linear function of load ($\mu_{x,y}(F_z)$) and it is modified by the current combined slip condition (terms to the right of $\mu_{x,y}$). See [45] for a complete definition of the tire model. We will use the $\lambda_{1,2}$ terms to provide a way of scaling the friction

coefficient on the front and rear axle, respectively. The front and rear axle is allowed to vary by $\pm 5\%$ while constrained such that the sum of the multipliers are identical to the baseline case: i.e, $\lambda_1 + \lambda_2 = 2$. Note that λ_1 and λ_2 modify both the lateral and longitudinal coefficient of friction (μ_x and μ_y in (5.7)). This is denoted as $\lambda_1 \mu_{x,y}(F_z)$ and $\lambda_2 \mu_{x,y}(F_z)$ for the front and rear axles, respectively. In addition to modifying the tire friction front and rear, we will also adjust the location of the slip angle where the maximum lateral force occurs. In the simplified Pacejka formulation, this is also a linear function of load; i.e., $\alpha_{max} = \alpha_{peak}(F_z)$. Again, we will introduce decision variables $\lambda_{3,4}$ to scale these terms by $\pm 5\%$ for the front and rear axles while keeping the sum of the changes equivalent to the baseline; i.e., $\lambda_3 + \lambda_4 = 2$. See also Table 5.2 for the definition of these multipliers $\lambda_1, ..., \lambda_4$. In the following, we use the short hand: $\lambda = [\lambda_1, \lambda_2, \lambda_3, \lambda_4]$. Finally, the optimization of tire selection for a particular driver (driving style) can be posed as follows:

$$
\begin{array}{ll}
\min\limits_{\lambda} & J_{global} = t(s_{finish}) - t(s_{start}) \\
 & \boxed{\begin{array}{l} \text{Sub MPC Problem:} \quad for\ i = 1, 2, ..., N-1 \\ \hline \text{Optimal Control Problem (3.29)} \\ \\ \min\limits_{\mathbf{u}} \quad J^i_{MPC}(\mathbf{Z}^i_{driver}) \\ s.t. \quad \mathbf{x}' - f(s, \mathbf{x}, \mathbf{u}, \lambda) = 0 \\ \vdots \\ s^i_f = s^i_o + s_{horizon} \\ s^i \in \begin{bmatrix} s^i_o & s^i_f \end{bmatrix} \\ s^{i+1}_o = s^i_o + s_{MPC},\ s_{MPC} = s/N \\ \mathbf{x}^{i+1}_0 = \mathbf{x}^i(s^{i+1}_o) \end{array}} \\
s.t. & \lambda_j \in [0.95, 1.05],\ j = 1, 2, ...4 \\
 & \lambda_1 + \lambda_2 = 2 \\
 & \lambda_3 + \lambda_4 = 2
\end{array}
\tag{5.8}
$$

Parameter	Description	$\lambda^*_{driverA}$	$\lambda^*_{driverB}$
λ^*_1	Multiplier on front axle friction	1.03	1.05
λ^*_2	Multiplier on rear axle friction law	0.97	0.95
λ^*_3	Multiplier on front axle slip angle at peak lateral force	0.98	1.00
λ^*_4	Multiplier on rear axle slip angle at peak lateral force	1.02	1.00

Table 5.2: Optimal decision variables for each driver.

In this problem, the outer loop searches for the optimal set of parameters $\lambda^* = [\lambda^*_1, \lambda^*_2, \lambda^*_3, \lambda^*_4]$ that minimizes the total maneuvering time in the section of interest, Turn 17 (T17). The problem is solved for each driver model ($\mathbf{Z}_{driver}$); therefore, the local MPC weight schedule is fixed per driver. The outer loop decision variables (λ) enter into the inner loop via the vehicle dynamics equations in $f(s, \mathbf{x}, \mathbf{u}, \lambda)$; specifically, the tire model (5.7). The problem is then solved similarly to the fitting process above with the outer loop being solved via MATLAB's GA implementation [165] and the inner loop's optimal control problem via GPOPS-II [111].

The optimal parameters obtained for each driver are given in Table 5.2 and the performance gains are listed in Table 5.3. It can be seen that each driver has a different set of parameters that minimize their global maneuvering time. Driver A's style has more potential than driver B with the parameters that we are tuning with; however, both drivers can benefit from the tuning. Note that the optimization chooses a more oversteering setup (decreased rear grip and/or increased rear axle slip angle) for both drivers which corroborate the authors' experience that this setup is ideal for optimal maneuvering times. This scenario is used to motivate the possible uses of this framework and demonstrate that different drivers not only drive differently, there maybe be a different set of parameters that best suit each driver. Realistically these parameters will be tuned while balancing with other objectives such as stability and driver workload in addition to maneuvering time; however, this is a first step at applying a minimum-time maneuvering simulation to tailor vehicle parameters to a particular driving style.

	Units	Driver A	Driver B
Baseline Measurement	s	23.51	23.50
Baseline Simulation	s	23.63	23.62
Optimized Tire	s	22.88	22.97
Optimized Tire Time Improvement	s	0.75	0.65
Optimized Tire Improvement Percentage	%	3.2%	2.8%

Table 5.3: Table of maneuvering times in Turn 17.

5.5 Conclusions

The ability to model individual driving style is an important topic to both the motorsports and high-performance automotive industries. Literature has shown local minima exist in the solution space for minimum-time vehicle maneuvering problems and experience has demonstrated that different driving styles can yield identical performance with different trajectories and control histories. In this chapter, we presented a mathematical framework for capturing driving style differences between drivers in the form of a cascaded optimization. We utilize an inner loop MPC with a blended-cost function which was motivated by previous work and literature. This controller finds the optimal vehicle inputs ($\mathbf{u}$) to negotiate the maneuver. An outer loop optimizer finds the optimal cost function to be used in each local MPC horizon. By varying the objective function used for different horizons around the track, we can match simulation to onboard vehicle measurements. This mathematical framework is then exercised for a case study on Sebring International Raceway. In this study, onboard measurements from two professional drivers that negotiated the circuit with nearly identical maneuvering times were used as the baseline data. Turn 17 was a key corner where their trajectories varied considerably, despite the identical maneuvering times. The cascaded optimization framework was able to reproduce the key differences exhibited in the onboard measurement and yield a model for each driver.

Using the identified model of each driver, a scenario was constructed to optimize tire parameters to suit the individual driver's style. Therein, another cascaded optimization

was used where the inner loop MPC operated on a fixed schedule of objectives (from the identified driver model), and the outer loop optimized key tire parameters. It was shown that performance advantages could be gained for each driver and the optimal set of tire parameters differ between the drivers. This mathematical framework could be applied similarly to a supplier submission process where a supplier will present the customer with several variants, test, evaluate feedback, and make design decisions for the next submission. Data could be collected, the driver's weights ($\mathbf{Z}$) could be identified, and then a design direction for the vehicle (λ^*) could be established using these known weights ($\mathbf{Z}$). The new tire design direction λ^* will, in turn, affect the way the driver drives (and affect the driver model $\mathbf{Z}$); thus, the complete process is iterative just like the supplier submission process. In this chapter, we have outlined the computational details of the first loop of this iterative process.

Future work could further explore several aspects of this research. First, additional data could be considered to expand the scope of drivers studied (resources such as the Revs Vehicle Dynamics Database [11] could be a great resource). Model fidelity could be increased to capture essential effects such as the track friction along the circuit and laterally across the track that would improve the model to measurement correlation. Next, while we limited the inner loop MPC to two objectives, additional objectives could be added to improve the correlation. The outer loop fit of the data is sensitive to the weighting choices (i.e., $\mathbf{Q}$ and $\mathbf{R}$). Further studies could consider better ways to weight these problems. Rather than concentrating on a blended-cost MPC, it would be of interest to look at other aspects of the MPC process to mimic driving styles. For example, instead of fixing the MPC horizon as we have done, perhaps, a variable MPC horizon could be scheduled via an outer loop optimizer to yield the differences we seek to model. This would be analogous to fitting the drivers' look ahead distance as a function of the path distance traveled.

Modeling individual drivers will be a key problem as vehicles continue to advance. Just as tunability increases, so does the ability of customization. If there are ways to model different drivers, one can use our approach described herein to optimize the vehicle

(components) to suit particular drivers.

Chapter 6

Conclusions and Future Work

6.1 Conclusions

In motorsports and high-performance vehicle development, professional drivers are relied upon to influence design and tuning direction for vehicles. In many cases, they perform final validation work of a vehicle. It has been established that different drivers have different driving styles and these styles affect the vehicle design and tuning directions. Most work to date has explored modeling an 'ideal' driver to simulate vehicles, however, modeling the 'human' element of driving is less understood. In this dissertation, we aim to mathematically model the driving style differences between drivers. A cascaded optimization framework was proposed to model these style differences. This framework was then applied to a case study to demonstrate the ability of the framework to model style differences and then use the models to tune tires for specific driving styles.

6.2 Summary of Contributions

In this work, we have presented a framework for modeling driving style and applied this methodology to onboard vehicle measurements. Using this framework, we were able to capture key differences in style between two drivers and then optimize the vehicle for each style. The remainder of this section summarizes the key contributions of this work.

6.2.1 Cascaded Optimization Framework

A cascaded optimization was proposed as the mathematical framework to model differences in driving style. The inner loop uses a model predictive controller to optimize the vehicle inputs that minimize a local blended cost function. The outer loop learns the optimal objective schedule used in each MPC horizon in the inner loop. This process is analogous to a human learning a particular circuit or maneuver. We applied this framework first to show how varying the cost function in each horizon can outperform a traditional fixed-cost, time-optimal MPC.

While this was done for a minimum-time vehicle maneuvering problems, it can easily be extended into any MPC process where a global objective is known. It is a general method for injecting a local MPC horizon with pertinent information outside of that horizon. One example could be minimum fuel problems where it is necessary to simulate a trajectory that minimizes fuel over a route, and road information outside of an MPC horizon could be useful to globally reduce fuel usage. Another example is traffic flow problems. Typically the MPC horizon is limited to a relatively short horizon to deal with the immediate control action to safely navigate the environment. If future traffic information, like lane closures, blockages, or traffic conditions from vehicle to vehicle communication could be incorporated into the model predictive controller at each horizon, then it could globally improve MPC performance.

In addition to outperforming the fixed-cost MPC, we were able to obtain multiple objective weight schedules that were all able to outperform the fixed-cost MPC; but, had very different control trajectories. This demonstrates local minima in the minimum-time vehicle maneuvering solution space. This is the key phenomena we used to explain how different driving styles were able to achieve nearly identical performance. The following lists the key contributions of this work:

- Outperformed traditional fixed-cost MPC by varying local MPC objectives
  - This was demonstrated for multiple vehicles and multiple tracks

- The variable MPC cost structure could be used as a general method for incorporating preview information outside of local MPC horizon into each local optimization and improve global performance.
- Identified local minima that could be used to explain/model different driving styles

6.2.2 Optimal Racing Line Reconstruction

In this phase, we proposed a novel optimal control based technique to reconstruct the racing line from a limited set of measurements. Traditional methods of reconstruction incur too much error to be useful, and none proposed to date are able to represent the measurement (usually collected in the time domain) in the path distance traveled domain. This is the domain used in simulation and allows for better comparison between simulations and measurements. Our reconstruction technique uses a simple particle motion model to ensure natural vehicle motion and a previously fit model of the track to identify the racing line traveled. This was accomplished by using a limited set of measurements: lateral and longitudinal acceleration and velocity. This racing line reconstruction technique was applied to a case study, and we were able to demonstrate nearly identical performance between two drivers with different driving styles. The following list summarizes the contributions of this work:

- Proposed optimal control based method to reconstruct racing line from a limited set of measurements.
- Demonstrated different driving styles with nearly identical performance

6.2.3 Application of Cascaded Optimization Framework to Identifying a Driver Model

The cascaded optimization framework was applied to the on-vehicle measurements in order to identify a driver model for each driver. The objective for the outer loop, in this

case, was to best match vehicle simulation to the onboard vehicle measurements. The result is a model of the two drivers that was able to capture key differences in driving style.

Using these driver models, we then used another cascaded optimization to optimize tire parameters for each driver model. It was shown that for the parameters studied, the optimal parameters varied for each driver. This validates our hypothesis, if we are able to capture the difference between drivers in simulation, we then can optimize a vehicle for a particular driver. The following list summarizes these contributions:

- Used a cascaded optimization framework to identify a driver model for two different driving styles.
  - Key differences in style between drivers were preserved in simulation compared to measurement.
- Using the identified driver models, the vehicle parameters were able to be tuned to a particular driver.

6.3 Future Work

There are many possible areas to advance this topic. Listed below are a few possibilities.

6.3.1 Scope of Driving Styles Studied

In this work, we relied on one case study of two professional drivers that were able to achieve nearly identical global performance while exhibiting different styles. It would be ideal to expand further the number of drivers studied with this framework. Resources such as the publicly available Revs database [11] could be an excellent resource for expanding this work.

6.3.2 The MPC Framework

While MPC was chosen as a good framework for modeling the human decision process [18], it causes much of the computational burden in the cascaded algorithm; in fact, the MPC process is the reason that we treat the problem hierarchically. If the entire problem could be treated with optimal control alone, then optimization parameters (such as the tire parameters studied in Section 5.4) could be solved simultaneously with the state and control trajectories. This would allow for a much more computationally friendly problem. While we use the cascaded optimization to schedule objectives used in each MPC horizon, perhaps there are other ways to incorporate the learning process within an optimal control framework. One idea may be to place equality constraints in the vehicle trajectory (i.e. $e_y(s_{constraint}) = e_{y_{constraint}}$). An outer loop optimization could then 'learn' the optimal constraint locations and magnitudes much like a driver learns apex points on a track. This learning process could then be extended to other items that a professional driver learns (such as braking points). By including these constraints, multiple driving styles could be modeled in an optimal control framework and alleviate some of the computational burdens of the MPC process.

6.3.3 Blended Cost MPC

In this dissertation, we chose to include two terms in the blended cost function: minimum-time and maximum exit velocity over each horizon. Model to measurement correlation could be improved by augmenting this cost to include other terms such as minimum or maximum lateral position on the track to force the vehicle to return to the center or push it to the boundaries over a horizon.

6.3.4 Outer Loop Optimization

As was discussed in Chapter 5, the choice of weighting parameters $\mathbf{Q}$ and $\mathbf{R}$ have a significant effect on the quality of the overall fit of the simulation to the reference measurements. In this work, we chose our optimal weighting parameters $\mathbf{Q}$ and $\mathbf{R}$ based on

experience. Future work could look at a more systematic way to determine optimal weighting and achieve a better 'fit' of simulation results to measurement.

Alternate techniques for finding the optimal weights $\mathbf{Z}_{driver}$ could also be explored. One idea could be to train neural networks with the measurements rather than using genetic algorithms.

6.3.5 Alternate MPC Horizon

In this work, we explored a blended, multi-objective cost MPC. There could be other ways to optimize the MPC process to model the human driver. One idea could be to optimize the MPC horizon distance ($s_{horizon}$) in each segment via the cascaded optimization. This would be analogous to modeling a variable driver's look ahead distance and could potentially yield similar results as the blended cost MPC.

6.3.6 MPC Improvements

In our work, we chose to apply an optimal control solver with mesh refinement in each MPC horizon; this is fairly computationally intensive since we are solving many optimal control problems over the full maneuver. While we optimized this as much as we could (via the use of automatic differentiation and solver settings), many other optimal control codes exist and could potentially provide performance improvements while retaining an accurate solution.

6.3.7 Alternate Applications of the Cascaded Optimization

As mentioned in the contributions above, the cascaded optimization structure was a general method of modifying the local MPC optimal control problem to take into account information outside of the current preview horizon. This idea can extend beyond minimum-time vehicle maneuvering problems and could be examined in any MPC process where a global objective is known. The two areas mentioned in the contribution sections could be potential examples: minimum-fuel planning problems, and traffic flow problems.

6.4 List of publications

The following publications were the completed during my doctoral studies:

Journals:

1. J. R. Anderson, J. Adcox, B. Ayalew, M. Knauff, T. Rhyne, and S. Cron. Interaction of a slip-based antilock braking system with tire torsional dynamics. Tire Science And Technology, 43(3):182–194, 2015.

2. J. R. Anderson and E. McPillan. Simulation of the wear and handling performance trade-off by using multi-objective optimization and TameTire. Tire Science And Technology, 44(4):280–290, 2016.

3. J. R. Anderson and B. Ayalew. Modelling minimum-time manoeuvering with global optimisation of local receding horizon control. *Vehicle System Dynamics*, pages 1-24, 2018.

4. J. R. Anderson and B. Ayalew. An optimal control approach to race line reconstruction from limited onboard data. *Vehicle System Dynamics* (Submitted, under review), 2018.

5. J. R. Anderson and B. Ayalew. A cascaded optimization approach for modeling a professional drivers unique driving style. *Vehicle System Dynamics* (Submitted, under review), 2018.

Conference Proceedings:

1. J. R. Anderson, B. Ayalew, J. Adcox, M. Knauff, T. Rhyne, and S. Cron. Interaction of a slip-based anti-lock braking system with tire torsional dynamics. In M. Kaliske, editor, 33rd Annual Meeting and Conference on Tire Science and Technology. The Tire Society, September 2014.

2. J. R. Anderson and E. McPillan. Simulation of the wear and handling performance tradeoff utilizing multi-objective optimization and TameTire. In submitted for presentation at the 2015 Tire Society meeting, and for consideration for publication in the journal Tire Science and Technology, 2015.

3. C. Wang, Q. Wang, J. R. Anderson, and B. Ayalew. Sprung mass motion emulation in a braking test rig. In ASME 2015 International Design Engineering Technical Conference and Computers and Information in Engineering Conference. American Society of Mechanical Engineers, August 2015.

4. J. R. Anderson, B. Ayalew, and T. Weiskircher. Modeling a professional driver in ultra-high performance maneuvers with a hybrid cost MPC. In American Control Conference (ACC), 2016, pages 1981-1986, Boston, MA, USA, July 2016. IEEE.

5. J. R. Anderson and B. Ayalew. Global optimization of local weights in mixed-cost MPC for minimum time vehicle maneuvering. In 2017 IEEE Conference on Control Technology and Applications (CCTA), pages 560-565, Kohala Coast, Hawaii, USA, August 2017. IEEE.

Appendices

Appendix A Vehicle Model

In this chapter, the vehicle model described in [20] is adopted as it is a reasonable compromise of model fidelity and computational cost. It is comprised of three degrees of freedom for the sprung mass, longitudinal velocity (v_x), lateral velocity (v_y), and rotation about the vertical axis ($\dot{\psi}$). The individual wheel dynamics are not explicitly modeled and instead, the four wheel slip ratios (κ_p) (where p denotes the four wheel positions) are modeled as control inputs to the system. This formulation allows us to eliminate the four wheel dynamics that are much faster than the other vehicle dynamics and can cause numerical issues (such as dense meshes) when solving the optimal control problem.

$$\dot{v_x} = v_y\dot{\psi} + \frac{F_x}{m} \tag{A.1}$$

$$\dot{v_y} = -v_x\dot{\psi} + \frac{F_y}{m} \tag{A.2}$$

$$\begin{aligned} I_{zz}\ddot{\psi} = a(\cos(\delta)(F_{y_{fr}} + F_{y_{fl}}) + \sin(\delta)(F_{x_{fr}} + F_{x_{fl}}))+ \\ t_f(F_{y_{fr}}\sin(\delta) - F_{x_{fr}}\cos(\delta))+ \\ t_f(F_{x_{fl}}\cos(\delta) - F_{y_{fl}}\sin(\delta))+ \\ t_rF_{x_{rl}} - b(F_{y_{rr}} + F_{y_{rl}}) - t_rF_{x_{rr}} \end{aligned} \tag{A.3}$$

where m and I_{zz} are the mass and moment of inertia, respectively. Total lateral and longitudinal forces acting at the Center of Gravity (Cg) are denoted by F_x and F_y.

$$\begin{aligned} F_x = \cos(\delta)(F_{x_{fl}} + F_{x_{fr}}) - \sin(\delta)(F_{y_{fl}} + F_{y_{fr}}) \\ +F_{x_{rl}} + F_{x_{rr}} + Fax \\ F_y = \cos(\delta)(F_{y_{fl}} + F_{y_{fr}}) + \sin(\delta)(F_{x_{fl}} + F_{x_{fr}}) \\ +F_{y_{rl}} + F_{y_{rr}} \end{aligned} \tag{A.4}$$

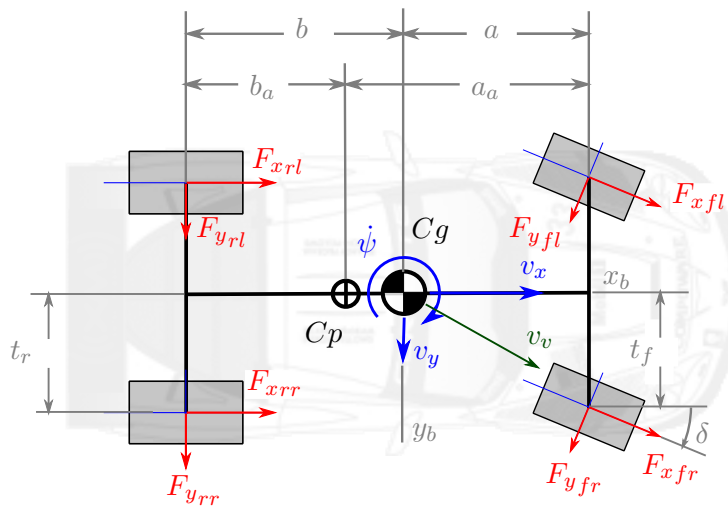

Figure A.1: Vehicle top view. Note: body-fixed coordinates x_b and y_b are located vertically at the ground plane.

The individual tire lateral and longitudinal forces are denoted by F_{xp} and F_{y_p}. The subscript $(\cdot)_p$ again represents the four wheel positions; $p \in \{fl, fr, rl, rr\}$ denotes front left, front right, rear left, rear right position. The vehicle is assumed to be front wheel steering only. The steering angle is represented by δ. The vehicle dimensions a, b represent values from the Cg to the front and rear axle. The dimension t_f, t_r represent half of the vehicle's front and rear track width. These dimensions can be seen in Figure A.1.

A.1 Aerodynamics

The speed-dependent aerodynamic forces act at the center of pressure (Cp) which is located via the parameters a_a, b_a. They are the distance of the center of pressure to the front and rear axle. The lift and drag forces (F_{ax}, F_{az}) are modeled as:

$$F_{az} = \frac{1}{2} C_L \rho A v_x^2 \tag{A.5}$$

$$F_{ax} = \frac{1}{2} C_D \rho A v_x^2 \tag{A.6}$$

where the lift and drag coefficients (C_L, C_D) are assumed constant. The vehicle's frontal area is denoted with A. The air density is denoted with ρ. Other aerodynamic effects such as yaw and pitch coupling are neglected for the purposes of this work.

A.2 Tires

The tire's frictional forces are calculated via an empirical formula that responds to changes in loads, lateral slip angle, and longitudinal slip ratio. It is based on the simplified Pacejka tire model presented in [45, 20] and detailed in Appendix B. The slip ratio (κ) and slip angle (α) are calculated by:

$$\kappa = -\left(1 + \frac{R\omega}{v_{xtire}}\right) \tag{A.7}$$

and,

$$\alpha = -\arctan\left(\frac{v_{y_{tire}}}{v_{xtire}}\right) \tag{A.8}$$

where R is the effective rolling radius of the tire and v_{xtire}, $v_{y_{tire}}$ are the longitudinal and lateral velocities of the tire accounting for vehicle rotation.

A.3 Tire Loads

Modeling tire loads presents a unique challenge because of the algebraic relationship that exists between the tire loads and the forces the tires can produce (which affect tire loads). This is typically handled one of a few ways in the literature. First, approximations of the lateral and longitudinal forces acing at the Cg can be made and then the four wheel loads can be solved for via the equilibrium equations (A.13) discussed below. From Newton's second law, The forces acting on the Cg should be proportional to mass times acceleration. This is fully explained in [45] and was the method employed in Chapter 3. Lateral acceleration was approximated as $a_y = \dot{\psi} v_x$. Since torque input was explicitly modeled in this chapter, total longitudinal force was modeled as the sum of torques on the four wheel positions divided by the effective rolling radius of the tires. Alternately, the tire

loads can be found by modeling the tire vertical dynamics. Stiffness and deflection of the tires can be explicitly modeled as discussed in [100]. The tire loads can also be treated as dynamic states with simple lags to account for the suspension dynamics as explained in [97]. A final method (which is what we will use in the remainder of our work) treats the tire loads as inputs to the system dynamics and not as system states [140]. In order to have the system obey equilibrium conditions, equality constraints are placed in the optimal control formulation. These constraints are derived by summing the forces and moments about the body-fixed coordinates (x_b, y_b) seen in Figure A.1 and enforcing a roll stiffness distribution $D \in [0, 1]$ such that the load transfer on the front axle is a fixed proportion of the total load transfer. First, summing the moments in the vertical direction:

$$\sum F_z = Fz_{L1} + Fz_{R1} + Fz_{L2} + Fz_{R2} + Faz = 0 \tag{A.9}$$

Next, balance moments about body-fixed x axis:

$$\sum M_{x_b} = t_r(Fz_{L2} - Fz_{R2}) + t_f(Fz_{L1} - Fz_{R1}) + hF_y = 0 \tag{A.10}$$

Then, sum moments about the body-fixed y axis:

$$\sum M_{y_b} = b(Fz_{R2} + Fz_{L2}) - a(Fz_{R1} + Fz_{L1}) + ...hF_x + (a_a - a)F_{az} = 0 \tag{A.11}$$

Finall, a fixing the front axle load transfer to be a proportion of the total load transfer, we can write the following:

$$Fz_{R1} - Fz_{L1} = D(Fz_{R1} + Fz_{R2} - Fz_{L1} - Fz_{L2}) \tag{A.12}$$

This yields the following linear system of equations:

$$\begin{bmatrix} 1 & 1 & 1 & 1 \\ -t_f & t_f & -t_r & t_r \\ -a & -a & b & b \\ D-1 & 1-D & D & -D \end{bmatrix} \begin{bmatrix} Fz_{fl} \\ Fz_{rl} \\ Fz_{rl} \\ Fz_{rr} \end{bmatrix} = \begin{bmatrix} -mg - F_{az} \\ -h_{cg}F_y \\ (a_a - a)F_{az} + hF_x \\ 0 \end{bmatrix} \tag{A.13}$$

Note that h_{cg} represents the Cg height.

A.4 Path Intrinsic Coordinate System

The path intrinsic coordinate system provides a convenient mechanism to bound the vehicle motion to stay within the track width boundaries. In this coordinate system the vehicle motion is modeled with respect to the road centerline as depicted in Figure A.2. The heading angle deviation (e_ψ) represents the difference between the path heading and the vehicle heading angle while the lateral deviation (e_y) refers to the vehicle lateral deviation from the path centerline. The vehicle speed in the path reference frame is denoted as $\dot{s}$. The quantities $\dot{s}$, e_ψ, and e_y are calculated as follows:

$$\dot{s} = \frac{v_x \cos(e_\psi) - v_y \sin(e_\psi)}{1 - e_y C} \tag{A.14}$$

where C is the path curvature is assumed to be a known function of path distance i.e., $C = C(s)$.

$$\dot{e}_\psi = \dot{\psi} - C\dot{s} \tag{A.15}$$

$$\dot{e}_y = v_x \sin(e_\psi) + v_y \cos(e_\psi) \tag{A.16}$$

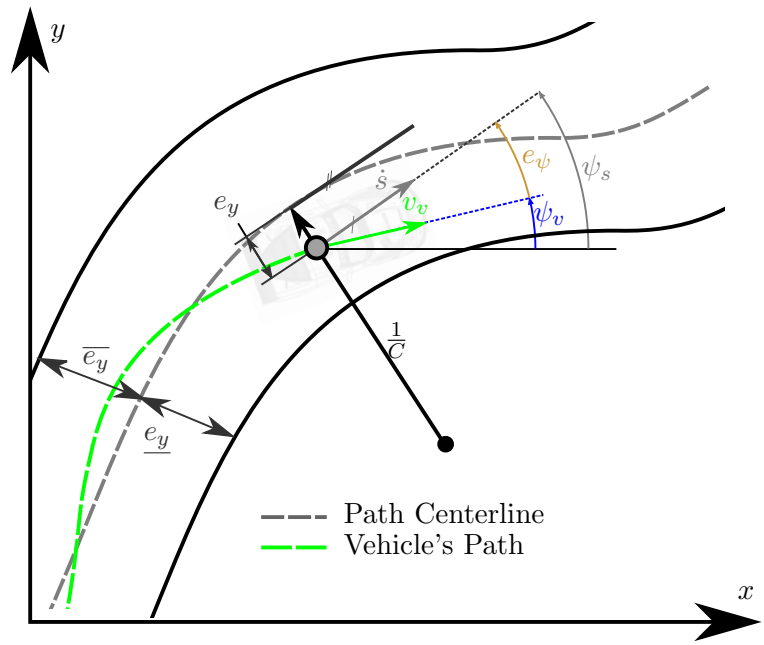

Figure A.2: Path intrinsic coordinate system. Note subscripts s and v refer to the path and vehicle frame respectively.

A.5 Distance Based Description

The vehicle dynamics can be written as:

$$\dot{\mathbf{x}} = f(\mathbf{x}, \mathbf{u}, t) \tag{A.17}$$

where, the vehicle states are: $\mathbf{x} = \begin{bmatrix} v_x, & v_y, & \dot{\psi}, & e_y, & e_\psi \end{bmatrix}^T$ and inputs are: $\mathbf{u} = \begin{bmatrix} \delta, \kappa_p, F_{zp} \end{bmatrix}^T$, where the subscript $(\cdot)_p$ denotes the four wheel positions.

For the purposes of time optimal control, it is of interest to change the independent variable of the system from time (t) to path distance travelled (s). This change of variables eliminates the free final time boundary condition that would arise if the system were written in the time domain. This transformation is achieved via application of the chain rule of differentiation to the system dynamics in (A.17).

$$\frac{d\mathbf{x}}{dt}\frac{dt}{ds} = \frac{d\mathbf{x}}{ds} = \frac{\dot{\mathbf{x}}}{\dot{s}} \tag{A.18}$$

The final system description can be written as:

$$\mathbf{x}' = f(\mathbf{x},\mathbf{u}, s) \tag{A.19}$$

where the operator $(\cdot)'$ denotes the spatial derivative $\frac{d}{ds}$. Note that time is added as an additional state in the state vector $\mathbf{x}$ with the state equation: $t = 1/\dot{s}$.

Appendix B Simplified Pacejka Tire Model

The tire model used in this work is a simplified tire model rooted in Pacejka's magic formula. It is fully described in [45, 20] and included here for completeness. Begin, the tire velocities are calculated to account for the chassis motion:

$$\begin{aligned} v_{xL1} &= v_x + \dot{\psi} w_f \qquad & v_{xR1} &= v_x - \dot{\psi} w_f \\ v_{yL1} &= v_y + \dot{\psi} w_f \qquad & v_{yR1} &= v_y + \dot{\psi} w_f \\ \\ v_{xL2} &= v_x + \dot{\psi} w_f \qquad & v_{xR2} &= v_x - \dot{\psi} w_f \\ v_{yL2} &= v_y - \dot{\psi} w_f \qquad & v_{yR2} &= v_y - \dot{\psi} w_f \end{aligned} \tag{B.1}$$

where $w_i,\ i \in \{f, r\}$ is half of the front or rear track width. The velocities are then rotated from the chassis to the tire coordinate system via the following rotation:

$$T = \begin{bmatrix} cos(\delta) & sin(\delta) \\ -sin(\delta) & cos(\delta) \end{bmatrix} \tag{B.2}$$

Now, for each of the wheel positions, the rotation can be carried out:

$$\begin{bmatrix} v_{xtire} \\ v_{ytire} \end{bmatrix} = T \begin{bmatrix} v_x \\ v_y \end{bmatrix} \tag{B.3}$$

The slip angle can be calculated by substituting the results in (B.3) into (A.8). Finally the slip angles are:

$$\alpha_{L1} = atan\left(\frac{-sin(\delta)(v_x + \dot{\psi}w_f) + cos(\delta)(v_y + \dot{\psi}a)}{cos(\delta)(v_x + \dot{\psi}w_f) + sin(\delta)(v_y + \dot{\psi}a)}\right) \tag{B.4}$$

$$\alpha_{R1} = atan\left(\frac{sin(\delta)(\dot{\psi}w_f - v_x) + cos(\delta)(v_y + \dot{\psi}a)}{cos(\delta)(v_x - \dot{\psi}w_f) + sin(\delta)(v_y + \dot{\psi}a)}\right) \tag{B.5}$$

$$\alpha_{L2} = atan\left(\frac{v_y - \dot{\psi}b}{v_x + \dot{\psi}w_r}\right) \tag{B.6}$$

$$\alpha_{R2} = atan\left(\frac{v_y - \dot{\psi}b}{v_x - \dot{\psi}w_r}\right) \tag{B.7}$$

The slip ratios can be calculated in a similar manor using the tire velocities calculated in (B.3) and substituting them into (A.7):

$$\kappa_{L1} = -\left(1 + \frac{R_f\omega_{L1}}{(cos(\delta)(v_x + \dot{\psi}w_f) + sin(\delta)(\dot{\psi}a + v_y))}\right) \tag{B.8}$$

$$\kappa_{R1} = -\left(1 + \frac{R_f\omega_{R1}}{(cos(\delta)(v_x - \dot{\psi}w_f) + sin(\delta)(\dot{\psi}a + v_y))}\right) \tag{B.9}$$

$$\kappa_{L2} = -\left(1 + \frac{R_r\omega_{L2}}{v_x + \dot{\psi}w_r}\right) \tag{B.10}$$

$$\kappa_{R2} = -\left(1 + \frac{R_r\omega_{R2}}{v_x - \dot{\psi}w_r}\right) \tag{B.11}$$

B.1 Tire Friction Calculations

The tire frictional forces are calculated by the following steps. First, current maximum longitudinal and lateral coefficients are identified by linearly interpolating the set maximum friction coefficients of friction at reference loads:

$$\mu_{xmax} = (F_z - F_{z1})\frac{\mu_{xmax2} - \mu_{xmax1}}{F_{z2} - F_{z1}} + \mu_{xmax1} \tag{B.12}$$

$$\mu_{y_{max}} = (F_z - F_{z1})\frac{\mu_{y_{max2}} - \mu_{y_{max1}}}{F_{z2} - F_{z1}} + \mu_{y_{max1}} \tag{B.13}$$

$$\tag{B.14}$$

The corresponding slip angles and ratios where the peaks occur are similarly calculated:

$$\alpha_{max} = (F_z - F_{z1})\frac{\alpha_{max2} - \alpha_{max1}}{F_{z2} - F_{z1}} + \alpha_{xmax1} \tag{B.15}$$

$$\kappa_{max} = (F_z - F_{z1})\frac{\kappa_{max2} - \kappa_{max1}}{F_{z2} - F_{z1}} + \kappa_{y_{max1}} \tag{B.16}$$

$$\tag{B.17}$$

The subscripts $(\cdot)_i,\ where;\ i \in 1, 2$ represent reference tire parameters. Next, the tire slip quantities are normalized by the peak values:

$$\alpha_n = \frac{\alpha}{\alpha_{max}} \tag{B.18}$$

$$\kappa_n = \frac{\kappa}{\kappa_{max}} \tag{B.19}$$

Slip is then characterized by a combined-slip coefficient:

$$\rho = \sqrt{\alpha_n^2 + \kappa_n^2} \tag{B.20}$$

Next, the operating longitudinal and lateral friction coefficients are described by:

$$\mu_x = \mu_{x_{max}} sin\left(Q_x atan(S_x \rho)\right) \tag{B.21}$$

$$\mu_y = \mu_{y_{max}} sin\left(Q_y atan(S_y \rho)\right) \tag{B.22}$$

where

$$S_x = \frac{\pi}{2atan(Q_x)} \tag{B.23}$$

$$S_y = \frac{\pi}{2atan(Q_y)} \tag{B.24}$$

Finally the tire forces are given by:

$$Fx = \mu_x F_z \frac{\kappa_n}{\rho} \tag{B.25}$$

$$Fy = \mu_y F_z \frac{\kappa_n}{\rho} \tag{B.26}$$

Bibliography

[1] Peter Wright and Tony Matthews. Formula 1 technology. Technical report, SAE Technical Paper, 2001.

[2] D Brayshaw. The use of numerical optimisation to determine on-limit handling behaviour of race cars [phd thesis]. *Department of Automotive, Mechanical and Structural Engineering, Cranfield University*, 2004.

[3] Anil V Rao. A survey of numerical methods for optimal control. *Advances in the Astronautical Sciences*, 135(1):497–528, 2009.

[4] Matthew P Kelly. Transcription methods for trajectory optimization: a beginners tutorial. *arXiv preprint arXiv:1707.00284*, 2017.

[5] D. Casanova. *On Minimum Time Vehicle Manoeuvering: The Theoretical Optimal Lap*. PhD thesis, Cranfield University, November 2000.

[6] Isaac watt boulton, 2018. [Online; accessed 15-May-2018].

[7] Giovanni Lurani. *History of the racing car: man and machine*. Thomas Y. Crowell Company, New York, 1972.

[8] Chris Gerdes. The future race car — 150mph, and no driver. `http://www.ted.com/talks/chris_gerdes_the_future_race_car_150mph_and_no_driver`, May 2012.

[9] Daniele Loiacono, Luigi Cardamone, and Pier Luca Lanzi. Automatic track generation for high-end racing games using evolutionary computation. *Computational Intelligence and AI in Games, IEEE Transactions*, 3(3):245–259, 2011.

[10] Francesco Biral, Fabrizio Zendri, Enrico Bertolazzi, Paolo Bosetti, Marco Galvani, Filippo Trivellato, and Mauro Da Lio. A web based "virtual racing car championship" to teach vehicle dynamics and multidisciplinary design. In *ASME 2011 International Mechanical Engineering Congress and Exposition*, pages 391–401. American Society of Mechanical Engineers, 2011.

[11] John C Kegelman, Lene K Harbott, and J Christian Gerdes. Insights into vehicle trajectories at the handling limits: analysing open data from race car drivers. *Vehicle system dynamics*, 55(2):191–207, 2017.

[12] Andreas Trabesinger. Formula 1 racing: Power games. *Nature*, 447(7147):900–903, June 2007.

[13] Timothy Cain. 2013 U.S. vehicle sales rankings by model - top 270 best-selling vehicles in america - every vehicle ranked, January 2014.

[14] Bob Ulrich. The signposts up ahead? Tire sales, 2014.

[15] Matthias Gerdts and Simon Karrenberg. Generating locally optimal trajectories for an automatically driven car. *Optimization and Engineering*, 10(4):439–463, 2009.

[16] Joseph Funke, Paul Theodosis, Rami Hindiyeh, Ganymed Stanek, Krisada Kritataki-rana, Chris Gerdes, Dirk Langer, Marcial Hernandez, B Muller-Bessler, and Burkhard Huhnke. Up to the limits: Autonomous audi tts. In *Intelligent Vehicles Symposium (IV), 2012 IEEE*, pages 541–547. IEEE, 2012.

[17] Roborace. `http://roborace.com`, 2017. [Online; accessed 9-April-2017].

[18] David J Cole. Occupant–vehicle dynamics and the role of the internal model. *Vehicle System Dynamics*, 56(5):661–688, 2017.

[19] Michal Maniowski. Optimisation of driver actions in rwd race car including tyre thermodynamics. *Vehicle System Dynamics*, 54(4):526–544, 2016.

[20] Giacomo Perantoni and David JN Limebeer. Optimal control for a formula one car with variable parameters. *Vehicle System Dynamics*, 52(5):653–678, 2014.

[21] Jeffery R. Anderson and Beshah Ayalew. Global optimization of local weights in mixed-cost MPC for minimum time vehicle maneuvering. In *2017 IEEE Conference on Control Technology and Applications (CCTA)*, pages 560–565, Kohala Coast, Hawai'i, USA, August 2017. IEEE.

[22] Jeffery Ryan Anderson and Beshah Ayalew. Modelling minimum-time manoeuvering with global optimisation of local receding horizon control. *Vehicle System Dynamics*, pages 1–24, 2018.

[23] Jeffery R. Anderson and Beshah Ayalew. An optimal control approach to race line reconstruction from limited onboard data. *Vehicle System Dynamics (Submitted, under review)*, 2018.

[24] Jeffery R. Anderson and Beshah Ayalew. A cascaded optimization approach for modeling a professional driver's driving style. *Vehicle System Dynamics (Submitted, under review)*, 2018.

[25] William F Milliken, Douglas L Milliken, et al. *Race Car Vehicle Dynamics*, volume 400. Society of Automotive Engineers Warrendale, 1995.

[26] H Scherenberg. Mercedes-benz racing design and cars experience. Technical Report 580042, SAE Technical Paper, 1958.

[27] R Roland, J Douglas, and CF Thelin. Computer simulation of watkins glen grand prix circuit performance. *Buffalo, New York: Cornell Aeronautical Laboratory*, 1971.

[28] R Griffiths. Minimum time simulation of a racing car. Master's thesis, School of Mechanical Engineering, Cranfield University, 1992.

[29] J Blasco-Figueroa. Minimum time manoeuvre based in the gg-speed envelope. Master's thesis, School of Engineering, Cranfield University, 2000.

[30] DL Brayshaw and MF Harrison. A quasi steady state approach to race car lap simulation in order to understand the effects of racing line and centre of gravity location. *Proceedings of the Institution of Mechanical Engineers, Part D: Journal of Automobile Engineering*, 219(6):725–739, 2005.

[31] AJ Tremlett, F Assadian, DJ Purdy, N Vaughan, AP Moore, and M Halley. Quasi-steady-state linearisation of the racing vehicle acceleration envelope: a limited slip differential example. *Vehicle System Dynamics*, 52(11):1416–1442, 2014.

[32] RG Dominy. Aerodynamic influences on the performance of the grand prix racing car. *Proceedings of the Institution of Mechanical Engineers, Part D: Journal of Automobile Engineering*, 198(2):87–93, 1984.

[33] RG Dominy. The influence of slipstreaming on the performance of a grand prix racing car. *Proceedings of the Institution of Mechanical Engineers, Part D: Journal of Automobile Engineering*, 204(1):35–40, 1990.

[34] Marco Gadola, Andrea Candelpergher, and Riccardo Adami. The impact of non-linear aerodynamics on racecar behaviour and lap time simulation. Technical report, SAE Technical Paper, 2002.

[35] Robert G Dominy. Sports prototype race car optimization. Technical report, SAE Technical Paper, 2002.

[36] Edward M Kasprzak, Kemper E Lewis, and Douglas L Milliken. Steady-state vehicle optimization using pareto-minimum analysis. Technical Report 983083, SAE Technical Paper, 1998.

[37] Kurt Hacker, Kemper Lewis, and Edward M Kasprzak. Racecar optimization and tradeoff analysis in a parallel computing environment. Technical Report 2000-01-3564, SAE Technical Paper, 2000.

[38] Blake Siegler, Andrew Deakin, and David Crolla. Lap time simulation: Comparison of steady state, quasi-static and transient racing car cornering strategies. Technical report, SAE Technical Paper, 2000.

[39] Nitin R Kapania, John Subosits, and J Christian Gerdes. A sequential two-step algorithm for fast generation of vehicle racing trajectories. *Journal of Dynamic Systems, Measurement, and Control*, 138(9):091005, 2016.

[40] John Subosits and J Christian Gerdes. Autonomous vehicle control for emergency maneuvers: The effect of topography. In *2015 American Control Conference (ACC)*, pages 1405–1410. IEEE, 2015.

[41] Sergio M Savaresi, Cristiano Spelta, Davide Ciotti, Marco Sofia, Enrico Rosignoli, and Emiliano Bina. Virtual selection of the optimal gear-set in a race car. *International Journal of Vehicle Systems Modelling and Testing*, 3(1-2):47–67, 2008.

[42] DL Brayshaw and MF Harrison. Use of numerical optimization to determine the effect of the roll stiffness distribution on race car performance. *Proceedings of the Institution of Mechanical Engineers, Part D: Journal of Automobile Engineering*, 219(10):1141–1151, 2005.

[43] David Vetturi Andrea Candelpergher, Marco Gadola. Developments of a method for lap time simulation. Technical report, SAE Technical Paper, 2000.

[44] Timo Völkl, Martin Muehlmeier, and Hermann Winner. Extended steady state lap time simulation for analyzing transient vehicle behavior. *SAE International Journal of Passenger Cars-Mechanical Systems*, 6(2013-01-0806):283–292, 2013.

[45] Daniel Kelly. *Lap Time Simulation with Transient Vehicle and Tyre Dynamics*. PhD thesis, Cranfield University, May 2008.

[46] Julian Timings and David Cole. Robust lap-time simulation. *Proceedings of the Institution of Mechanical Engineers, Part D: Journal of Automobile Engineering*, 228(10):1200–1216, 2014.

[47] M Tomizuka and DE Whitney. The human operator in manual preview tracking (an experiment and its modeling via optimal control). *Journal of Dynamic Systems, Measurement, and Control*, 98(4):407–413, 1976.

[48] Duane T McRuer and Ezra S Krendel. Dynamic response of human operators. Technical report, Department of Defense, 1957.

[49] David H Weir and Duane T McRuer. A theory for driver steering control of motor vehicles. Technical Report HS-005 311, 1968.

[50] JJ Rix and DJ Cole. Models of human learning applicable to the vehicle steering task. In *Proceedings of the 6th International Symposium on Advanced Vehicle Control*, pages 683–688, International Conference Center, Hiroshima, Japan, 2002.

[51] R.S. Sharp, D. Casanova, and P. Symonds. A mathematical model for driver steering control, with design, tuning and performance results. *Vehicle System Dynamics: International Journal of Vehicle Mechanics and Mobility*, 33(5):289–326, 2000.

[52] K. Guo and H. Guan. Modelling of driver/vehicle directional control system. *Vehicle System Dynamics*, 22:141–184, 1993.

[53] Charles C. Macadam. Understanding and modeling the human driver. *Vehicle System Dynamics: International Journal of Vehicle Mechanics and Mobility*, 40(1-3):101–134, 2003.

[54] Manfred Plöchl and Johannes Edelmann. Driver models in automobile dynamics application. *Vehicle System Dynamics*, 45(7-8):699–741, 2007.

[55] Chalres C. MacAdam. Application of an optimal preview control for simulation of closed-loop automobile driving. *IEEE Transactions on Systems, Man and Cybernetics*, 11(6):393–399, June 1981.

[56] The VehicleSim steer controller. Technical report, Mechanical Simulation, June 2011.

[57] Rainer Fischer, Torsten Butz, Martin Ehmann, and Mario Vockenhuber. A driver model for virtual control system development. *ATZautotechnology*, 11(6):22–25, 2011.

[58] Torsten Butz and Oskar von Stryk. Optimal control based modeling of vehicle driver properties. Technical report, DTIC Document, April 2005.

[59] Vivan Govender and David C Barton. Multibody system simulation and optimisation of the driving dynamics of a formula sae race car. Technical report, SAE Technical Paper, 2009.

[60] Efstathios Velenis and Panagiotis Tsiotras. Optimal velocity profile generation for given acceleration limits: Theoretical analysis. In *American Control Conference*, pages 1478–1483, Portland, OR, June 8-10 2005. IEEE.

[61] E Velenis and P Tsiotras. Optimal velocity profile generation for given acceleration limits; the half-car model case. In *2005 IEEE International Symposium on Industrial Electronics*, pages 355–360, Dubrovnik, Croatia, December 2005.

[62] Efstathios Velenis and Panagiotis Tsiotras. Minimum-time travel for a vehicle with acceleration limits: Theoretical analysis and receding-horizon implementation. *Journal of Optimization Theory and Applications*, 138(2):275–296, 2008.

[63] F. Braghin, F. Cheli, S. Melzi, and E. Sabbioni. Race driver model. *Computers and Structures*, 86:1503–1516, 2008.

[64] R Lot, M Massaro, and R Sartori. Advanced motorcycle virtual rider. *Vehicle System Dynamics*, 46(S1):215–224, 2008.

[65] RS Sharp. A method for predicting minimum-time capability of a motorcycle on a racing circuit. *Journal of Dynamic Systems, Measurement, and Control*, 136(4):041007, 2014.

[66] RS Sharp, M Thommyppillai, and SA Evangelou. Towards a model of a high-performance driver for circuit-racing cars. In *Proc. 10th Int. Symp. AVEC*, pages 713–718, 2010.

[67] Alessandro Saccon, John Hauser, and Alessandro Beghi. A virtual rider for motorcycles: Maneuver regulation of a multi-body vehicle model. *IEEE Transactions on Control Systems Technology*, 21(2):332–346, 2013.

[68] Ivan Fernandez Colunga and Andrew Bradley. Modelling of transient cornering and suspension dynamics, and investigation into the control strategies for an ideal driver in a lap time simulator. *Proceedings of the Institution of Mechanical Engineers, Part D: Journal of Automobile Engineering*, 228(10):1185–1199, 2014.

[69] Qilun Zhu and Robert Prucka. Control optimization of a charge sustaining hybrid powertrain for motorsports. Technical Report 2018-01-0416, SAE Technical Paper, 2018.

[70] Kirstin LR Talvala, Krisada Kritayakirana, and J Christian Gerdes. Pushing the limits: From lanekeeping to autonomous racing. *Annual Reviews in Control*, 35(1):137–148, 2011.

[71] Paul A Theodosis and J Christian Gerdes. Nonlinear optimization of a racing line for an autonomous racecar using professional driving techniques. In *ASME 2012 5th Annual Dynamic Systems and Control Conference joint with the JSME 2012 11th Motion and Vibration Conference*, pages 235–241. American Society of Mechanical Engineers, 2012.

[72] Guido Koch, John C. Kegelman, and Chris Gerdes. Analysis of measured racing lines: A path primitive based curve fitting approach. In *AVEC*, 2012.

[73] Paul A Theodosis and J Christian Gerdes. Generating a racing line for an autonomous racecar using professional driving techniques. In *ASME 2011 Dynamic Systems and Control Conference*, pages 853–850, 2011.

[74] Aliasghar Arab, Kaiyan Yu, Jingang Yi, and Dezhen Song. Motion planning for aggressive autonomous vehicle maneuvers. In *Automation Science and Engineering (CASE), 2016 IEEE International Conference on*, pages 221–226. IEEE, 2016.

[75] Thomas Lipp and Stephen Boyd. Minimum-time speed optimization over a fixed path. *International Journal of Control*, 1(1):1–15, 2014.

[76] Diederik Verscheure, Bram Demeulenaere, Jan Swevers, Joris De Schutter, and Moritz Diehl. Time-optimal path tracking for robots: A convex optimization approach. *Automatic Control, IEEE Transactions on*, 10(54):2318–2327, 2009.

[77] Jonathan How, Nicholas Pohlman, and Chan-Woo Park. Gps estimation algorithms for precise velocity, slip and race-track position measurements. Technical Report 2002-02-3336, SAE Technical Paper, 2002.

[78] Juan Pablo Samper Mejia, Paul A Theodosis, and J Christian Gerdes. Using a path-fitting algorithm to analyze the racing techniques of a skilled driver. In *ASME 2013 Dynamic Systems and Control Conference*, pages V003T47A006–V003T47A006. American Society of Mechanical Engineers, 2013.

[79] Luigi Cardamone, Daniele Loiacono, Pier Luca Lanzi, and Alessandro Pietro Bardelli. Searching for the optimal racing line using genetic algorithms. In Georgios N. Yannakakis and Julian Togelius, editors, *Computational Intelligence and Games (CIG), 2010 IEEE Symposium on*, pages 388–394, IT University of Copenhagen, Center for Computer Games Research, Copenhagen, Denmark, August 2010. IEEE.

[80] M. Botta, V. Gautieri, D. Loiacono, and P. L. Lanzi. Evolving the optimal racing line in a high-end racing game. In *2012 IEEE Conference on Computational Intelligence and Games (CIG)*, pages 108–115, Granada, Spain, September 2012. IEEE.

[81] Marco Gadola, David Vetturi, Danilo Cambiaghi, and Luca Manzo. A tool for lap time simulation. Technical report, SAE Technical Paper, 1996.

[82] Martin Mühlmeier and Norbert Müller. Optimization of the driving line on a race track. Technical Report 2002-01-3399, SAE, 2002.

[83] Julian P Timings and David J Cole. Vehicle trajectory linearisation to enable efficient optimisation of the constant speed racing line. *Vehicle system dynamics*, 50(6):883–901, 2012.

[84] HJ Pesch and M Gerdts. Simulation of test-drivers of automobiles at driving limit. In Willi Jäger and Hans-Joachim Krebs, editors, *Mathematics—Key Technology for the Future*, pages 74–83. Springer, Berlin, Germany, 2003.

[85] Matthias Gerdts. A moving horizon technique for the simulation of automobile test-drives. *ZAMM-Journal of Applied Mathematics and Mechanics*, 83(3):147–162, 2003.

[86] Donald E Kirk. *Optimal Control Theory: An Introduction*. Prentice Hall, Englewood Cliffs, New Jersey, 1970.

[87] Arthur Earl Bryson. *Applied optimal control: optimization, estimation and control*. Routledge, 2018.

[88] T. Fujioka and T. Kimura. Numerical simulation of minimum-time cornering behavior. *JSAE Review*, 13(1), 1992.

[89] J.P.M. Hendrikx, J.J.J. Meijlink, and R.F.C Kriens. Application of optimal control theory to inverse simulation of car handling. *Vehicle System Dynamics*, 26:449–461, 1996.

[90] D. Casanova and R.S. Sharp. Minimum time manoeuvring: The significance of yaw inertia. *Vehicle System Dynamics*, 34(34):77–115, 2000.

[91] Vittore Cossalter, Mauro Da Lio, Roberto Lot, and Lucca Fabbri. A general method for the evaluation of vehicle manoeuvrability with special emphasis on motorcycles. *Vehicle system dynamics*, 31(2):113–135, 1999.

[92] R.S. Sharp and Huei Peng. Vehicle dynamics applications of optimal control theory. *Vehicle System Dynamics*, 49(7):1073–1111, July 2011.

[93] David JN Limebeer and Anil V Rao. Faster, higher and greener: Vehicular optimal control. *IEEE Control Systems Magazine*, pages 37–56, April 2015.

[94] Aldo Sorniotti and Massimiliano Curto. Racing simulation of a formula 1 vehicle with kinetic energy recovery system. Technical Report 2008-01-2964, SAE Technical Paper, 2008.

[95] Nicola Dal Bianco, Enrico Bertolazzi, Francesco Biral, and Matteo Massaro. Comparison of direct and indirect methods for minimum lap time optimal control problems. *Vehicle System Dynamics*, 0(0):1–32, 2018.

[96] E Bertolazzi, F Biral, and M Da Lio. Symbolic–numeric indirect method for solving optimal control problems for large multibody systems. *Multibody System Dynamics*, 13(2):233–252, 2005.

[97] AJ Tremlett, M Massaro, DJ Purdy, E Velenis, F Assadian, AP Moore, and M Halley. Optimal control of motorsport differentials. *Vehicle System Dynamics*, 53(12):1771–1794, 2015.

[98] Fabiano Maggio, Francesco Biral, and Mauro Da Lio. How gearbox ratios influence lap time and driving style. an analysis based on time-optimal maneuvers. Technical Report 2003-32-0056, SAE Technical Paper, 2003.

[99] Bobbo Simon, Cossalter Vittore, Massaro Matteo, and Peretto Martino. Application of the "optimal maneuver method" for enhancing racing motorcycle performance. *SAE International Journal of Passenger Cars-Mechanical Systems*, 1(2008-01-2965):1311–1318, 2008.

[100] Roberto Lot and Nicola Dal Bianco. Lap time optimisation of a racing go-kart. *Vehicle System Dynamics*, 52(2):210–230, 2015.

[101] Roberto Lot and Nicola Dal Bianco. The significance of high-order dynamics in lap time simulations. In *IAVSD 2015: 24th International Symposium on Dynamics of Vehicles on Roads and Tracks*, Graz, AT, August 2015. CRC Press.

[102] Davide Tavernini, Matteo Massaro, Efstathios Velenis, Diomidis I Katzourakis, and Roberto Lot. Minimum time cornering: the effect of road surface and car transmission layout. *Vehicle System Dynamics*, 51(10):1533–1547, 2013.

[103] R Lot and M Da Lio. A symbolic approach for automatic generation of the equations of motion of multibody systems. *Multibody System Dynamics*, 12(2):147–172, 2004.

[104] Enrico Bertolazzi, Francesco Biral, and Mauro Da Lio. Symbolic-numeric efficient solution of optimal control problems for multibody systems. *Journal of computational and applied mathematics*, 185(2):404–421, 2006.

[105] Enrico Bertolazzi, Francesco Biral, and Mauro Da Lio. Real-time motion planning for multibody systems. *Multibody System Dynamics*, 17(2-3):119–139, 2007.

[106] John T Betts. *Practical methods for optimal control and estimation using nonlinear programming*, volume 19. Siam, Warrendale, PA, 2010.

[107] John T Betts. Survey of numerical methods for trajectory optimization. *Journal of guidance, control, and dynamics*, 21(2):193–207, 1998.

[108] Jonathon Allen. Computer optimization of cornering line. Master's thesis, Cranfield University, 1997.

[109] D. Casanova, R.S. Sharp, and P. Symonds. Sensitivity to mass variations of the fastest possible lap of a formula one car. *Vehicle System Dynamics Supplement*, 35(35):119–134, 2001.

[110] Boris Houska, Hans Joachim Ferreau, and Moritz Diehl. An auto-generated real-time iteration algorithm for nonlinear mpc in the microsecond range. *Automatica*, 47(10):2279–2285, 2011.

[111] Michael A Patterson and Anil V Rao. GPOPS-II: A matlab software for solving multiple-phase optimal control problems using hp-adaptive gaussian quadrature collocation methods and sparse nonlinear programming. *ACM Transactions on Mathematical Software*, 41(1):1–37, October 2014.

[112] Roberto Lot, Nicola Dal Bianco, Matteo Massaro, and Matteo Veneri. Optimal control of road vehicles: Direct and indirect approaches. In *15th European Automotive Congress 15th European Automotive Congress*, Madrid, Spain, October 2017.

[113] Divya Garg, Michael Patterson, William W Hager, Anil V Rao, David A Benson, and Geoffrey T Huntington. A unified framework for the numerical solution of optimal control problems using pseudospectral methods. *Automatica*, 46(11):1843–1851, 2010.

[114] Joseph C La Joie. Race car performance optimization. Technical report, SAE Technical Paper, 1994.

[115] M Da Lio. Valutazione della manovrabilit à dei motocicli attraverso l'esame della risposta nel dominio del tempo ad una manovra condotta in maniera ottima. Technical report, Department of Mechanical Engineering, University of Padova, Padova (Italy), May 1996 (In Italian).

[116] M Da Lio. Analisi della manovrabilit à dei veicoli. un approccio basato sul controllo ottimo. *ATA Journal*, 50(1):35–42 (In Italian), 1997.

[117] Blake Siegler and David Crolla. Racing car simulation and the virtual race track. In *2001 ASME International Mechanical Engineering Congress and Exposition*, pages 231–238, 2001.

[118] Blake Siegler and David Crolla. Lap time simulation for racing car design. Technical report, SAE Technical Paper, 2002.

[119] Daniele Casanova, Robin S Sharp, Mark Final, Bruce Christianson, and Pat Symonds. Application of automatic differentiation to race car performance optimisation. In *Automatic differentiation of algorithms*, pages 117–124. Springer, 2002.

[120] D.P. Kelly and R.S. Sharp. Time-optimal control of the race car: a numerical method to emulate the ideal driver. *Vehicle System Dynamics*, 48(12):1461–1474, 2010.

[121] Craig T Lawrence, Jian L Zhou, and André L Tits. User's guide for cfsqp version 2.0: Ac code for solving (large scale) constrained nonlinear (minimax) optimization problems, generating iterates satisfying all inequality constraints. Technical report, 1994.

[122] Günther Prokop. Modeling human vehicle driving by model predictive online optimization. *Vehicle System Dynamics*, 35(1):19–53, 2001.

[123] Efstathios Velenis and Panagiotis Tsiotras. Minimum time vs maximum exit velocity path optimization during. In *2005 IEEE international symposium on industrial electronics*, pages 355–360, Dubrovnic, Croatia, June 2005. IEEE.

[124] Efstathios Velenis, Panagiotis Tsiotras, and Jianbo Lu. Optimality properties and driver input parameterization for trail-braking cornering. *European Journal of Control*, 4:308–320, 2008.

[125] D. Casanova, R.S. Sharp, and P. Symonds. On the optimisation of the longitudinal location of the mass centre of a formula one car for two circuits. In *Proceedings of the 6th International Symposium on Automotive Control (AVEC 2002)*, volume 2, pages 6–12, Japan, Hiroshima, September 9–13 2002. Citeseer, SAE.

[126] Paola Falugi, Eric Kerrigan, and Eugene Van Wyk. Imperial college london optimal control software user guide (iclocs). *Department of Electrical and Electronic Engineering, Imperial College London, London, England, UK*, 2010.

[127] Roberto Lot and S Evangelou. Lap time optimization of a sports series hybrid electric vehicle. In *2013 World Congress on Engineering*, 2013.

[128] David JN Limebeer, G Perantoni, and AV Rao. Optimal control of formula one car energy recovery systems. *International Journal of Control*, 87(10):2065–2080, 2014.

[129] Mehdi Imani Masouleh and David JN Limebeer. Fuel minimization for a vehicle equipped with a flywheel and battery on a three-dimensional track. *IEEE Transactions on Intelligent Vehicles*, 2(3):161–174, 2017.

[130] Mehdi Imani Masouleh. *Optimal control and stability of four-wheeled vehicles*. PhD thesis, University of Oxford, 2017.

[131] Edward N Smith, Efstathios Velenis, Davide Tavernini, and Dongpu Cao. Effect of handling characteristics on minimum time cornering with torque vectoring. *Vehicle System Dynamics*, 56(2):221–248, 2018.

[132] Ricardo de Castro, Mara Tanelli, Rui Esteves Araujo, and Sergio M. Savaresi. Minimum-time manoeuvering in electric vehicles with four wheel-individual-motors. *Vehicle System Dynamics: International Journal of Vehicle Mechanics and Mobility*, 52(6):824–846, 2014.

[133] Julian P Timings and David J Cole. Minimum maneuver time calculation using convex optimization. *Journal of Dynamic Systems, Measurement, and Control*, 135(3):031015, 2013.

[134] Karl Berntorp, Bjorn Olofsson, Bo Bernhardsson, Kristoffer Lundahl, and Lars Nielsen. Models and methodology for optimal vehicle maneuvers applied to a hairpin turn. In *American Control Conference (ACC), 2013*, pages 2139–2146, Renaissance Washington, DC Downtown Hotel, Washington, DC, June 2013. IEEE.

[135] Karl Berntorp, Björn Olofsson, Kristoffer Lundahl, and Lars Nielsen. Models and methodology for optimal trajectory generation in safety-critical road–vehicle manoeuvres. *Vehicle System Dynamics*, pages 1–29, 2014.

[136] Kristoffer Lundahl, Karl Berntorp, Björn Olofsson, Jan Åslund, and Lars Nielsen. Studying the influence of roll and pitch dynamics in optimal road-vehicle maneuvers. In *23rd International Symposium on Dynamics of Vehicles on Roads and Tracks*, Qingdao, China, August 2013.

[137] Alessandro Rucco, Giuseppe Notarstefano, and John Hauser. An efficient minimum-time trajectory generation strategy for two-track car vehicles. *IEEE Transactions on Control Systems Technology*, 23(4):1505–1519, 2015.

[138] Michał Maniowski. Optimization of driving technique of rwd racing car for faster cornering. *Journal of KONES*, 22, 2015.

[139] M Maniowski. Optimization of driver and chassis of fwd racing car for faster cornering. In *The Dynamics of Vehicles on Roads and Tracks: Proceedings of the 24th Symposium of the International Association for Vehicle System Dynamics (IAVSD 2015), Graz, Austria, 17-21 August 2015*, page 77. CRC Press, 2016.

[140] Mehdi Imani Masouleh and David JN Limebeer. Optimizing the aero-suspension interactions in a formula one car. *IEEE Transactions on Control Systems Technology*, 24(3):912–927, 2016.

[141] Nicola Dal Bianco, Lot Roberto, and Gadola Marco. Minimum time optimal control simulation of a gp2 race car. *Proceedings of the Institution of Mechanical Engineers, Part D: Journal of Automobile Engineering*, page 0954407017728158, 2017.

[142] Giacomo Perantoni and David JN Limebeer. Optimal control of a formula one car on a three-dimensional track—part 1: Track modeling and identification. *Journal of Dynamic Systems, Measurement, and Control*, 137(5):051018, 2015.

[143] DJN Limebeer and G Perantoni. Optimal control of a formula one car on a three-dimensional track—part 2: Optimal control. *Journal of Dynamic Systems, Measurement, and Control*, 137(5):051019, 2015.

[144] Giacomo Perantoni. *Optimal control of vehicle systems*. PhD thesis, University of Oxford, 2013.

[145] Roberto Lot, Nicola Dal Bianco, and Koen Matthys. Lap time simulation and design optimisation of a brushed dc electric motorcycle for the isle of man tt zero challenge. *Vehicle System Dynamics*, 2017.

[146] RS Sharp, Patrick Gruber, and Ernesto Fina. Circuit racing, track texture, temperature and rubber friction. *Vehicle System Dynamics*, 54(4):510–525, 2016.

[147] D.P. Kelly and R.S. Sharp. Time-optimal control of the race car: influence of a thermodynamic tyre model. *Vehicle System Dynamics*, 50(4):641–662, April 2012.

[148] AJ Tremlett and DJN Limebeer. Optimal tyre usage for a formula one car. *Vehicle System Dynamics*, 54(10):1448–1473, 2016.

[149] Robin Verschueren, Stijn De Bruyne, Mario Zanon, Janick V Frasch, and Moritz Diehl. Towards time-optimal race car driving using nonlinear mpc in real-time. In *53rd IEEE Conference on Decision and Control*, pages 2505–2510, J.W. Marriott Hotel, Los Angeles, CA, USA, December 2014. IEEE.

[150] Robin Verschueren, Mario Zanon, Rien Quirynen, and Moritz Diehl. Time-optimal race car driving using an online exact hessian based nonlinear mpc algorithm. In *European Control Conference (ECC)*. IEEE, 2016.

[151] Matthias Gerdts. Solving mixed-integer optimal control problems by branch&bound: A case study from automobile test-driving with gear shift. *Optimal Control Applications and Methods*, 26(1):1–18, 2005.

[152] Sebastian Sager, Christian Kirches, and Hans Georg Bock. Fast solution of periodic optimal control problems in automobile test-driving with gear shifts. In *Decision and Control, 2008. CDC 2008. 47th IEEE Conference on*, pages 1563–1568. IEEE, 2008.

[153] Christian Kirches, Sebastian Sager, Hans Georg Bock, and Johannes P Schlöder. Time-optimal control of automobile test drives with gear shifts. *Optimal Control Applications and Methods*, 31(2):137–153, 2010.

[154] Peter Kühl, Joachim Ferreau, Jan Albersmeyer, Christian Kirches, Leonard Wirsching, Sebastian Sager, Andreas Potschka, Gerrit Schulz, Moritz Diehl, Daniel B Leineweber, et al. Muscod-ii users manual. *University of Heidelberg*, 2007.

[155] Vittore Cossalter, Roberto Lot, and Davide Tavernini. Optimization of the centre of mass position of a racing motorcycle in dry and wet track by means of the "optimal maneuver method". In Goele Pipeleers, editor, *Mechatronics (ICM), 2013 IEEE International Conference on*, pages 412–417, Department of Management and Engineering, University of Pado, Vicenza, VI, Italy, February 2013. IEEE.

[156] Christoph Voser, Rami Y Hindiyeh, and J Christian Gerdes. Analysis and control of high sideslip manoeuvres. *Vehicle System Dynamics*, 48(S1):317–336, 2010.

[157] Davide Tavernini, Efstathios Velenis, Roberto Lot, and Matteo Massaro. On the optimality of handbrake cornering. In *52nd IEEE Conference on Decision and Control*, pages 2233–2238. IEEE, 2013.

[158] Michał Maniowski. Multi-criteria optimization of chassis parameters of nissan 200 sx for drifting competitions. In *IOP Conference Series: Materials Science and Engineering*, volume 148, page 012019. IOP Publishing, 2016.

[159] Charles C MacAdam and Gregory E Johnson. Application of elementary neural networks and preview sensors for representing driver steering control behaviour. *Vehicle System Dynamics*, 25(1):3–30, 1996.

[160] Jorge Muñoz, German Gutierrez, and Araceli Sanchis. A human-like torcs controller for the simulated car racing championship. In *Proceedings of the 2010 IEEE Conference on Computational Intelligence and Games*, pages 473–480. IEEE, 2010.

[161] Bernhard Wymann, Eric Espié, Christophe Guionneau, Christos Dimitrakakis, Rémi Coulom, and Andrew Sumner. Torcs, the open racing car simulator. *Software available at http://torcs. sourceforge. net*, 4, 2000.

[162] Elias Yee and Jason Teo. Evolutionary spiking neural networks as racing car controllers. In *Hybrid Intelligent Systems (HIS), 2011 11th International Conference on*, pages 411–416. IEEE, 2011.

[163] Jeffery R. Anderson, Beshah Ayalew, and T. Weiskircher. Modeling a professional driver in ultra-high performance maneuvers with a hybrid cost MPC. In *American Control Conference (ACC), 2016*, pages 1981–1986, Boston Marriott Copley Place, Boston, MA, USA, July 2016. IEEE.

[164] Amedeo Tesi, Francesco Vinattieri, Renzo Capitani, and Claudio Annicchiarico. Development of an e-LSD control strategy considering the evolution of the friction torque with the wear depth. *SAE International Journal of Engines*, 9(2016-01-1136), 2016.

[165] Global optimization toolbox: User's guide (R2017a). Technical report, The MathWorks, March 2017.

[166] Hockenheim. `http://www.hockenheimring.de/en/history/`, 2017. [Online; accessed 31-March-2017].

[167] Nürburgring. `http://www.nuerburgring.de/en/fans-info/history.html`, 2017. [Online; accessed 31-March-2017].

[168] Roberto Lot and Francesco Biral. A curvilinear abscissa approach for the lap time optimization of racing vehicles. *IFAC Proceedings Volumes*, 47(3):7559–7565, 2014.

[169] Torsten Butz, Martin Ehmann, and Thieß-Magnus Wolter. A realistic road model for real-time vehicle dynamics simulation. Technical Report 2014-01-1068, SAE Technical Paper, 2004.

[170] Marko Lepetic, Gregor Klancar, Igor Skrjanc, Drago Matko, and Bostjan Potocnik. Time optimal path planning considering acceleration limits. *Robotics and Autonomous Systems*, 45(3):199–210, 2003.

[171] Sebring international raceway, 2017. [Online; accessed 17-October-2017].

[172] T. Weiskircher and B. Ayalew. Predictive control for autonomous driving in dynamic public traffic. In *Proceedings of the American Control Conference*, pages 3328–3333, Chicago, IL, July 2015. IEEE.

[173] Signal processing toolbox. Technical report, The MathWorks, 2014.

[174] Thomas Weiskircher, Qian Wang, and Beshah Ayalew. Predictive guidance and control framework for (semi-) autonomous vehicles in public traffic. *IEEE Transactions on control systems technology*, 2017.

[175] Piero Taruffi. *The technique of motor racing.* Motor Racing Publications, 1958.

[176] Matthew J Weinstein and Anil V Rao. Algorithm: Adigator, a toolbox for the algorithmic differentiation of mathematical functions in matlab using source transformation via operator overloading. *ACM Trans. Math. Softw.*, 2016.

[177] Andreas Wächter and Lorenz T Biegler. On the implementation of an interior-point filter line-search algorithm for large-scale nonlinear programming. *Mathematical programming*, 106(1):25–57, 2006.